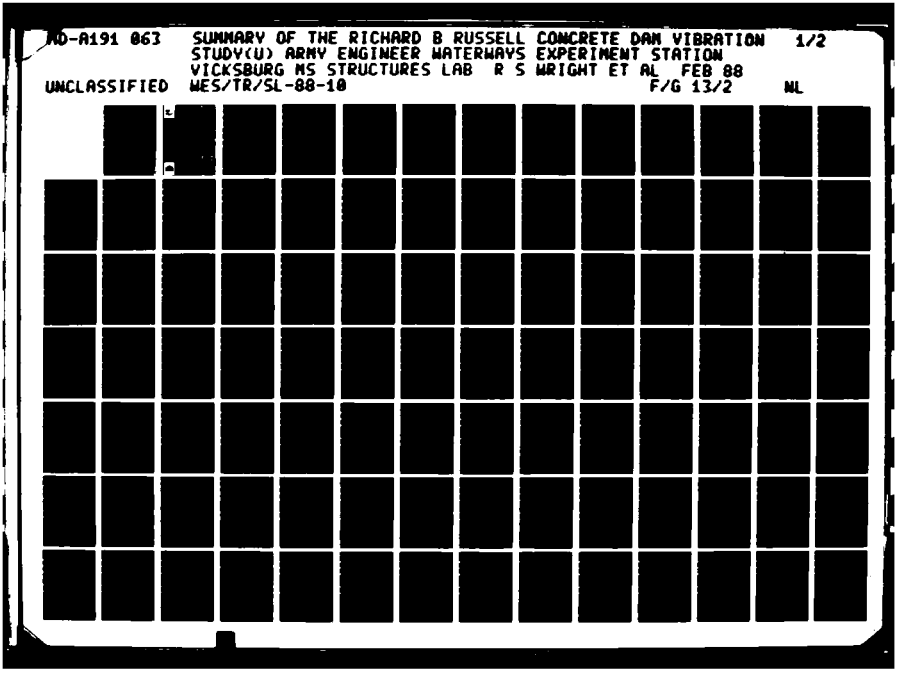
AD-A191 063 SUMMARY OF THE RICHARD B RUSSELL CONCRETE DAM VIBRATION 1/2
STUDY(U) ARMY ENGINEER WATERWAYS EXPERIMENT STATION
VICKSBURG MS STRUCTURES LAB R S WRIGHT ET AL FEB 88
UNCLASSIFIED WES/TR/SL-88-10 F/G 13/2 NL

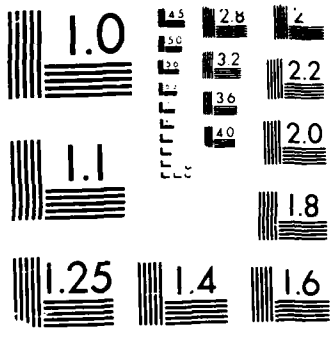

TECHNICAL REPORT SL-88-10

SUMMARY OF THE RICHARD B. RUSSELL CONCRETE DAM VIBRATION STUDY

by

R. Stephen Wright, Vincent P. Chiarito, Robert L. Hall

Structures Laboratory

DEPARTMENT OF THE ARMY
Waterways Experiment Station, Corps of Engineers
PO Box 631, Vicksburg, Mississippi 39180-0631

February 1988
Final Report

Prepared for DEPARTMENT OF THE ARMY
US Army Corps of Engineers
Washington, DC 20314-1000

and US Army Engineer District, Savannah
Savannah, Georgia 31402-0889

Unclassified

SECURITY CLASSIFICATION OF THIS PAGE

REPORT DOCUMENTATION PAGE

Form Approved
OMB No 0704-0188
Exp Date Jun 30 1986

AD-A191063

1a REPORT SECURITY CLASSIFICATION Unclassified	1b RESTRICTIVE MARKINGS
2a SECURITY CLASSIFICATION AUTHORITY	3 DISTRIBUTION/AVAILABILITY OF REPORT Approved for public release; distribution unlimited.
2b DECLASSIFICATION/DOWNGRADING SCHEDULE	
4 PERFORMING ORGANIZATION REPORT NUMBER(S) Technical Report SL-88-10	5 MONITORING ORGANIZATION REPORT NUMBER(S)
6a NAME OF PERFORMING ORGANIZATION USAEWES Structures Laboratory 6b OFFICE SYMBOL (If applicable)	7a NAME OF MONITORING ORGANIZATION
6c ADDRESS (City, State, and ZIP Code) PO Box 631 Vicksburg, MS 39180-0631	7b ADDRESS (City, State, and ZIP Code)
8a NAME OF FUNDING/SPONSORING ORGANIZATION See reverse 8b OFFICE SYMBOL (If applicable)	9 PROCUREMENT INSTRUMENT IDENTIFICATION NUMBER
8c ADDRESS (City, State, and ZIP Code) Washington, DC 20314-1000; Savannah, GA 31402-0889	10 SOURCE OF FUNDING NUMBERS PROGRAM ELEMENT NO / PROJECT NO / TASK NO / WORK UNIT ACCESSION NO

11 TITLE (Include Security Classification)
Summary of the Richard B. Russell Concrete Dam Vibration Study

12 PERSONAL AUTHOR(S)
Wright, R. Stephen; Chiarito, Vincent P.; Hall, Robert L.

13a TYPE OF REPORT	13b TIME COVERED	14 DATE OF REPORT (Year, Month, Day)	15 PAGE COUNT
Final report	FROM _____ TO _____	February 1988	119

16 SUPPLEMENTARY NOTATION
Available from National Technical Information Service, 5285 Port Royal Road, Springfield, VA 22161.

17 COSATI CODES		
FIELD	GROUP	SUB-GROUP

18 SUBJECT TERMS (Continue on reverse if necessary and identify by block number)
Concrete dams
Finite element analysis
Hydrodynamic interaction
Modal assurance criterion
Structure-foundation interaction
Vibration response test

19 ABSTRACT (Continue on reverse if necessary and identify by block number)

Linear elastic three-dimensional finite element (FE) analyses of a concrete gravity dam modeled both with and without reservoir effects were conducted to determine natural frequencies and mode shapes of the dam. These analyses were compared with experimental results from prototype vibration tests before and after reservoir impoundment. Mode shapes comparisons between the prototype and the FE model results were evaluated using a modal assurance criterion. Flexible and rigid foundation models were used in the analyses, and the reservoir was modeled as added mass to the dam. The comparison of analytical and experimental results provided a basis for assessing the accuracy of linear elastic FE models for predicting dynamic properties of concrete gravity dams.

The correlation between experimental and FE mode shapes was the most favorable for the dam without reservoir using a fixed foundation. Analytical estimates of natural frequencies were higher than those actually measured by experiment. The FE model with flexible foundation gave estimates closest to the frequencies determined by the experiment.

20 DISTRIBUTION/AVAILABILITY OF ABSTRACT	21 ABSTRACT SECURITY CLASSIFICATION
☒ UNCLASSIFIED/UNLIMITED ☐ SAME AS RPT ☐ DTIC USERS	Unclassified
22a NAME OF RESPONSIBLE INDIVIDUAL	22b TELEPHONE (Include Area Code) / 22c OFFICE SYMBOL

DD FORM 1473, 84 MAR 83 APR edition may be used until exhausted
All other editions are obsolete

SECURITY CLASSIFICATION OF THIS PAGE

Unclassified

8a. NAME OF FUNDING/SPONSORING ORGANIZATION (Continued).

US Army Corps of Engineers;
US Army Engineer District, Savannah

PREFACE

This study was conducted during September 1981 through September 1987 by the US Army Engineer Waterways Experiment Station (WES) under the sponsorship of the Office, Chief of Engineers (OCE), US Army, and the US Army Engineer District, Savannah. The Technical Monitor was Mr. Lucian Guthrie, OCE.

This work was conducted under the supervision of Mr. Bryant Mather, Chief, Structures Laboratory (SL), WES; Mr. James T. Ballard, Assistant Chief, SL; and Dr. Jimmy P. Balsara, Chief of the Structural Mechanics Division. Dr. Paul F. Mlakar and CPT Robert Volz were involved in the planning and directing phases of the work.

Acknowledgment is made to Mr. Xiaru Wang and Mr. Yangyou Chen for developing the finite element grid of the dam and for conducting parameter studies on isolated monoliths with and without foundation interaction. Mr. Robert Cole, Structural Analysis Group, is acknowleged for developing a computer routine to compare mode shapes using the modal assurance criterion. Acknowledgment is also made to Mr. James L. Pickens and Mr. Rick Floyd, Instrumentation Services Division, for instrumentation support; to Mr. Stafford S. Cooper and Mr. Donald Douglas, Geotechnical Laboratory, for their efforts in conducting the field tests; and to Mr. Alton M. Alexander, Evaluation and Monitoring Unit, SL, for the concrete material property testing and help with the data analysis. Finally, the support of personnel at the Richard B. Russell Area Office is acknowledged. This report was prepared by Mr. R. Stephen Wright, Mr. Vincent P. Chiarito, and Dr. Robert L. Hall, SL, and was edited by Ms. Lee T. Byrne of the Information Products Division, Information Technology Laboratory, WES.

COL Dwayne G. Lee, CE, is the Commander and Director of WES. Dr. Robert W. Whalin is the Technical Director.

CONTENTS

CONVERSION FACTORS, NON-SI TO SI (METRIC)
UNITS OF MEASUREMENT

Non-SI units of measurement used in this report can be converted to SI (metric) units as follows:

Multiply	By	To Obtain
feet	0.3048	metres
feet per second	0.3048	metres per second
inches	25.4	millimetres
kips (force) per square inch	6.894757	megapascals
miles (US statute)	1.609	kilometres
pounds (force)	4.448222	newtons
pounds (force) per cubic foot	157.08748	newtons per cubic metre
pounds (force) per foot	14.593904	newtons per metre
pounds (force) per inch	175.1268	newtons per metre
pounds (force) per square inch	0.006894757	megapascals

SUMMARY OF THE RICHARD B. RUSSELL CONCRETE DAM VIBRATION STUDY

PART I: INTRODUCTION

1. The Richard B. Russell Dam, recently built by the US Army Corps of Engineers (CE), is approximately 170 miles* from the mouth of the Savannah River between Georgia and South Carolina. As shown in Figure 1, the crest of the concrete gravity part of the dam is 1,884 ft long. It is composed of 13 nonoverflow, 8 intake, and 11 spillway monoliths, the tallest of which is approximately 200 ft high.

2. Results of prototype vibration tests of the Richard B. Russell Dam, with and without reservoir, were compared with linear elastic three-dimensional dynamic finite element (FE) analyses of the dam (Chiarito and Mlakar 1983; Bevins, Chiarito, and Hall, in preparation). This comparison provides a basis for assessing the accuracy of linear elastic FE models for predicting dynamic properties of concrete gravity dams.

3. A modal assurance criterion** (MAC) was used to compare the results of experimental and analytical structural dynamics (Allemang and Brown 1982). (See Appendix B for a discussion of the modal assurance criterion.)

4. The grid for the three-dimensional FE analyses of the dam is shown in Figure 2. Four FE analyses were conducted:

a. Fixed base or foundation, without reservoir.

b. Fixed base, with reservoir.

c. Flexible base, without reservoir.

d. Flexible base, with reservoir.

The flexible base was modeled with vertical and horizontal springs using a spring constant computed from material properties of the foundation. Concentrated masses were added to model the mass due to the reservoir and the tainter gates.

---

* A table of factors for converting non-SI units of measurement to SI (metric) units is presented on page 3.

** Certain technical terms are defined in the Glossary, Appendix E.

PART II: PROTOTYPE TESTS

5. Two forced vibration tests were made on the Richard B. Russell Dam before and after impoundment of the reservoir to determine the natural frequencies, mode shapes, modal damping ratios, and relative joint movements (Chiarito and Mlakar 1983; Bevins, Chiarito, and Hall, in preparation). The first low-level forced vibration test (test 1), before reservoir impoundment, was conducted during January and February 1982 with a mean headwater elevation of 343. The second test (test 2), with reservoir impoundment, was conducted during June and July 1984 with a mean headwater elevation of 470. These tests provided an experimental measure of the prototype hydrodynamic interaction and a comparison of the changes of the dynamic properties produced by the reservoir.

6. The dam was excited at monoliths 7, 16, and 22 by a crest-mounted inertial mass. The force input was in an upstream-downstream direction. As shown in Figures 3 and 4, respectively, three arrays of servo accelerometers measured the horizontal crest accelerations of 31 monoliths in the first test and all 32 monoliths in the second test. Measurements from the drive point on monolith 16 overlapped measurements from drive points on monoliths 7 and 22.

7. In each test, accelerometers were placed at different elevations in the three drive point monoliths to measure the horizontal motions in the vertical planes. Figures 5 and 6 show the cross-sectional accelerometer locations for the first and second tests, respectively. Pressure gages were also placed on monolith 7 in the second test (Figure 6).

8. Relative joint motion arrays were positioned at three locations in test 1 and two locations in test 2. They consisted of two accelerometers closely spaced on each side of the joint being monitored. Tests 1 and 2 joint accelerometer locations are shown in Figure 7.

9. The abutments of the sides of the dam restrained the end monoliths with some degree of fixity. However, the abutment on the Georgia side was not complete during the first test and was approximately 60 ft below the completed crest elevation 495. Therefore, a portion of monolith 1 was unrestrained on the Georgia side during the first test.

10. Static and dynamic measurements on 6- by 12-in. concrete cylinders from the dam are summarized in Tables 1 through 3. Dynamic modulus of elasticity of seven rock core samples are listed in Table 4. The in situ elastic

modulus of the foundation, E_f, was estimated from the dynamic modulus of elasticity, cross-hole seismic velocity, and pulse velocity of the rock core samples. As discussed in Appendix A, the estimated value for E_f was 6.05×10^6 psi.

11. The mode shapes measured of the crest of the dam from the two vibration tests are shown in Figures 8 through 12. The response at monolith 22, a drive point measurement, was neglected because it was an order of magnitude larger than the other responses. This extremely large response seemed to be in error and distorted the mode shapes. By visual inspection of these modes, the responses in the midsection of the dam compared well, but differed at the ends of the dam. Slight shifts in the maximum response points towards the ends of the dam are an indication that the hydrodynamic effects added mass to the dam's midsection. Note that the fourth crest flexural mode, Figure 11, was determined for test 2 only. This is because the vibrator locations may have been nodes of the fourth mode in test 1 (Chiarito and Mlakar 1983). (The locations of the nodes were possibly different for tests 1 and 2.)

12. As expected, the reservoir impoundment decreased the natural frequencies of the dam due to the added mass. The damping estimates and natural frequencies from test 1 and 2 are shown in Tables 5 and 6, respectively. With the exception of mode 5, the reservoir had little effect on the damping estimates. Percent decreases in natural frequencies were the largest for mode 1 (10.1 percent), with smaller decreases for the higher modes (Bevins, Chiarito, and Hall, in preparation). (As discussed later, natural frequencies from finite element analyses are also included in Table 6 for comparison.)

13. The MAC was used to compare the crest mode shapes (Allemang and Brown 1982). (Monolith 22 was not used in computing the MAC because excessive local responses were recorded in test 2 at this monolith.) Table 7 summarizes the results. Mode 3 showed reasonable agreement, but the other modes had fair to poor correlation. Possible explanations of the poorer correlation between mode shapes include the following:

a. The force input was not large enough to completely excite the entire structure at the lower frequencies. (A typical force is shown in Figure 13). Ideally, two or more force inputs would be better. By visual inspection of modes 1 and 2, the midsection of the dam agrees well, but at the ends the shapes differ. This would account for the low MAC.

b. A high degree of modal coupling (closely spaced resonance frequencies) existed at the higher frequencies.

c. The friction forces between monoliths may have been different for test 1 and 2. Tests 1 was conducted in winter, and test 2 was conducted in summer. Thus, expansion and contraction of the material could have changed the normal and frictional forces between monoliths.

14. Except at elevation 430 (normalized height was 0.65), the experimentally measured pressures on the upstream face of monolith 7 in the second test with reservoir (Bevins, Chiarito, and Hall, in preparation) were close to theoretical values calculated by a simplified procedure developed by Fenves and Chopra (1986). (Due to a scaling error in the gage calibration, an excessively large pressure was recorded at elevation 430.) The theoretical pressures are based on the fundamental cantilever mode shape and maximum acceleration of a two-dimensional section. The measured pressure distribution also was in agreement with pressures measured during vibration testing of the Pine Flat Dam (Rea, Liaw, and Chopra 1972). The magnitude of the experimentally and theoretically determined hydrodynamic pressure for the fundamental frequency (5.3 Hz) of the dam is plotted in Figure 14 as a function of elevation along the centerline of monolith 7. (The extremely large pressure at elevation 430 is not shown in Figure 14.) As shown in Figure 14, theoretical pressures were computed for two concrete moduli to establish a band in which the experimental pressures should fall. This is because the monolith was constructed using different concrete strengths for the exterior and interior mass (Tables 1 and 2). Evidence of low signal-to-noise ratio can be seen in the pressure distribution in Figure 14 (i.e., the points do not form a smooth distribution).

15. Measurements from both tests at the relative joint motion arrays indicated relative motions between monoliths. The nonlinear behavior of the dam is attributed mostly to the monoliths' joint behavior.

PART III: FINITE ELEMENT MODEL

Finite Element Program

16. A structural analysis program for the static and dynamic response of linear systems was used to calculate the natural frequencies and mode shapes of the dam (Bathe, Wilson, and Peterson 1973). This program is coded in FORTRAN 66 and was run on the Honeywell DPS 8 mainframe computer at the US Army Engineer Waterways Experiment Station:

17. The program contains the following element types:

a. Three-dimensional truss element.

b. Three-dimensional beam element.

c. Plane stress and plane strain element.

d. Two-dimensional axisymmetric solid.

e. Three-dimensional solid.

f. Variable-number-nodes thick shell and three-dimensional elements.

g. Thin plate or thin shell element.

h. Boundary element.

i. Pipe element (tangent and bend).

These structural elements can be used in static or dynamic analyses to model a large number of two- or three-dimensional structural problems. The capacity of the program depends mainly on the total number of nodal points in the system, the number of eigenvalues needed in the dynamic analysis, and the computer used. Practically no restriction is placed on the number of elements used, the number of load cases, or the order and bandwidth of the stiffness matrix. Each nodal point in the system can have from zero to six displacement degrees of freedom. Because the element stiffness and mass matrices are assembled in condensed form, the program is equally efficient in the analysis of one-, two-, or three-dimensional systems.

18. The formation of the structure matrices is carried out in the same manner in a static or dynamic analysis. Four types of dynamic analysis can be performed by the program:

a. Determination of system mode shapes and frequencies only.

b. Response spectrum analysis.

c. Frequency response analysis.

d. Dymamic response analysis for arbitrary time-dependent loads using mode superposition or step-by-step direct integration of the equations of motion.

19. The structural mode shapes and frequencies can be obtained by two distinct algorithms:

a. The determinant search method is used for small problems in which the total stiffness matrix can be kept in the core of the computer.

b. The subspace iteration method is used for large problems in which only portions of the stiffness matrix can be retained in the core of the computer.

A subspace iteration method was used to solve for the undamped natural frequencies and mode shapes presented in this report.

Parameter Studies

20. The grid for the FE model was developed by conducting parameter studies of isolated nonoverflow, spillway, and intake monoliths. Modal analyses were used to obtain appropriate FE grid sizes for each of the monoliths. A compatible grid was found for all of the monoliths, thus making possible the generation of the nodal and element data with the computer (Chiarito 1985). Favorable results were obtained when modal analyses of each monolith using uniform grids were compared with analyses using the grid for the entire three-dimensional FE model. Figures 15 through 17 show typical sections of the monoliths and the resulting three-dimensional grids of each monolith. (The resulting three-dimensional FE grid of the dam was shown previously in Figure 2.)

21. Figure 15 shows the penstock tube opening in the intake monolith modeled as solid, or "smeared-hole," elements with 29 percent less stiffness and density than the mass concrete. Modal analyses showed good agreement between a finer FE grid that included the penstock opening and the grid shown in Figure 5 using solid elements.

22. Studies were also performed to obtain a suitable Winkler spring representation of the foundation. Comparisons of two-dimensional and three-dimensional FE dynamic analyses on the nonoverflow section using Winkler springs with analyses using an FE foundation grid and a fixed foundation are presented in Appendix A.

Material Properties

23. The concrete properties used in the FE analyses were taken from previous measurements on 6- by 12-in. concrete cylinders, as summarized in Tables 1 through 3. The concrete samples tested in 1982 and 1984 were 5 and 17, respectively. Generally higher concrete strengths were measured in 1982 than in 1984; however, one cannot conclude that the concrete was stronger in 1982 than it was in 1984 because, statistically, not enough samples were tested in 1982 to indicate any definite change in concrete strength between 1982 and 1984. For example, the cylinder strengths for the 3-ksi design strength concrete determined from the 2 samples tested in 1982 fell within one standard deviation of the 14 samples tested in 1984. This statistical information indicates that if 14 concrete samples had been tested in 1982, the range of data would have been similar to the 1984 results.

24. Dynamic modulus of elasticity values used were 5.1×10^6 psi for exterior mass concrete and 4.26×10^6 psi for interior mass concrete. From previous foundation tests, the dynamic elastic modulus of the foundation used to compute the spring constant was 6.05×10^6 psi, as discussed in Appendix A. Using elastic theory, the average horizontal and vertical spring constant was 4×10^{10} lb/ft in the flexible base model (Timoshenko and Goodier 1970).

Element Types

25. Four element types were used to model the dam. Variable-number-nodes (8 to 21 nodes) three-dimensional solid elements were used to model the mass concrete of the nonoverflow, intake, and spillway monoliths (Bathe, Wilson, and Peterson 1973). Plate elements were used to model the concrete spillway piers, the concrete training walls at spillway monoliths 16 and 26, and the concrete deck of the spillway bridge. Beam elements were used to model the steel girders of the spillway bridge, and Winkler springs were used along the base of the model in the flexible base analysis.

Boundary Conditions

26. By definition, only the X , Y , and Z translations were defined on the three-dimensional thick-shell elements. All degrees of freedom were

deleted along the base of the model for the fixed base analysis. For the flexible base analysis, the longitudinal (Y) translations and all rotations were fixed along the base of the model. Except at the dam abutment interface, horizontal and vertical springs were placed at all nodes on the base in the X and Z directions.

27. In order to model the restraint due to the abutments, nodes along the two end sections (monoliths 1 and 32) had all degrees of freedom deleted (i.e., nodes fixed). However, a few of the nodes had translational degrees of freedom defined on the Georgia side for the model of the dam without reservoir. As was discussed previously, this abutment was not complete at the time of the first vibration test.

28. For the model without reservoir, 5,127 and 5,609 degrees of freedom were used for the fixed base and flexible base FE models, respectively. For the model with reservoir, 5,100 and 5,582 degrees of freedom were used for the fixed base and flexible base FE models, respectively.

Modeling of Added Mass

29. Concentrated masses were added at nodes thought to be in contact with the reservoir to model the reservoir mass and the tainter gates. A constant 49.6-ft-wide mass of reservoir was applied to the model with reservoir. Studies (see Appendix C) showed that this constant width of reservoir added the same amount of mass as a modified Westergaard (1933) analysis. A typical nonoverflow monolith for the dam was analyzed with a constant 49.6-ft-wide mass of reservoir. As discussed in Appendix C, the fundamental frequency compared well with the result obtained from an approximate procedure by Chopra (1978). The mass of the reservoir acting on the tainter gates and the mass of the gate was applied at the trunnion locations on the spillway piers.

PART IV: FINITE ELEMENT MODEL RESULTS

Dam Without Reservoir

30. The three-dimensional shapes (eigenvectors) shown in Figures 18 and 19 include the first nine major bending modes of the dam crest computed from the FE model with fixed base. At 7.7 Hz (eigenvector 2), the major response is associated with the sidesway of the roadway and concrete spillway pier system. The other eigenvectors show that the major responses of the dam are associated with bending of the dam perpendicular to the longitudinal axis of the dam. The fifth eigenvector, at 10.4 Hz (i.e., the fourth bending mode of the crest), is the shape computed by the FE analysis but not measured experimentally. As mentioned previously, it is possible that the vibration exciters were located at nodes of that mode shape during the first vibration test (Chiarito and Mlakar 1983).

31. Previously, initial three-dimensional FE analyses were conducted for the entire dam without reservoir (Chiarito 1985). The main differences between the initial analyses and the latest analyses were that the initial analyses did not model the training walls at monoliths 16 and 26 and had more defined degrees of freedom at the dam abutment interfaces. Material properties were slightly different, and the initial analyses did not add the weight of the tainter gates. The initial analyses had natural frequencies approximately 5 percent greater than the latest analyses.

32. Also, three-dimensional dynamic FE analyses were conducted on isolated monoliths, and two-dimensional FE analyses were conducted on the nonoverflow monolith. Foundation and reservoir effects were not included in these analyses, and dynamic modulus of elasticity values were used. The fundamental frequencies calculated for the isolated nonoverflow, intake, and spillway monoliths were 9.8 Hz, 6.9 Hz, and 11.3 Hz, respectively. These results indicate that the intake sections are the most flexible part of the dam and that the spillway monoliths are the stiffest part of the dam. Also, the fundamental frequency for the two-dimensional analysis of the nonoverflow section was 8.4 Hz. Previously, a two-dimensional analysis of the nonoverflow section using a static modulus of elasticity estimated a fundamental frequency of 7.63 Hz (Norman 1979).

33. The calculated fundamental frequency of the entire dam without

reservoir was 7.1 Hz for a fixed foundation. This frequency was less than the fundamental frequencies of the nonoverflow and spillway monoliths but slightly more than the fundamental frequency of the intake monolith. As expected, the intake sections increased the flexibility of the entire dam.

Dam With Reservoir

34. The three-dimensional shapes (eigenvectors) shown in Figures 20 and 21 are the first eight major bending modes of the dam crest and two mode shapes associated with sidesway of the roadway and concrete spillway pier system. These eigenvectors were calculated from the FE model with fixed base. The eigenvectors not shown are also associated with sidesway of the spillway pier system.

Comparisons of Dam With and Without Reservoir

35. Tables 8 and 9 summarize results of the FE analyses with and without reservoir for fixed and flexible bases, respectively. The FE mode shapes with and without reservoir were compared using MAC. Most mode shapes compared well, except at the higher frequencies. Figures 22 through 31 show the trend toward poorer correlation among FE fixed and flexible base, mode shapes, with and without reservoir, as the frequency increases.

36. As expected, the frequencies computed from the model of the dam with reservoir were lower than from the model without reservoir. Table 6, presented earlier, is a summary of the natural frequencies determined by experiment and analysis.

PART V: COMPARISON OF FINITE ELEMENT MODEL TO PROTOTYPE TEST RESULTS

Dam Without Reservoir

37. Comparisons of the dam crest mode shapes are shown in Figures 32 through 36. Note that the mode numbers correspond to bending modes of the dam crest. As mentioned previously, the fourth mode was not measured experimentally, but was determined analytically. Table 10 summarizes the results of these analytical and experimental mode shape comparisons. Based upon the results of the MAC values, the correlation between analytical and experimental mode shapes was favorable. Overall, the model with a fixed base had slightly better mode shape correlation than did the model with a flexible base, possibly because the base of the dam was more rigid than modeled by the FE flexible base analysis. For a qualitative comparison, the mode shapes all appear to have the largest amplitude in the same general location on the crest of the dam. The MAC does indicate quantitatively how good the comparison is among modes.

38. As shown in Table 6, the frequencies estimated by the FE models were higher than frequencies measured experimentally (16 to 30 percent higher for the FE fixed base model, and 9 to 18 percent higher for the flexible base model). This is reasonable since the FE models are approximations of the dam using a discrete number of degrees of freedom. The FE model in this case is stiffer than the actual dam. The flexible base model estimated frequencies closer to the experimentally measured frequencies than did the fixed base model because foundation interaction decreases the frequency (Norman and Stone 1979).

39. Comparisons of the experimental mode shapes in cross section with results from the FE model with fixed foundation are shown in Figures 37 through 56. Note that the frequencies of the cross-sectional modes correspond with the crest modal frequencies. Table 11 summarizes the results. The correlation between most mode shapes was favorable, and the governing mode shape in cross section resembled the fundamental mode shape of a cantilever beam. However, at the lower frequencies, the mode shapes for spillway monolith 22 (Figures 52 through 56) exhibited discontinuities at the bottom of the pier. This is probably because the force input was not large enough to completely

excite the entire monolith at the lower frequencies. As noted previously, the spillway monoliths are the stiffest part of the dam. From a three-dimensional dynamic FE analysis of an isolated spillway monolith, the fundamental frequency was 11.3 Hz. This is higher than the first four experimentally measured natural frequencies of the dam without reservoir (5.9 Hz to 8.2 Hz).

40. Comparisons of analytical mode shapes in cross section with a design mode shape proposed by Chopra (1978) were conducted and are presented in Appendix D. The results were favorable, indicating that the proposed design mode shape is sufficiently accurate for design purposes.

Dam With Reservoir

41. Comparisons of the dam crest mode shapes are shown in Figures 57 through 61. Note that the mode numbers correspond to bending modes of the dam crest. Table 12 summarizes the results of these comparisons. (The response at monolith 22 was not used in computing the MAC because excessive local responses were recorded in test 2 at this monolith.) Crest mode shape correlation between experiment and analysis was not as favorable as with the dam without reservoir. The fixed model had higher MAC values than the flexible base model for the first three modes, possibly because the prototype foundation stiffness was greater than modeled in the FE flexible base analysis.

42. Various factors may have caused the low correlation between experimental and analytical mode shapes. As discussed previously, errors in the experimental mode shapes may be due partly to a force input that was not large enough to completely excite the entire dam at the lower frequencies. Also, a high degree of modal coupling (closely spaced resonance frequencies) existed at a higher frequencies.

43. Furthermore, inadequacies in the FE model assumptions could have produced a lower correlation between experimental and analytical mode shapes:

a. The modified Westergaard (1933) added mass concept to model the reservoir effects may not be valid at the higher frequencies (Bevins, Chiarito, and Hall, in preparation). Westergaard's method assumes that water is incompressible. This assumption is valid when the forcing frequency is less than the natural frequency of the dam/reservoir system, but for frequencies higher than this, the method overestimates the hydrodynamic effects (Chakrabarti and Chopra 1974). Comparing FE results with and without reservoir, the FE analyses indicated that the percent reductions in natural frequencies were greater for the higher modes. This is

inconsistent with the experimental results, which indicated that the first mode had the largest decrease in natural frequency due to reservoir interaction.

b. The FE model did not include the effects of the added mass of the soil at the abutments. The abutment of the Georgia side of the dam was not complete at the time the first vibration test was made. The additional soil during the second test might have caused a slight increase in the stiffness of the structure at the Georgia-side abutment.

c. Nonlinearitites due to joint slippage were not modeled.

44. Similar to the case of the dam without reservoir, the frequencies estimated by the FE models were higher than measured experimentally (7 to 17 percent higher for the FE fixed base model, and up to 8 percent higher for the FE flexible base model). The flexible base model frequencies compared better with the experiment then did the fixed base model frequencies because foundation interaction reduces the calculated frequencies.

45. Comparisons of the experimental mode shapes in cross section with results from the FE model with fixed foundation are shown in Figures 62 through 71. (Comparisons for monolith 22 were not made because only two accelerometers were mounted on monolith 22). Note that the frequencies of the cross-sectional modes correspond with the crest modal frequencies. Table 13 summarizes the results. The correlation between most mode shapes was favorable, and the governing mode shape in cross section resembled the fundamental mode shape of a cantilever beam.

46. It should be noted that some dam crest experimental mode shapes had better correlation with FE results of a different mode of vibration. The fourth experimental mode shape at 7.5 Hz resembled a fourth normal mode of vibration of a beam fixed at both ends (Harris and Crede 1961). However, this mode shape had a better correlation with the third FE crest flexural mode. Engineering judgment was used in interpreting the experimental mode at 7.5 Hz as a fourth mode of vibration. However, it is possible that the experimental modes exhibited measured local behavior not determined by the model. In this way, the MAC can aid in illustrating complex responses not computed by the model, but measured in the prototype test.

PART VI: CONCLUSIONS

47. By visual inspection of the mode shapes with and without reservoir, hydrodynamic interaction changed the mode shapes of the dam, with the largest differences occurring at the ends of the dam. The dam's midsection had similar responses with and without reservoir interaction; however, slight shifts in the maximum response points towards the ends of the dam indicate that hydrodynamic effects added mass to the dam's midsection. Various factors could have caused fairly low correlations between experimental mode shapes for the tests with and without reservoir. The force input was not large enough to completely excite the entire structure at the lower frequencies, causing scatter in estimates of the mode shapes. Ideally, two or more force inputs would be better. Also, a high degree of modal coupling existed at the higher frequencies, and the friction forces between monoliths may have been different because the tests were conducted during different seasons.

48. The experimental natural frequencies were reduced by the hydrodynamic effects, with the percent change in the first mode the largest (10.' percent). With the exception of the fifth mode, the reservoir impoundment had little effect on the damping estimates.

49. The hydrodynamic pressures measured in the second test with reservoir were close to the predicted values for the fundamental frequency (except at elevation 430), and the pressure distribution was similar to distributions measured at Pine Flat Dam (Rea, Liaw, and Chopra 1972). The theoretical hydrodynamic pressures were based on a two-dimensional response of an isolated nonoverflow monolith (monolith 7). The fundamental mode shape of a cantiliver beam was used to compute the theoretical pressure distribution. Because the experimental and analytical cross-sectional mode shapes of the entire dam resembled the fundamental mode shape of a cantilever beam, the use of a two-dimensional model was valid for predicting the pressure distribution on this nonoverflow monolith. Further pressure measurements and analyses would be needed to confirm if the theoretical pressure distribution is valid for the other parts of the dam.

50. Measurements from both tests at the relative joint motion arrays indicated relative motions between monoliths. The nonlinear behavoir of the dam is attributed primarily to the monoliths' joint behavior.

51. Despite a few experimental errors, no gross anomalies existed, and

the dynamic properties determined are reasonable. It can be concluded that the dam appears to be structurally sound as built.

52. Three-dimensional linear FE analyses have been compared with previous experimental estimates of the modal parameters of a concrete gravity dam. Using available dynamic material properties of the dam concrete and the foundation, a three-dimensional FE model was successfully developed to estimate the linear elastic modal properties of the dam. The fourth mode shape was not measured experimentally for the dam without reservoir, but was computed by the three-dimensional FE analyses.

53. The MAC was useful for evaluating the correlation between the experimental and the FE mode shapes. Favorable correlations of the crest mode shapes were computed for the dam without reservoir, indicating that a reasonable three-dimensional FE model was developed for computing the first three natural modes of vibrations. Various factors may have caused a lower correlation between the experimental and analytical crest mode shapes for the dam with reservoir. Low force input at lower frequencies caused poorer estimates in experimental mode shapes at certain locations, and a high degree of modal coupling existed at the higher frequencies. The effects of the soil-dam interaction at the abutments and the reservoir effects may not have been modeled adequately. Also, nonlinearities due to joint slippage were not modeled. The correlation between most cross-sectional shapes was favorable, and the governing mode shape in cross section resembled the fundamental mode shape of a cantilever beam.

54. It has been shown that a proposed design cross-sectional mode shape by Chopra (1978) is sufficiently accurate for design purposes. Chopra presents a simplified analysis procedure for computing stresses due to earthquake ground motion in the horizontal direction. The simplified procedure uses the fundamental mode of vibration of a two-dimensional model of the dam. The design mode shape resembles the fundamental mode shape of a cantilever beam. As discussed by Chopra, the response of concrete gravity dams to earthquake ground motion is primarily due to the fundamental mode of vibration. The experimental cross-sectional mode shapes of the entire dam resembled Chopra's design mode shape (i.e. the fundamental mode shape of a cantilever beam). Further studies would have to be performed to determine the validity of Chopra's method versus the analysis of the entire dam. These further studies would compare the stresses from the analysis of the entire dam with the

stresses from Chopra's simpified procedure.

55. Analyses of isolated nonoverflow, intake, and spillway monoliths were useful because they showed the relative stiffness of the parts of the dam. The calculated fundamental frequencies of the isolated monoliths indicated that the intake sections were the most flexible part of the dam and that the spillway monoliths were the stiffest part of the dam. Furthermore, the calculated fundamental frequency (7.1 Hz) of the entire dam without reservoir for a fixed foundation was less than the fundamental frequencies of the nonoverflow and spillway monoliths (9.8 Hz and 11.3 Hz, respectively) but slightly more than the fundamental frequency of the intake monolith (6.9 Hz). It can be concluded from these analyses that the intake sections increased the flexibility of the entire dam.

56. The three-dimensional analyses estimated frequencies up to 30 percent higher than those measured experimentally. This is reasonable since the FE models are an approximation of the dam using a discrete number of degrees of freedom. Due to foundation interaction, the FE mode with flexible foundation predicted natural frequencies closer to the experimentally measured values than did the FE model with rigid foundation.

57. In general, it appears that three-dimensional linear FE analyses can give a good estimate of the natural frequencies of concrete gravity dams with or without reservoir effects. The FE analyses can adequately estimate the bending mode shapes of concrete gravity dams without reservoir impoundment. These analyses can adequately estimate the bending mode shapes of concrete gravity dams with reservoir if the reservoir effects are appropriately modeled.

PART VII: RECOMMENDATIONS FOR FURTHER STUDY

58. The effects of the hydrodynamic interaction should be studied further. Additional analyses could be performed using a more appropriate distribution of added masses due to reservoir impoundment. The added mass distribution should be consistent with results from the latest research on hydrodynamic interaction. Possibly a better correlation would then be achieved between analysis and the prototype test with reservoir impoundment.

59. Other refinements in the FE analysis should include more accurate modeling of soil-structure interaction and a model for the joint slippage between monoliths.

60. Studies should be performed on the data collected measuring the movement of the dam before and after reservoir impoundment. This would give an estimate of the flexibility of the interacting dam-foundation system.

61. Further pressure measurements and analyses would be needed to confirm if the theoretical pressure distribution (Fenves and Chopra 1986) is valid for the entire dam. Also further studies would have to be performed to determine the validity of Chopra's simplified method of analysis (Chopra 1978) versus the analysis of the entire dam. These further studies would compare the stresses from the analysis of the entire dam with the stresses from Chopra's simplified procedure.

REFERENCES

Allemang, R. J., and Brown, D. L. 1982 (Nov). "A Correlation Coefficient for Modal Vector Analysis," Proceedings of the 1st Interactional Modal Analysis Conference, pp 110-116.

Bathe, K. J., Wilson, E. L., and Peterson, F. E. 1973. "SAPIV: A Structural Analysis Program for Static and Dynamic Response of Linear Systems," University of California, Earthquake Engineering Research Center, Richmond, Calif.

Bevins, Tommy L., Chiarito, Vincent P., and Hall, Robert L. "Vibration Test of Richard B. Russell Concrete Dam After Reservoir Impoundment," Technical Report SL-87- , in preparation, US Army Engineer Waterways Experiment Station, Vicksburg, Miss.

Chakrabarti, P., and Chopra, Anil K. 1974 (June). "Hydrodynamic Effects in Earthquake Response of Gravity Dams," Journal of the Structures Division, American Society of Civil Engineers, Vol 100, No. ST6, pp 1211-1224.

Chiarito, Vincent P. 1985 (Jan). "Linear Finite Element Comparison with Experimental Modal Analysis for a Concrete Gravity Dam," Proceedings of the Third International Modal Analysis Conference, Vol 1, pp 59-65.

Chiarito, Vincent P., and Mlakar, Paul F. 1983. "Vibration Test of Richard B. Russell Concrete Dam Before Reservoir Impoundment," Technical Report SL-83-2, US Army Engineer Waterways Experiment Station, Vicksburg, Miss.

Chopra, Anil K. 1978. "Earthquake Resistant Design of Concrete Gravity Dams," Journal of the Structural Division, American Society of Civil Engineers, Vol 104, No. ST6, pp 953-971.

Fenves, Gregory, and Chopra, Anil K. 1986. "Simplified Analysis for Earthquake Resistant Design of Concrete Gravity Dams," Report No. EERC-85/10, University of California, Berkeley, Calif.

Harris, C. N., and Crede, C. E., ed. 1961. Shock and Vibration Handbook, McGraw-Hill, New York.

Norman, C. Dean. 1979. "Earthquake Analysis of the Modified Geometry of the Concrete Nonoverflow Section, Richard B. Dam," Technical Report SL-79-14, US Army Engineer Waterways Experiment Station, Vicksburg, Miss.

Norman, C. Dean, and Stone, Harry E. 1979. "Earthquake Analysis of the Gravity Dam Monoliths of the Richard B. Russell Dam," Technical Report SL-79-8, US Army Engineer Waterways Experiment Station, Vicksburg, Miss.

Rea, D., Liaw, C. Y., and Chopra, Anil K. 1972. "Dynamic Properties of Pine Flat Dam," Report No. EERC-72/7, University of California, Berkeley Calif.

Timoshenko, S. P., and Goodier, J. N. 1970. Theory of Elasticity, 3d ed., McGraw-Hill, New York.

Westergaard, H. M. 1933. "Water Pressure on Dams During Earthquakes," Transactions, American Society of Civil Engineers, Vol 98, pp 418-433.

Table 1

Results from Uniaxial Compression Test

Cylinder No.	Poisson's Ratio	Initial Elastic Concrete Modulus 10^6 psi	Uniaxial Compressive Strength ksi	Date Cast 1981	Date* Tested
		4 ksi Design Strength Concrete			
5,037	0.21	4.67	6.36	5 Mar	1
5,811	0.24	4.12	4.97	10 Jul	2
		3 ksi Design Strength Concrete			
5,464	0.18	4.51	5.68	8 May	1
5,765	0.16	3.45	5.20	2 Jul	2
5,468	0.16	3.76	4.55	9 May	
5,563	0.18	3.96	4.95	29 May	
5,735	0.16	4.09	4.85	26 Jun	
6,112	0.16	4.90	6.16	19 Sep	
6,140	0.19	4.45	5.22	25 Sep	
5,166	0.20	4.91	5.86	20 Mar	1
5,512	0.16	3.70	4.81	14 May	2
5,655	0.13	3.92	5.25	12 Jun	
5,708	0.15	4.12	4.81	19 Jun	
5,214	0.16	4.02	4.72	25 Mar	
5,519	0.18	4.46	5.11	15 May	
6,016	0.15	4.22	6.30	27 Aug	
6,083	0.18	4.92	7.27	11 Sep	
6,187	0.13	3.24	3.87	1 Oct	
		2 ksi Design Strength Concrete			
4,954	0.20	3.44	3.45	25 Feb	1
5,833	0.19	3.50	3.40	17 Jul	1
4,993	0.18	3.45	3.13	28 Feb	2
5,993	0.18	2.63	3.17	21 Aug	2

* 1 = 6 May 1982, 2 = 27 Aug 1984.

Table 2

Initial Elastic Concrete Modulus

Cylinder No.	E_{static} $\times 10^6$ psi*	$E_{dynamic}$ $\times 10^6$ psi*	Percent Increase	Date* Tested
		4 ksi Design Strength Concrete		
5,037	4.67	5.59	20	1
5,811	4.12	4.61	12	2
			16 Average	
		3 ksi Design Strength Concrete		
5,765	3.45	4.72	72	2
5,468	3.76	4.48	19	
5,563	3.96	4.63	17	
5,735	4.09	4.72	15	
6,112	4.90	5.64	15	
6,140	4.45	4.92	11	
5,512	3.70	5.34	44	
5,655	3.92	4.81	23	
5,708	4.12	4.77	16	
5,214	4.02	5.08	26	
5,519	4.46	5.08	14	
6,016	4.22	5.48	30	
6,083	4.92	5.73	16	
6,187	3.24	4.92	52	
5,464	4.51	5.43	20	1
5,166	4.91	5.81	18	1
			23 Average	
		2 ksi Design Strength Concrete		
4,993	3.45	3.85	12	2
5,993	2.63	4.09	56	2
4,954	3.44	4.54	32	1
5,833	3.50	4.54	29	1
			32 Average	

* 1 = 6 May 1982, 2 = 27 Aug 1984.

Table 3

Dynamic Measurements on 6- by 12-in. Concrete Cylinders

Design Strength ksi	Cylinder No.	Frequency Hz	Dynamic Modulus $\times 10^6$ psi	Cast Date 1981	Test Date*	Concrete Type**	Damping Ratio %
4.0	5,037	4,023	5.59	5 Mar	1	B	0.331
	5,811	3,725	4.61	10 Jul	2	B	--
		Average	5.10				
3.0	5,464	3,961	5.43	8 May	1	A	0.323
	5,765	3,725	4.72	2 Jul	2	A	--
	5,468	3,700	4.48	9 May		B	--
	5,563	3,725	4.63	29 May		B	--
	5,735	3,750	4.72	26 Jun		B	--
	6,112	4,075	5.64	19 Sep		B/O	--
	6,140	3,825	4.92	25 Sep		B/O	--
	5,512	3,775	5.34	14 May		C	--
	5,655	3,775	4.81	12 Jun		C	--
	5,708	3,775	4.77	19 Jun		C	--
	5,166	4,129	5.81	20 Mar	1	B/O	0.422
	5,214	3,900	5.08	25 Mar	2	C/O	--
	5,519	3,900	5.08	15 May			--
	6,016	4,000	5.48	27 Aug			--
	6,083	4,075	5.73	11 Sep			--
	6,187	3,675	4.92	1 Oct			--
		Average	5.10				
2.0	4,954	3,627	4.54	25 Feb	1	A	0.373
	5,833	3,625	4.54	17 Jul	1	A	0.364
	4,993	3,425	3.85	28 Feb	2	A	--
	5,993	3,500	4.09	21 Aug	2	A	--
		Average	4.26				

* 1 = 6 May 1982, 2 = 26 Aug 1984.

** A = 6-in. aggregate with fly ash, B = 3-in. aggregate with fly ash, B/O = 3-in. aggregate without fly ash, C = 1/2-in. aggregate with fly ash, and C/O = 1/2-in. aggregate without fly ash.

Table 4

Dynamic Modulus of Elasticity of

Rock Core Samples

	Modulus of Elasticity × 10^6 psi		
	Static (Initial Tangent)	Dynamic*	
	7.14	0.54†	
	5.20	5.78	
	12.90	0.40†	
	5.20	7.43	
	13.79	1.05†	
	3.18	3.90	
	5.97	0.24†	
7 sample average	7.63	9.60	(estimate)
3 sample average	4.53	5.70	

* The dynamic modulus was estimated from the three-sample average by applying the same ratio of dynamic to static modulus.

$$9.60 = \frac{5.70}{4.53} \times 7.63$$

† Not used in average. Sample contained healed fractures that probably interfered with frequency reading.

Table 5

Experimental Damping Estimates Before and After

Reservoir Impoundment

Crest Mode No.	Damping Before Impoundment percent	Damping After Impoundment percent
1	4.29	4.41
2	2.07	2.76
3	3.11	3.69
4	Not measured	1.52
5	5.16	2.90

Table 6

Summary of Experimental and Analytical Frequencies, Hz

Crest Mode No.	Prototype Vibration Test Without Reservoir	Finite Element Analysis Without Reservoir		Prototype Vibration Test With Reservoir	Finite Element Analysis With Reservoir	
		Fixed Base	Flexible Base		Fixed Base	Flexible Base
1	5.9	7.1	6.6	5.3	6.2	5.7
2	6.8	7.9	7.4	6.2	6.8	6.4
3	7.6	9.3	8.7	7.3	7.8	7.3
4	Not measured	10.4	9.6	7.5	8.2	7.6
5	8.2	10.7	10.0	8.1	8.7	8.0

Table 7

Experimental Mode Shape Comparisons

Crest Mode No.	Prototype Vibration Test Without Reservoir Frequency Hz	Protype Vibration Test With Reservoir Frequency, Hz	MAC*
1	5.9	5.3	0.16
2	6.8	6.2	0.20
3	7.6	7.3	0.49
4	Not measured	7.5	N/A
5	8.2	8.1	0.02

* Modal Assurance Criterion.

Table 8

Finite Element Fixed Base Mode Shape Comparisons

Crest Mode No.	Analysis Without Reservoir Frequency, Hz	Analysis With Reservoir Frequency, Hz	MAC*
1	7.1	6.2	1.00
2	7.9	6.8	0.99
3	9.3	7.8	0.96
4	10.4	8.2	0.38
5	10.7	8.7	0.30

* Modal Assurance Criterion.

Table 9

Finite Element Flexible Base Mode Shape Comparisons

Crest Mode No.	Analysis Without Reservoir Frequency, Hz	Analysis With Reservoir Frequency, Hz	MAC*
1	6.6	5.7	1.00
2	7.4	6.4	1.00
3	8.7	7.3	0.91
4	9.6	7.6	0.96
5	10.0	8.0	0.83

* Modal Assurance Criterion.

Table 10

Crest Mode Comparisons - Dam Without Reservoir

(Experiment versus Analysis)

Crest Mode No.	Prototype Vibration Test Frequency, Hz	Three-Dimensional Finite Element Analyses			
		Fixed Base Frequency, Hz	MAC*	Flexible Base Frequency, Hz	MAC*
1	5.9	7.1	0.73	6.6	0.74
2	6.8	7.9	0.63	7.4	0.63
3	7.6	9.3	0.64	8.7	0.61
4	Not measured	10.4	--	9.6	--
5	8.2	10.7	0.41	10.0	0.13

* Modal Assurance Criterion.

Table 11

Cross Section Comparisons Without Reservoir

(Experiment versus Analysis)

Crest Mode No.	Experimental Frequency, Hz	Finite Element Fixed Base Frequency, Hz	Modal Assurance Criterion Monolith 7	Monolith 16	Monolith 22
1	5.9	7.1	0.73	0.37	0.00
2	6.8	7.9	0.40	0.74	0.00
3	7.6	9.3	0.73	0.94	0.47
4	Not measured	10.4	--	--	--
5	8.2	10.7	0.72	0.79	0.84

Table 12

Crest Mode Comparisons - Dam With Reservoir

(Experiment versus Analysis)

Crest Mode No.	Prototype Vibration Test Frequency, Hz	Three-Dimensional Finite Element Analyses			
		Fixed Base Frequency, Hz	MAC*	Flexible Base Frequency, Hz	MAC*
1	5.3	6.2	0.20	5.7	0.19
2	6.2	6.8	0.44	6.4	0.38
3	7.3	7.8	0.63	7.3	0.51
4	7.5	8.2	0.15	7.6	0.36
5	8.1	8.7	0.09	8.0	0.33

* Modal Assurance Criterion.

Table 13

Cross-Section Comparisons With Reservoir

(Experiment versus Analysis)

Crest Mode No.	Experimental Frequency, Hz	Finite Element Fixed Base Frequency, Hz	Modal Assurance Monolith 7	Monolith 16
1	5.3	6.2	0.73	0.03
2	6.2	6.8	0.81	0.90
3	7.3	7.8	0.49	0.92
4	7.5	8.2	0.53	0.89
5	8.1	8.7	0.54	0.88

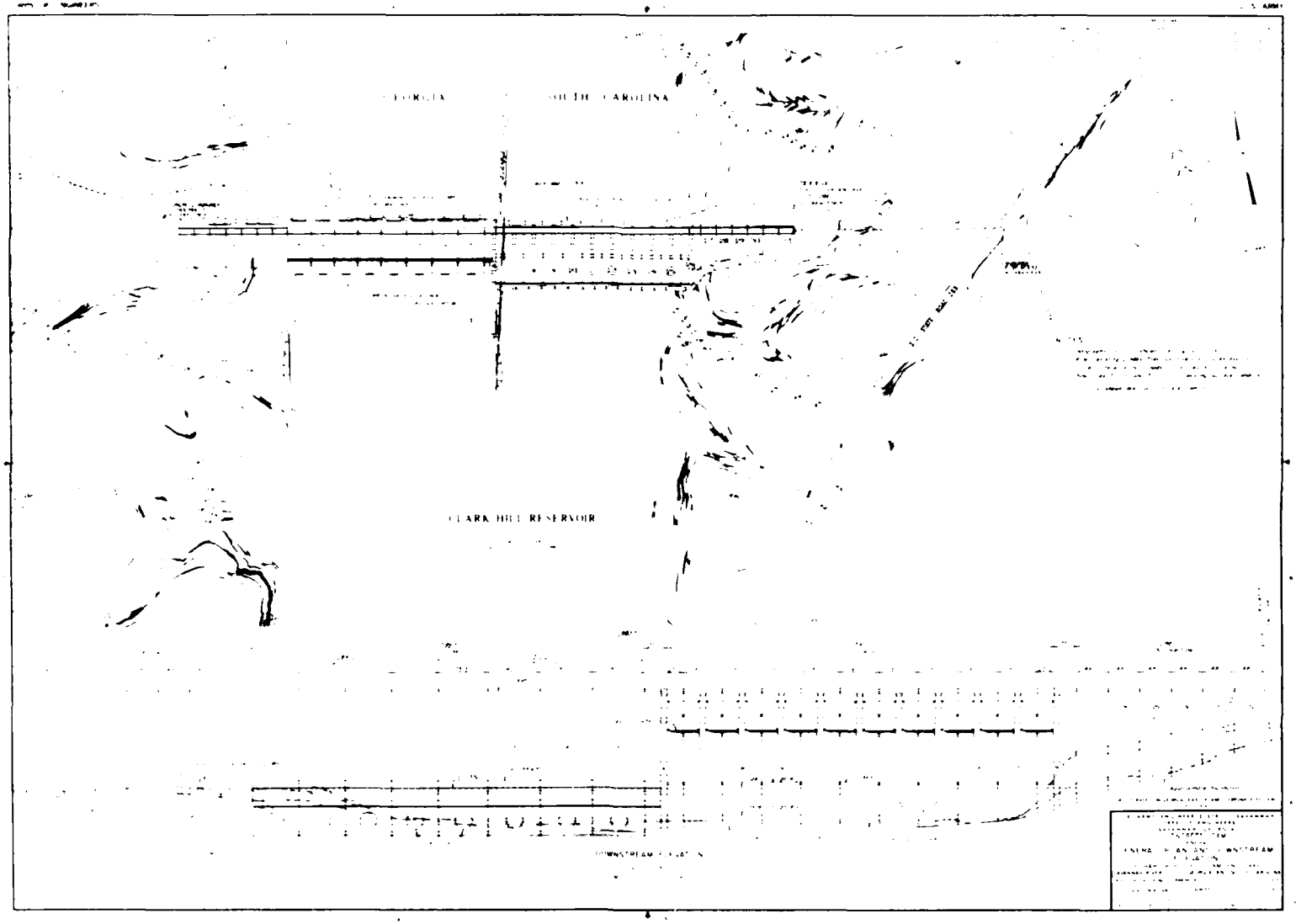

Figure 1. Plan and elevation of Richard B. Russell Dam

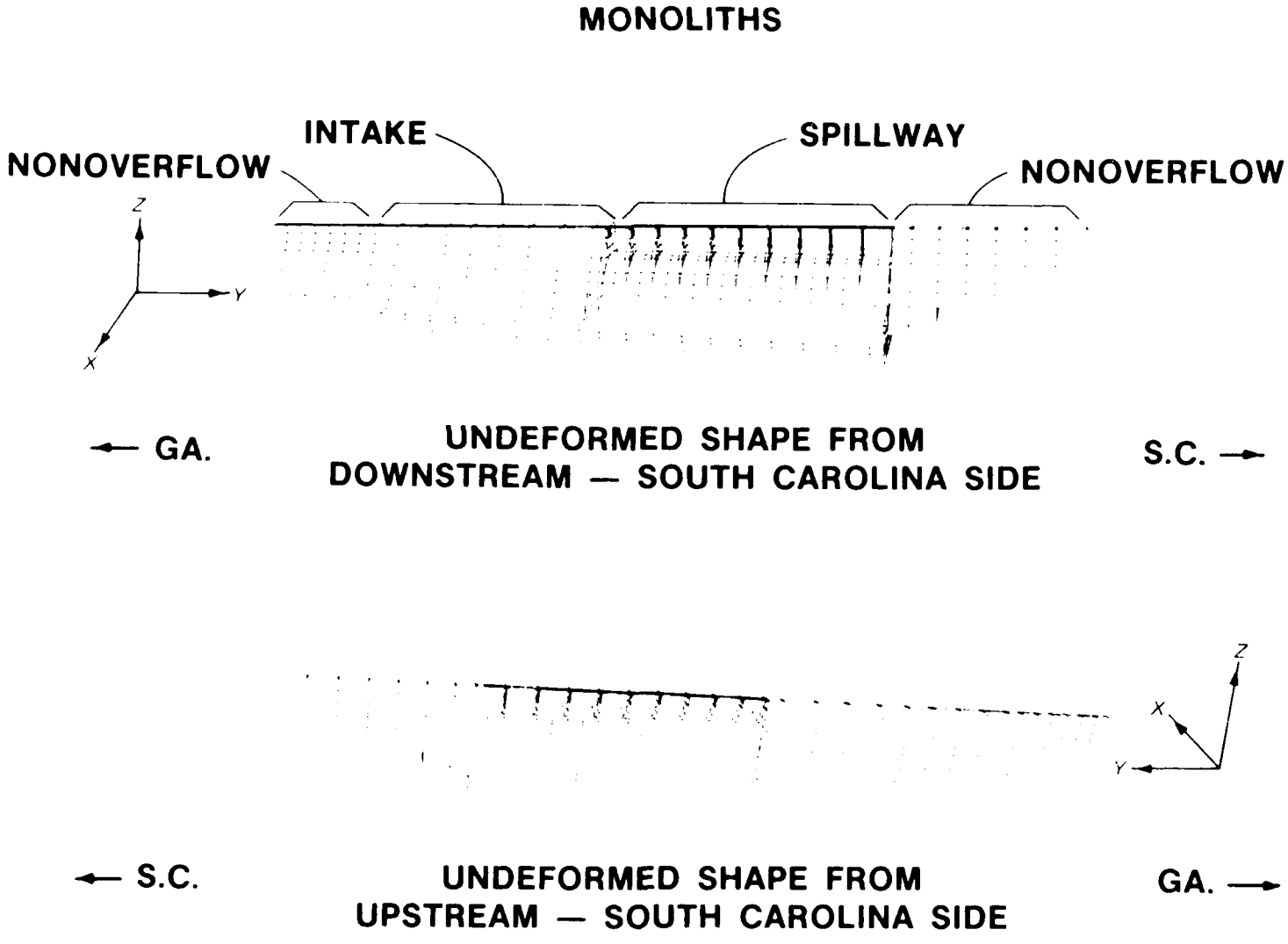

Figure 2. Finite element grid of Richard B. Russell Dam

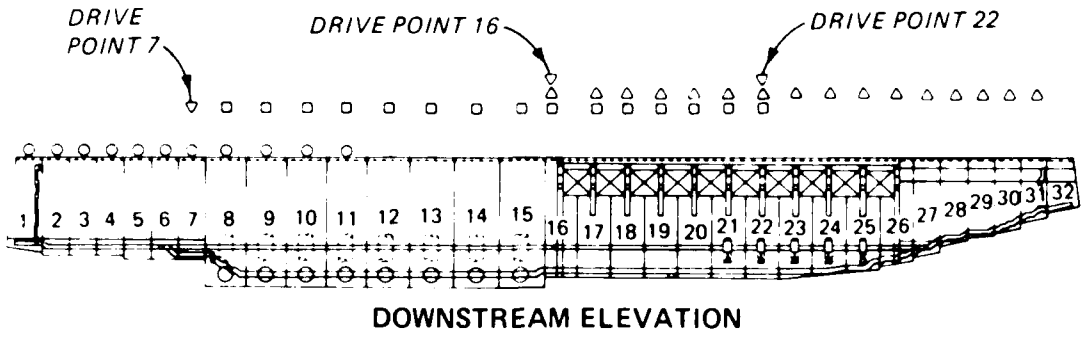

DOWNSTREAM ELEVATION

LEGEND

- ▽ DRIVE POINT
- ○ DRIVE POINT 7 CREST ACCELEROMETERS
- □ DRIVE POINT 16 CREST ACCELEROMETERS
- △ DRIVE POINT 22 CREST ACCELEROMETERS

Figure 3. Crest accelerometer locations for test 1

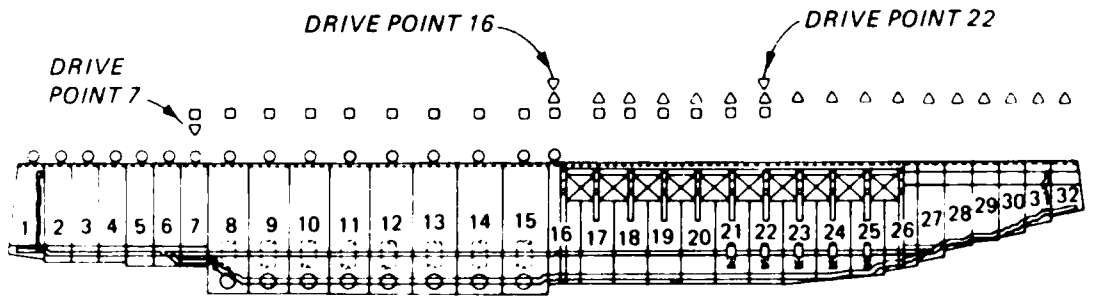

DOWNSTREAM ELEVATION

LEGEND

- ▽ DRIVE POINT
- ○ DRIVE POINT 7 CREST ACCELEROMETERS
- □ DRIVE POINT 16 CREST ACCELEROMETERS
- △ DRIVE POINT 22 CREST ACCELEROMETERS

Figure 4. Crest accelerometer locations for test 2

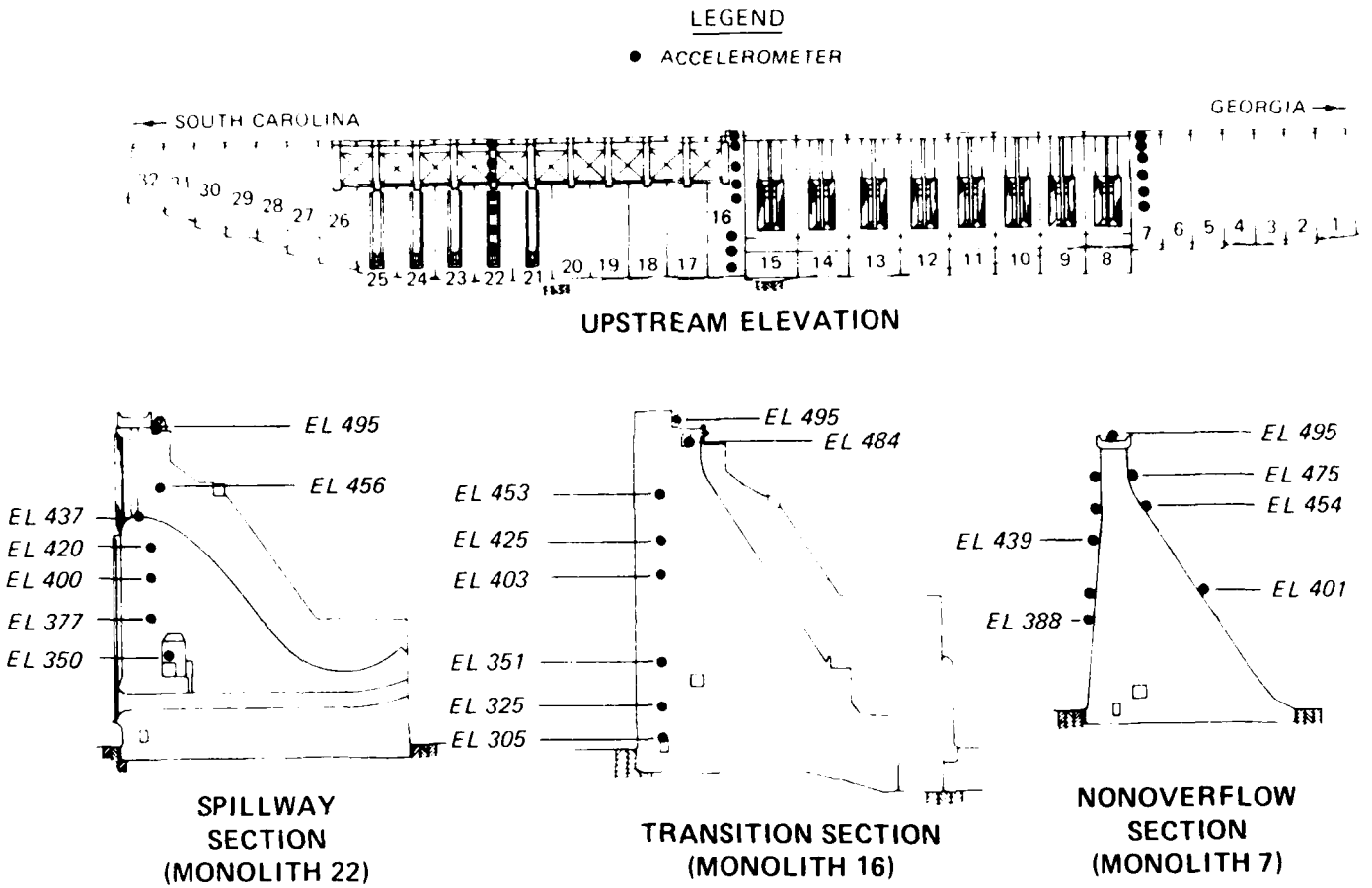

Figure 5. Cross-sectional accelerometer locations for test 1

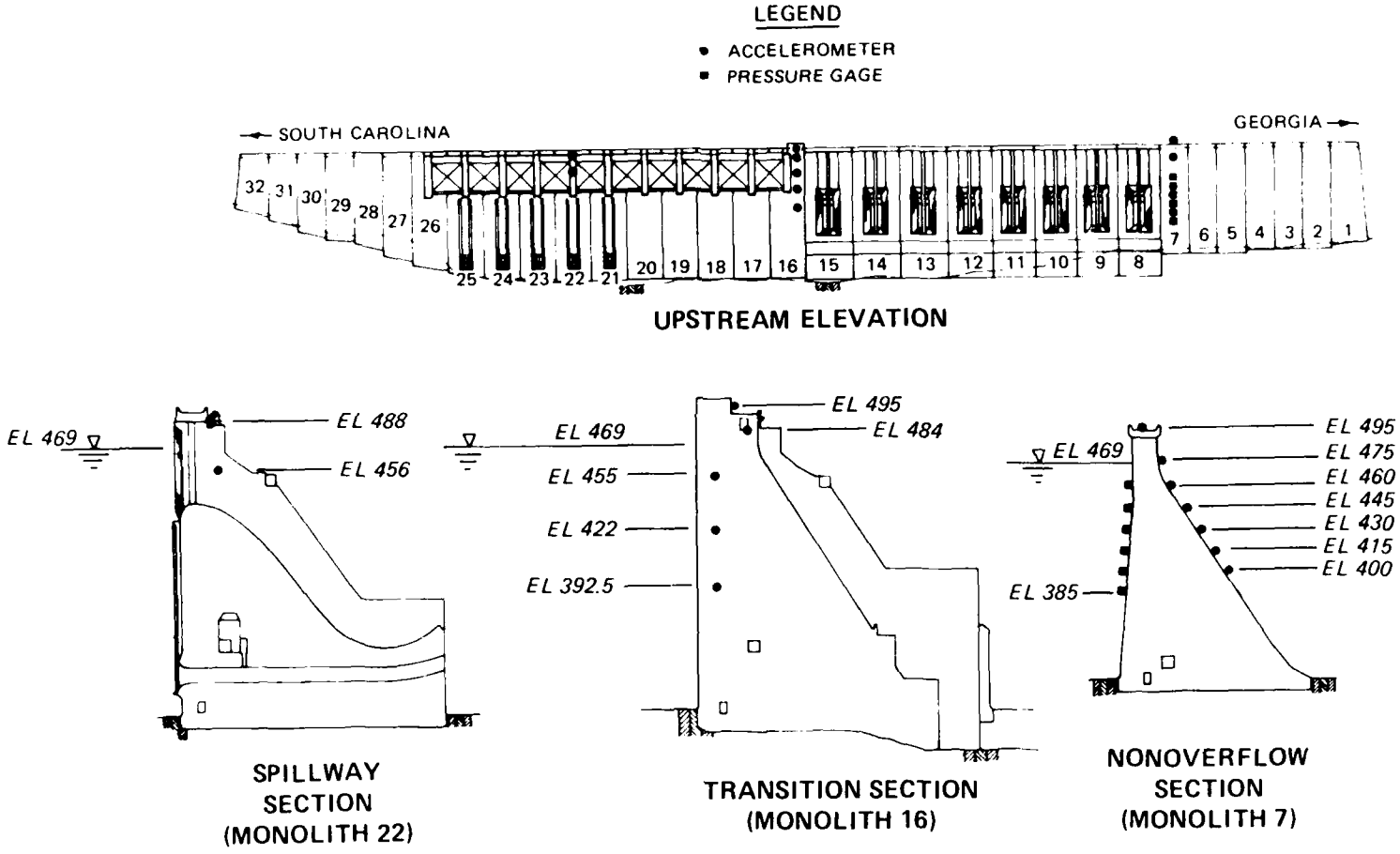

Figure 6. Cross-sectional accelerometer and pressure gage locations for test 2

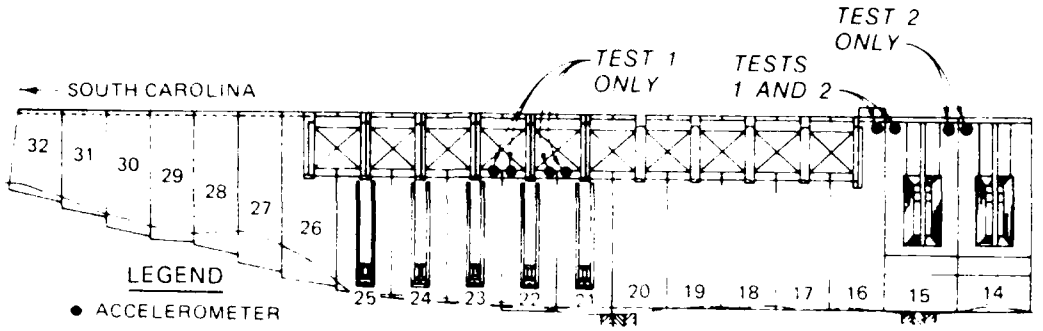

Figure 7. Relative joint motion accelerometer locations for tests 1 and 2

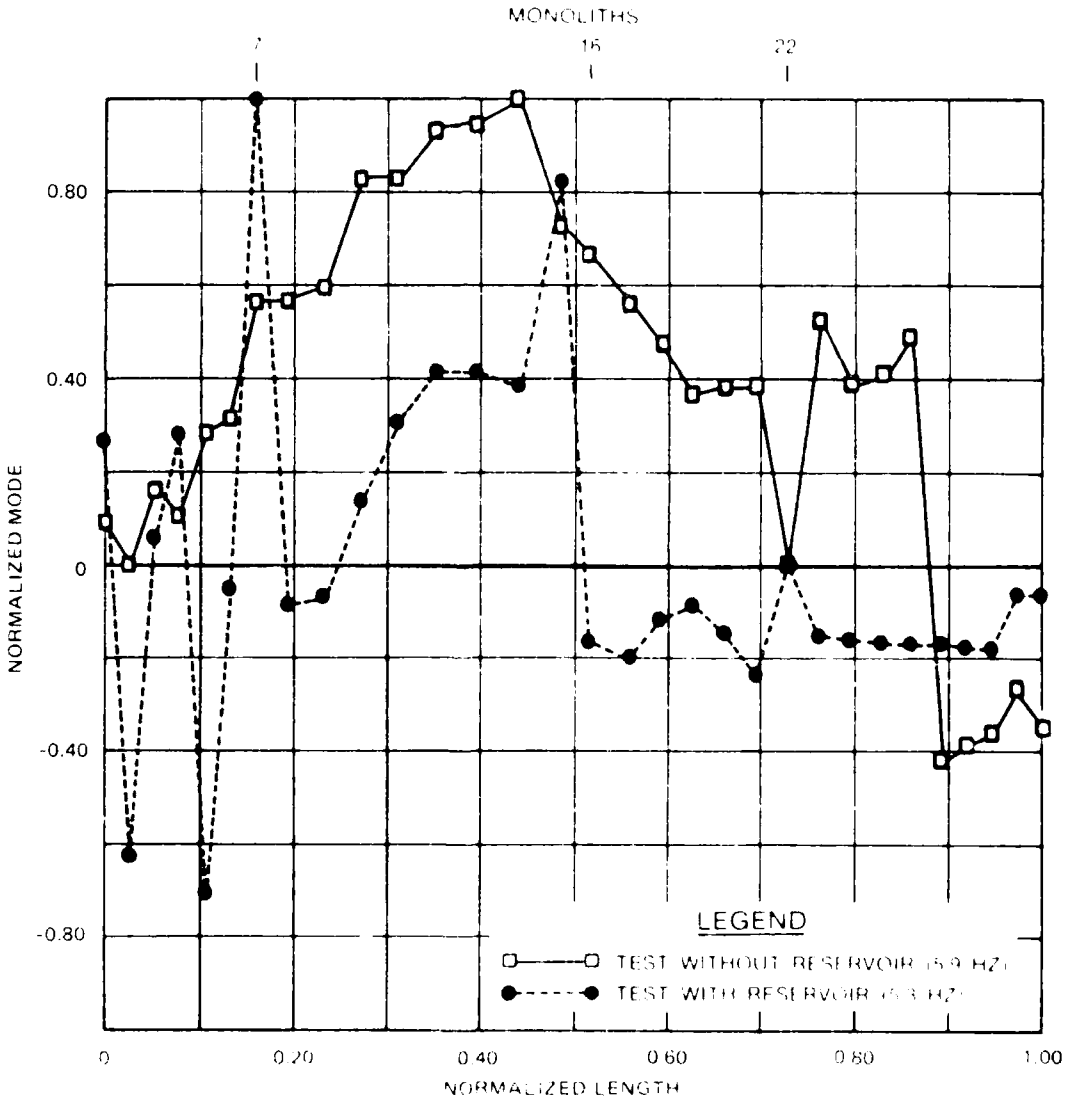

Figure 8. Experimental mode shape comparisons

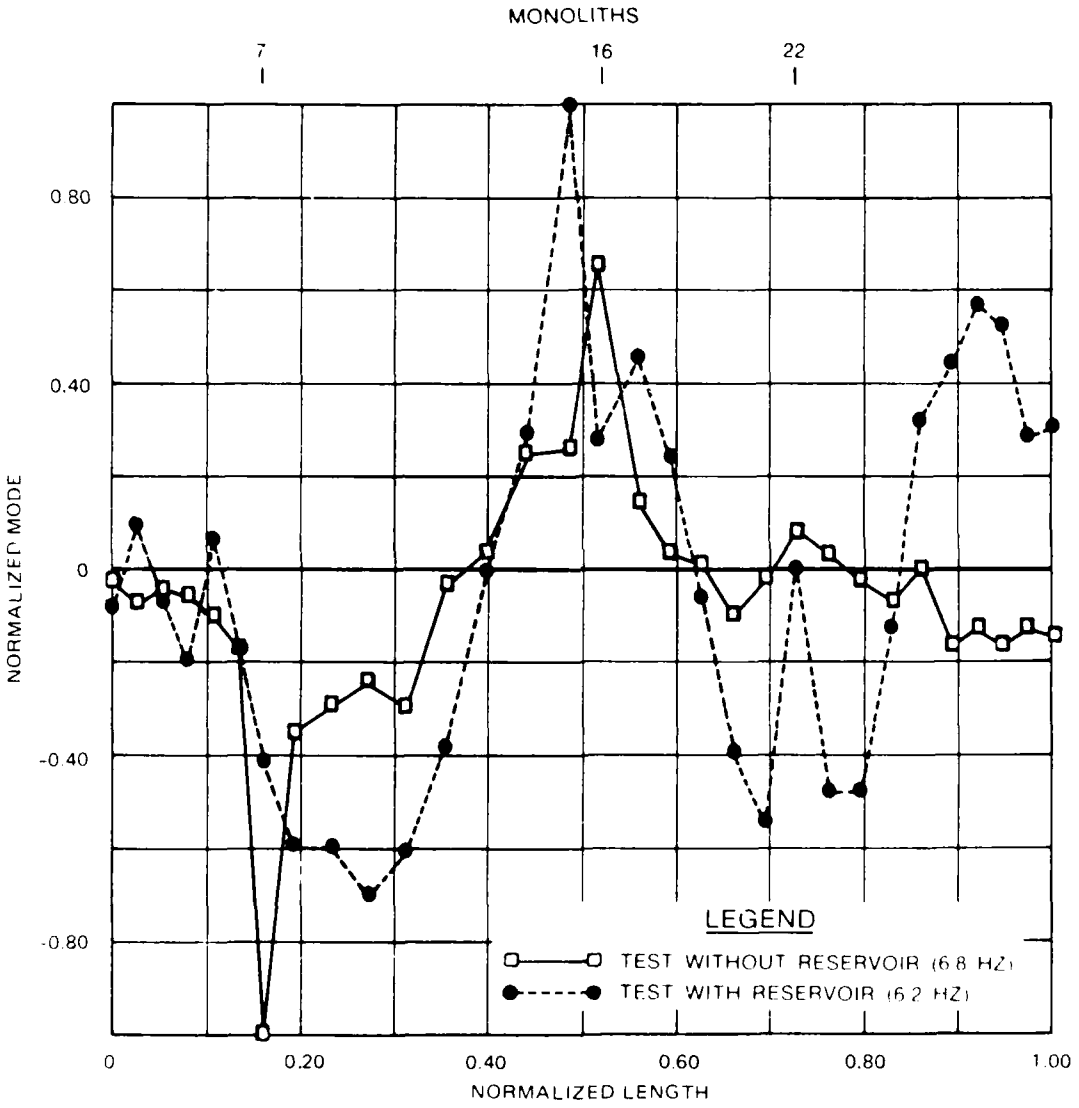

Figure 9. Experimental mode shape 2 comparisons

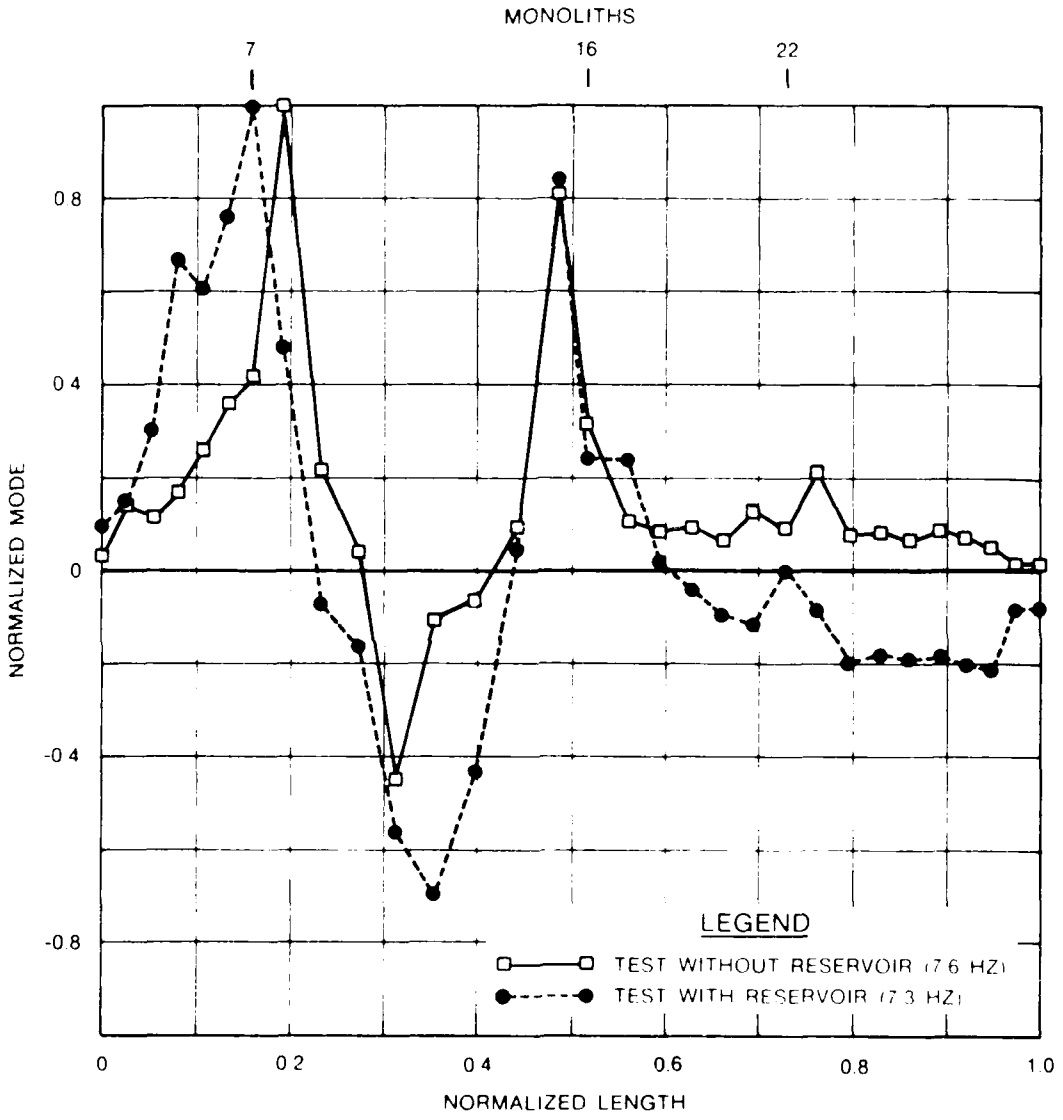

Figure 10. Experimental mode shape 3 comparisons

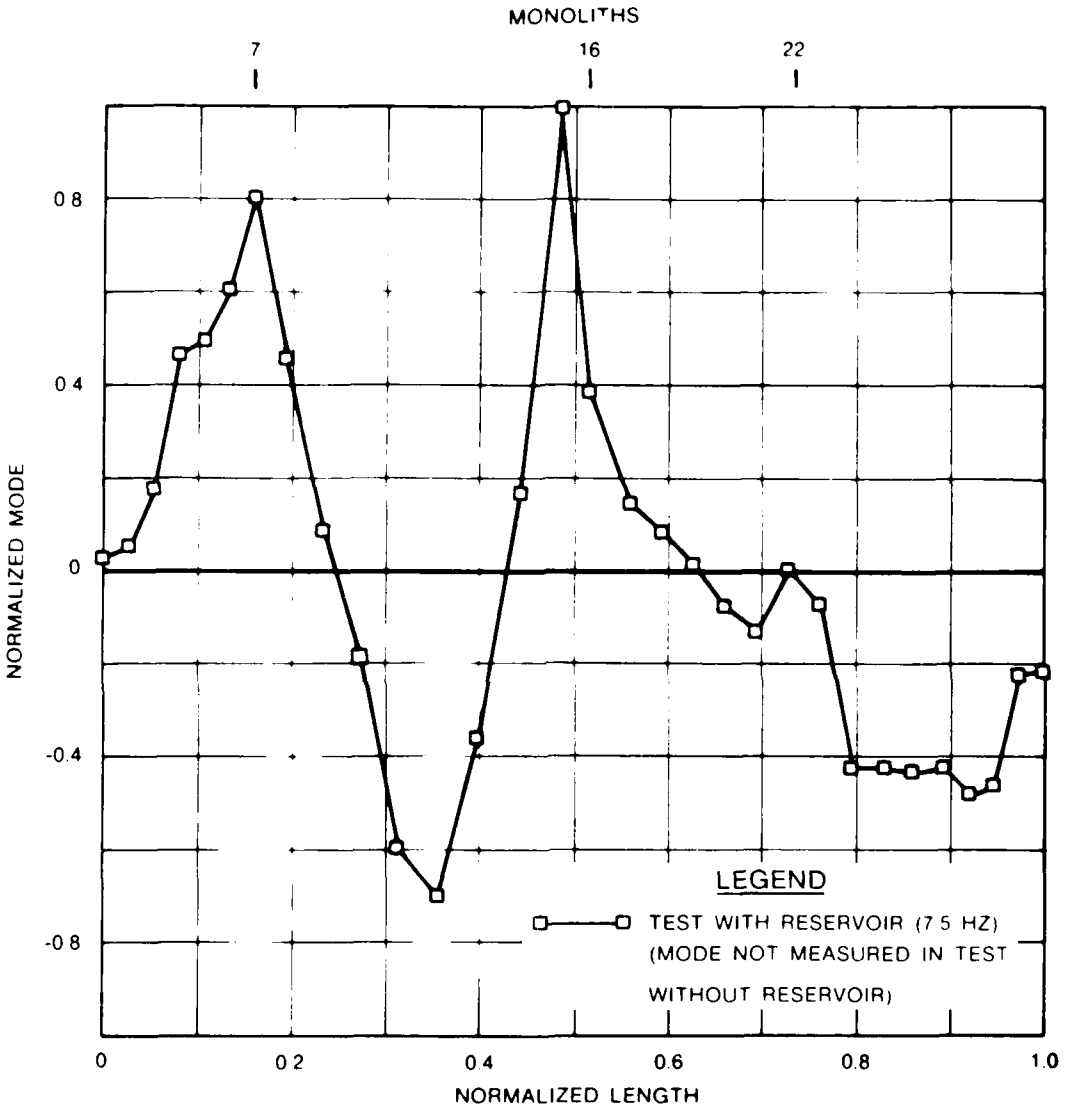

Figure 11. Experimental mode shape 4 comparisons

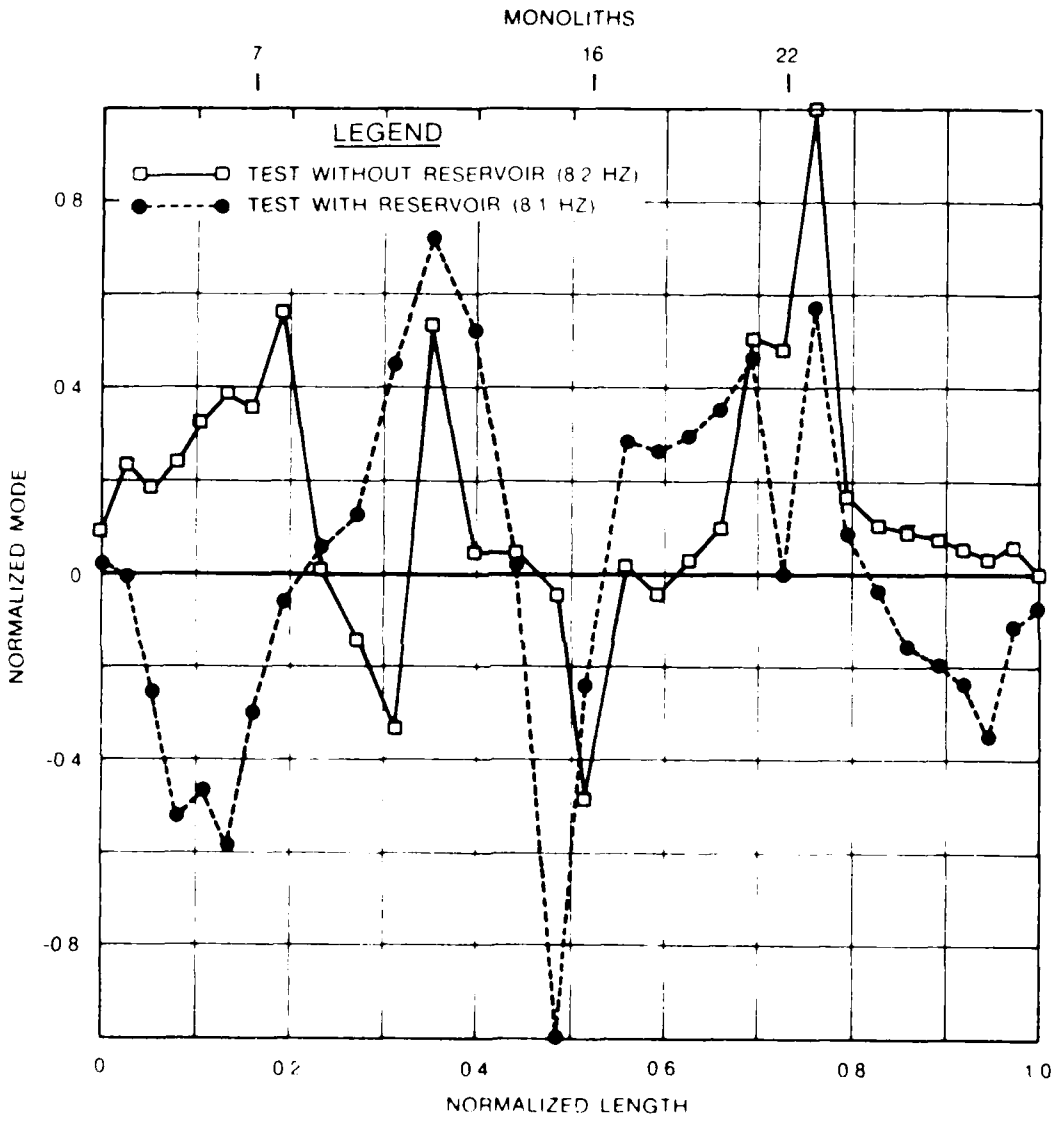

Figure 12. Experimental mode shape 5 comparisons

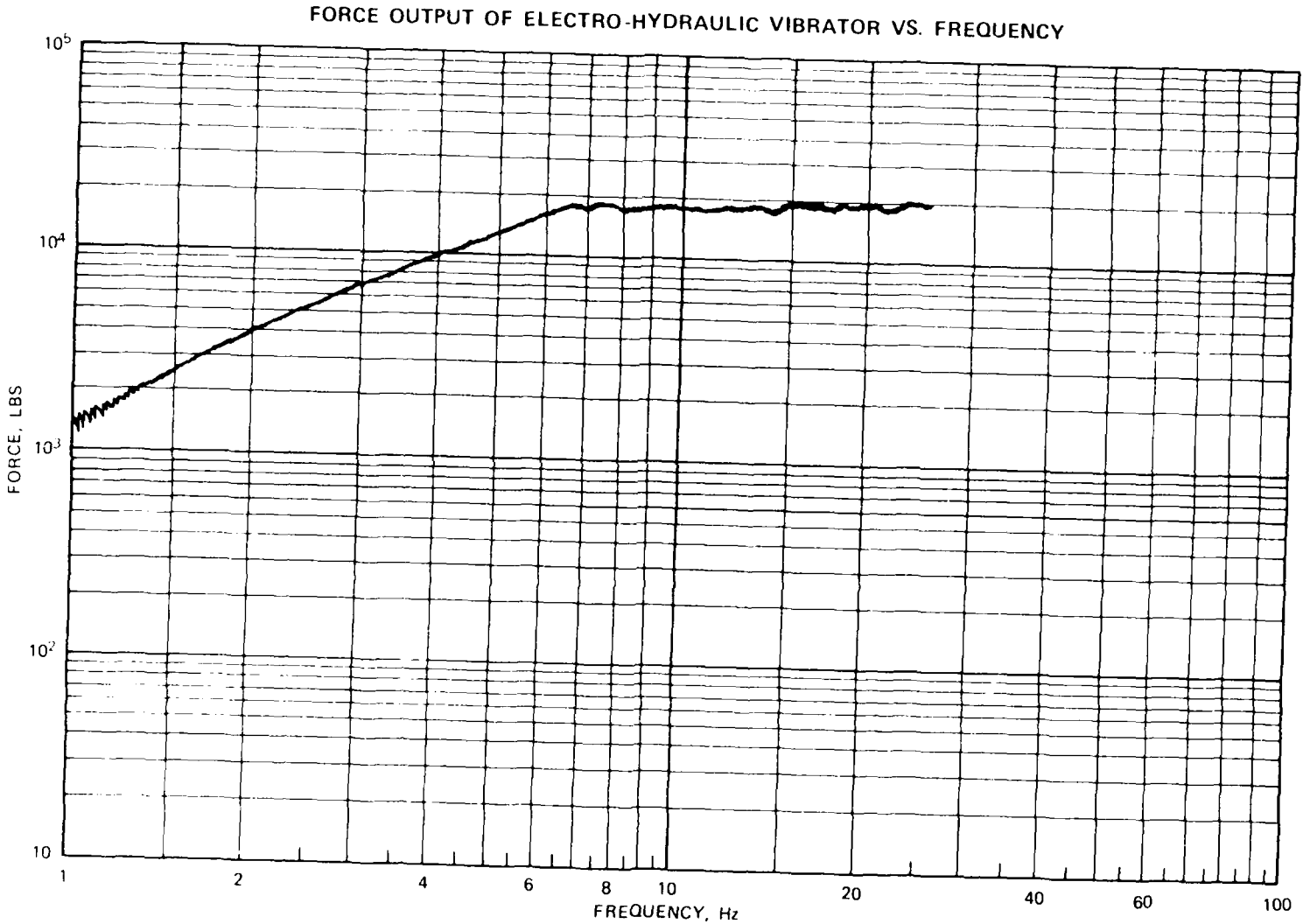

Figure 13. Typical force spectrum

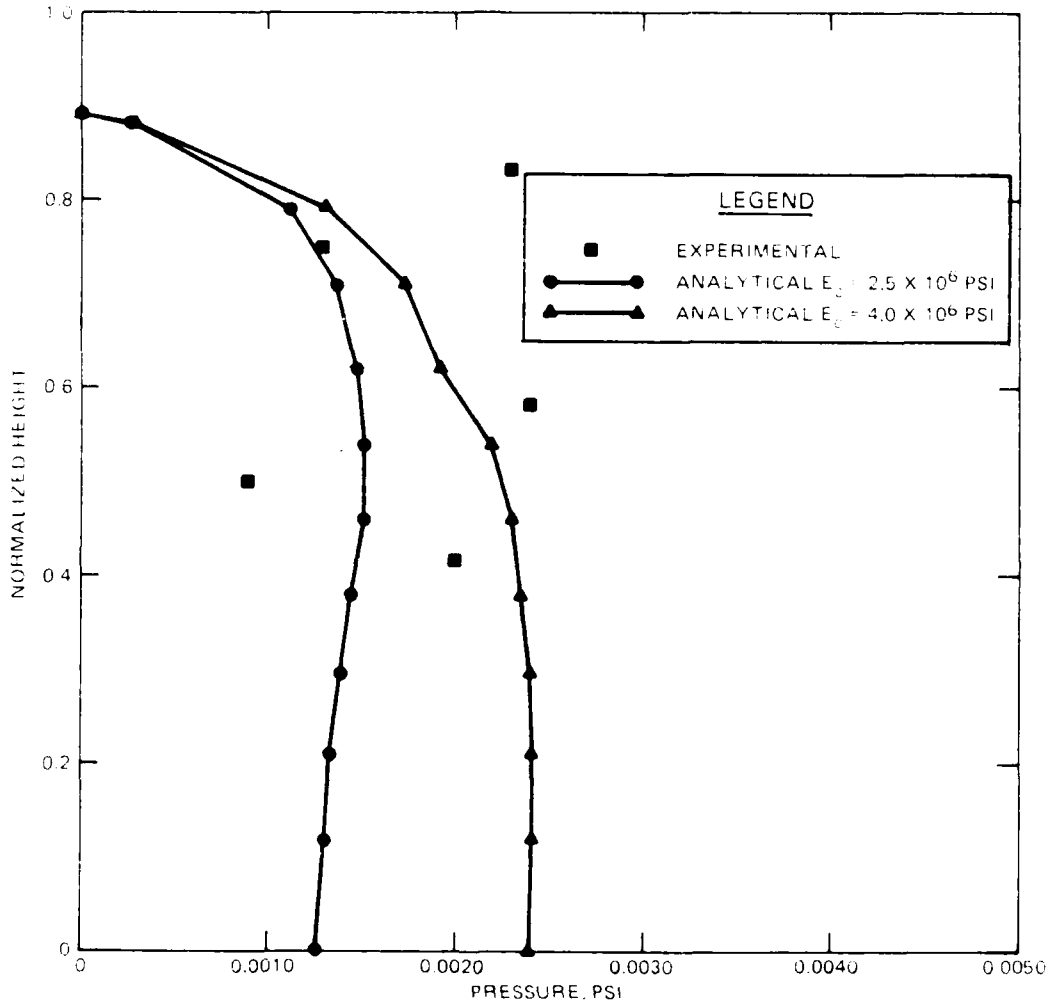

Figure 14. Comparisons of experimentally measured and theoretical hydrodynamic pressures

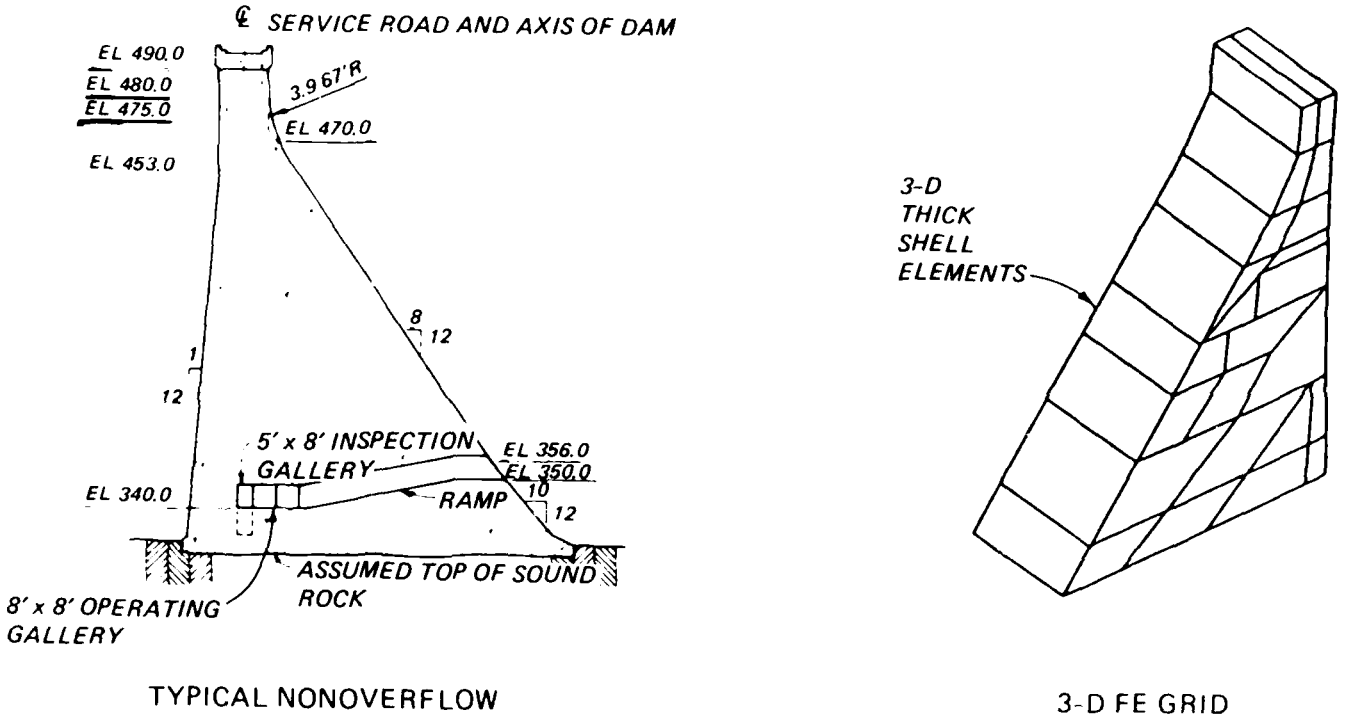

Figure 15. Isolated nonoverflow monolith

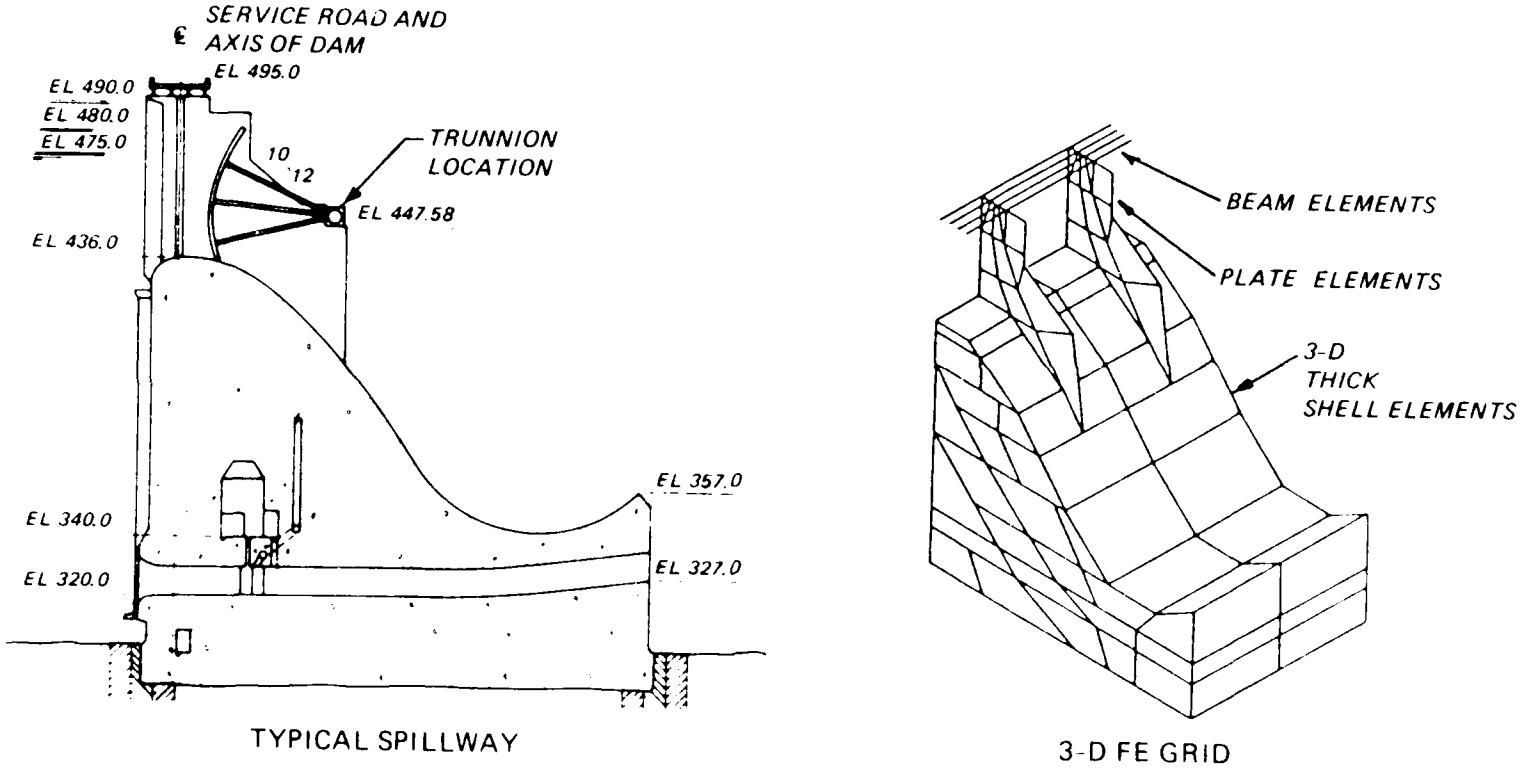

Figure 16. Isolated spillway monolith

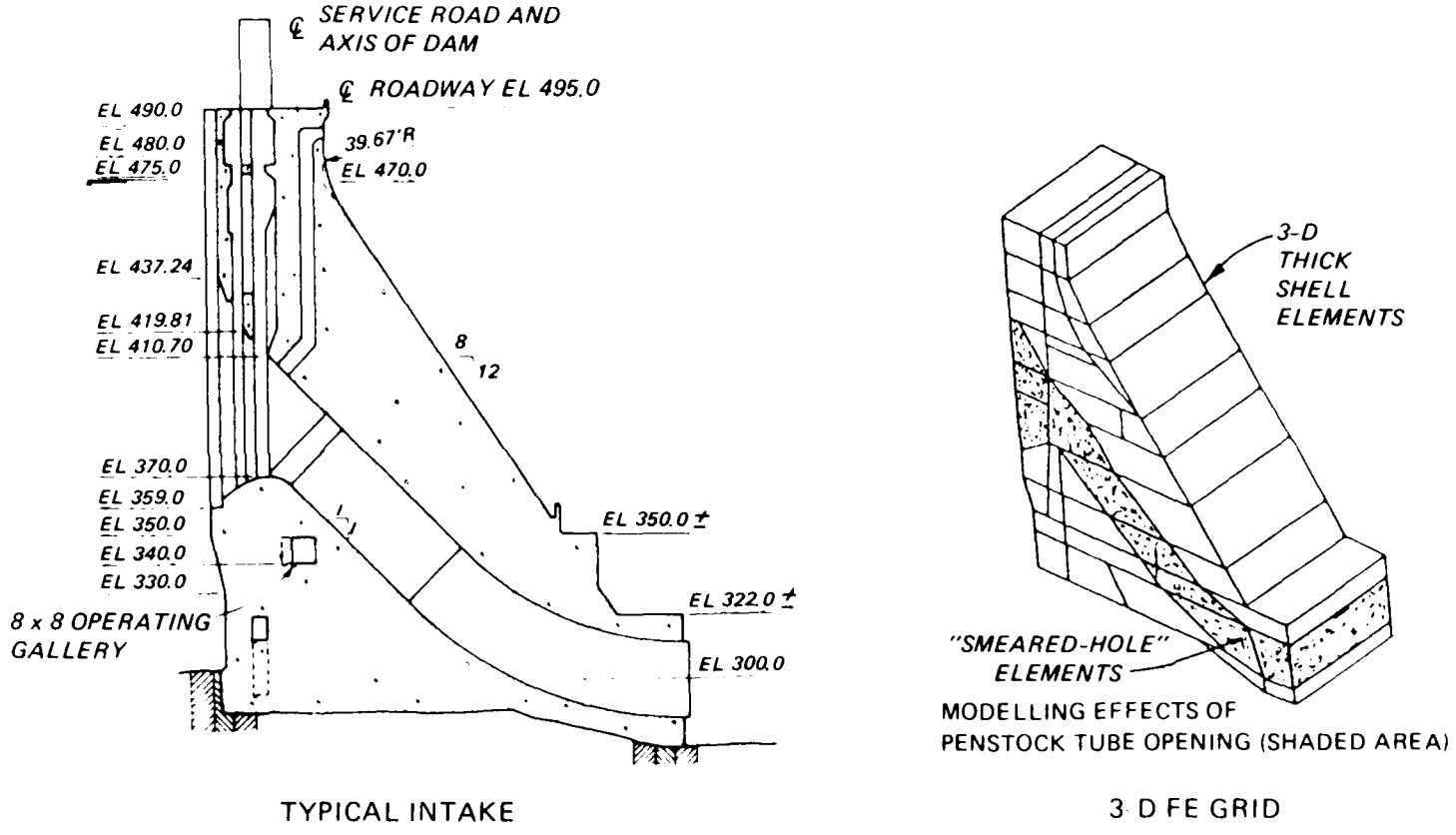

Figure 17. Isolated intake monolith

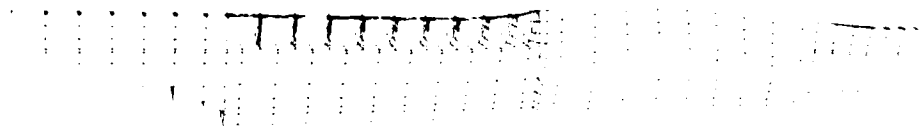

EIGENVECTOR NO. 1, 7.1 Hz (CREST MODE NO. 1)

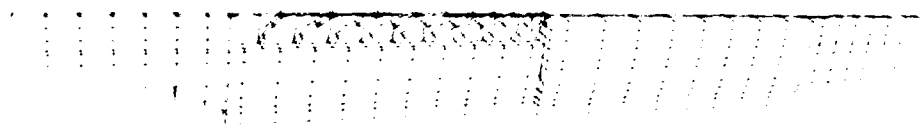

EIGENVECTOR NO. 2, 7.7 Hz

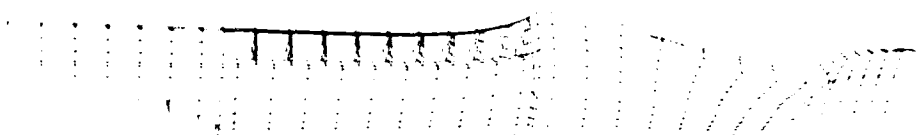

EIGENVECTOR NO. 3, 7.9 Hz (CREST MODE NO. 2)

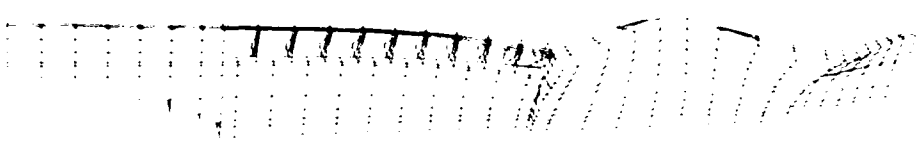

EIGENVECTOR NO. 4, 9.3 Hz (CREST MODE NO. 3)

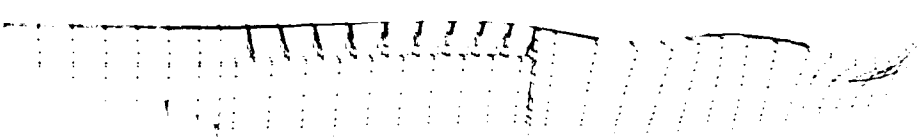

EIGENVECTOR NO. 5, 10.4 Hz (CREST MODE NO. 4)

Figure 18. Eigenvectors Nos. 1-5 from FE model without reservoir and with fixed base

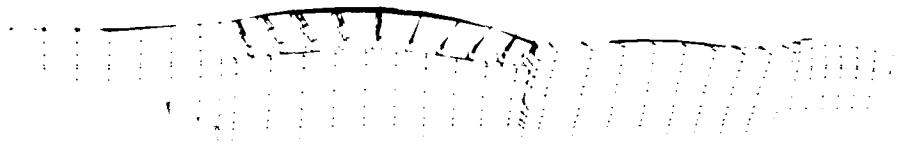

EIGENVECTOR NO. 6, 10.7 Hz (CREST MODE NO. 5)

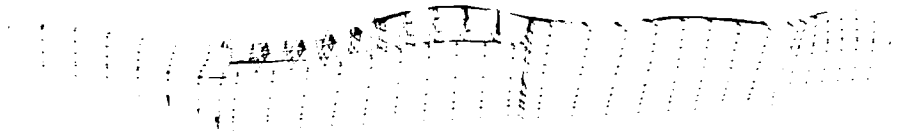

EIGENVECTOR NO. 8, 11.3 Hz (CREST MODE NO. 6)

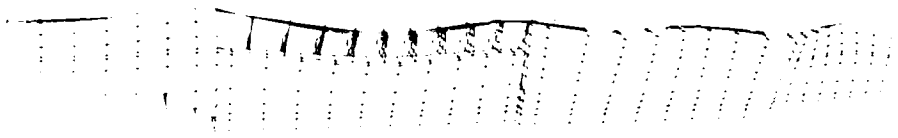

EIGENVECTOR NO. 9, 11.7 Hz (CREST MODE NO. 7)

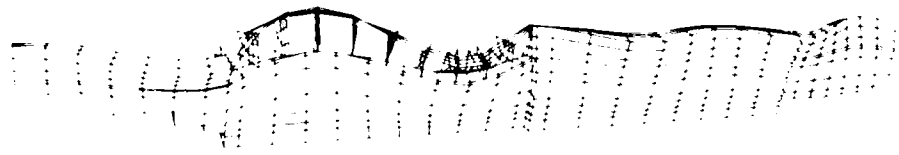

EIGENVECTOR NO. 11, 12.3 Hz (CREST MODE NO. 8)

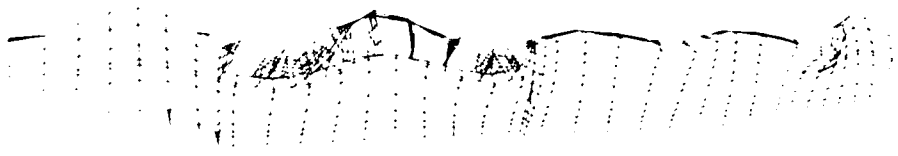

EIGENVECTOR NO. 14, 13.5 Hz (CREST MODE NO. 9)

Figure 19. Eigenvectors Nos. 6, 8, 9, 11, and 14 from FE model without reservoir and with fixed base

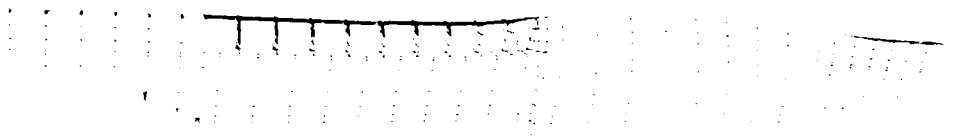

EIGENVECTOR NO. 1, 6.2 Hz (CREST MODE NO. 1)

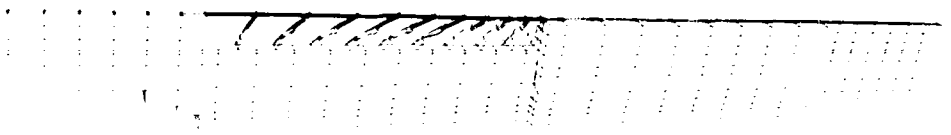

EIGENVECTOR NO. 2, 6.3 Hz

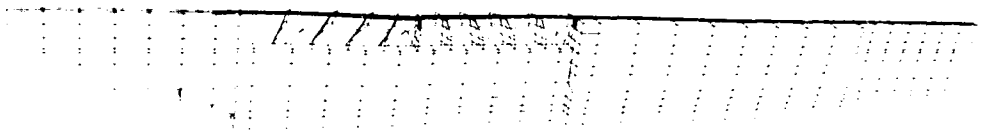

EIGENVECTOR NO. 3, 6.6 Hz

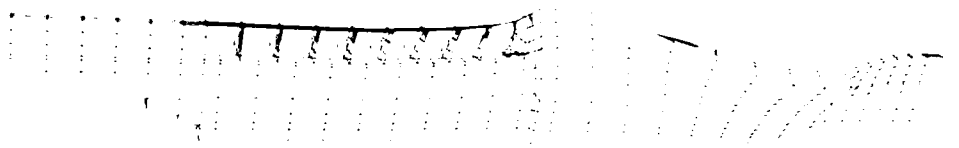

EIGENVECTOR NO. 11, 6.8 Hz (CREST MODE NO. 2)

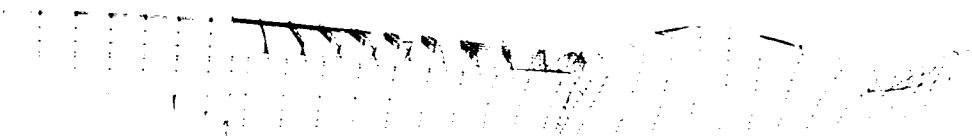

EIGENVECTOR NO. 14, 7.8 Hz (CREST MODE NO. 3)

Figure 20. Eigenvectors Nos. 1, 2, 3, 11, and 14 from FE model with reservoir and fixed base

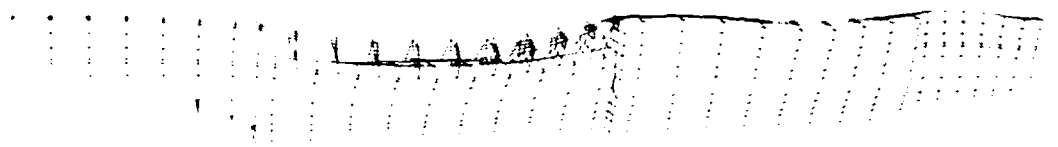

EIGENVECTOR NO. 16, 8.2 Hz (CREST MODE NO. 4)

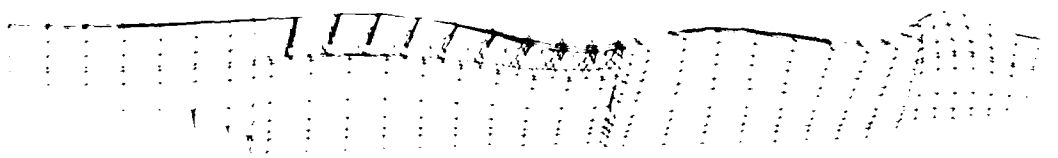

EIGENVECTOR NO. 17, 8.7 Hz (CREST MODE NO. 5)

EIGENVECTOR NO. 18, 9.1 Hz (CREST MODE NO. 6)

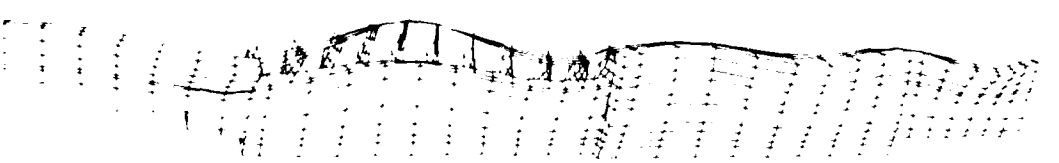

EIGENVECTOR NO. 19, 9.7 Hz (CREST MODE NO. 7)

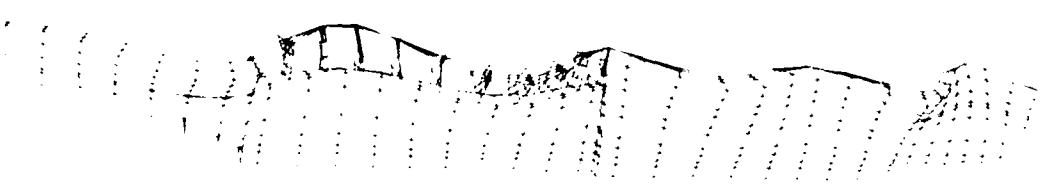

EIGENVECTOR NO. 20, 10.0 Hz (CREST MODE NO. 8)

Figure 21. Eigenvectors Nos. 16-20 from FE model with reservoir and fixed base

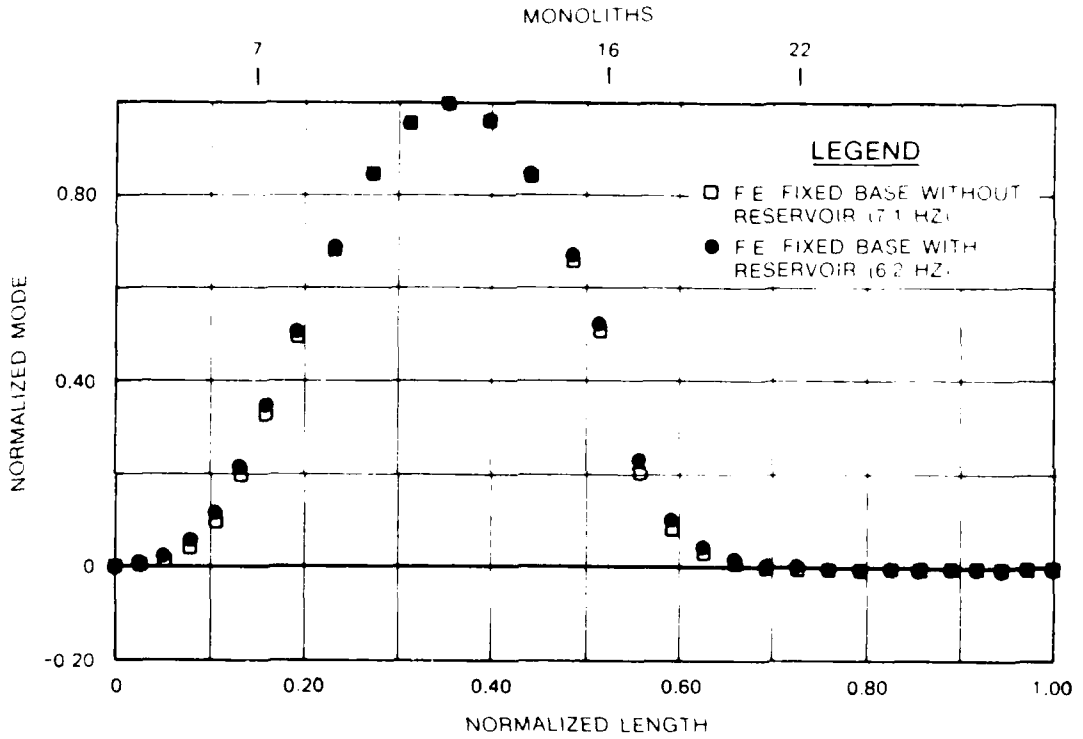

Figure 22. FE fixed base model mode shape 1 comparisons

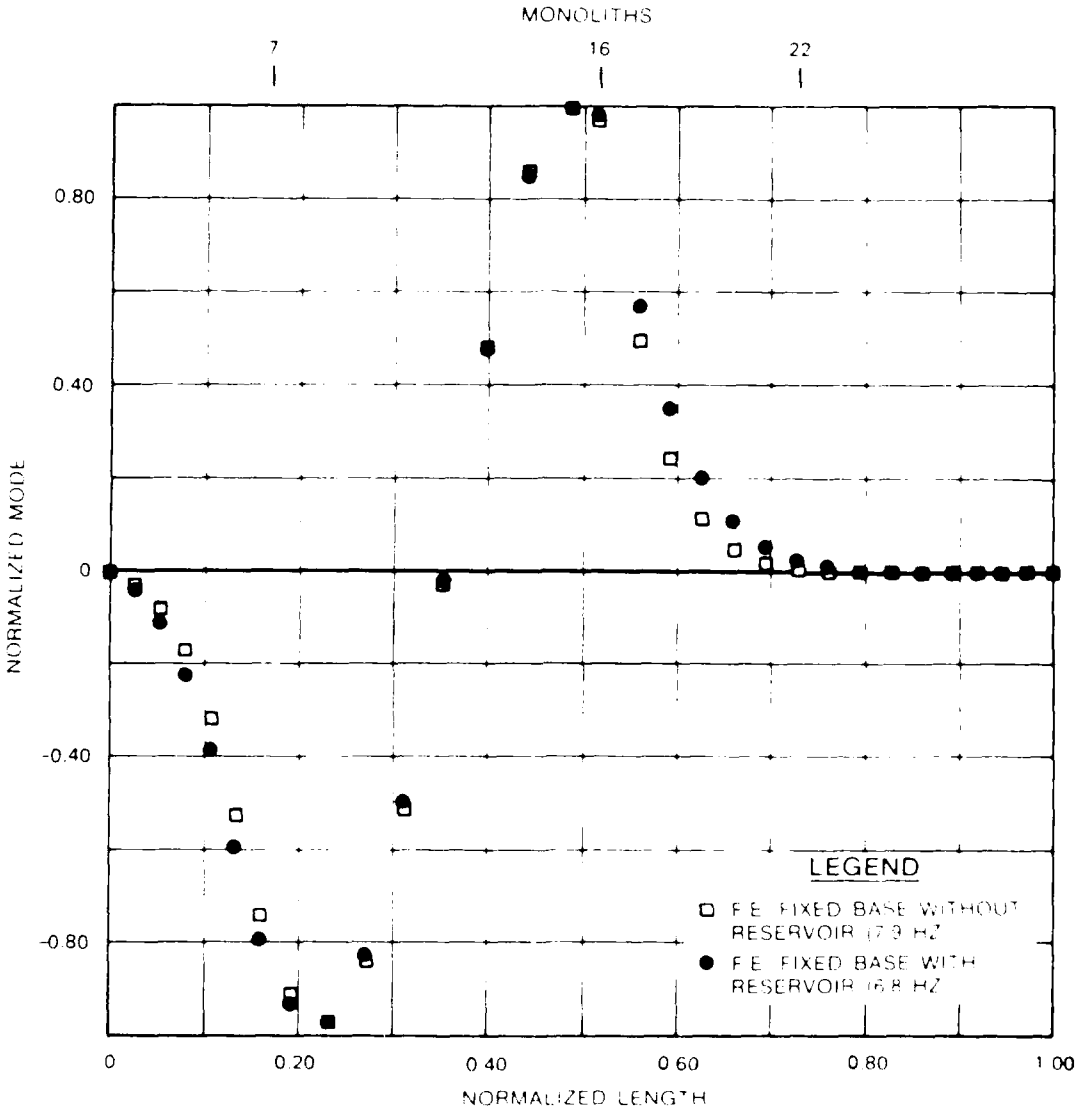

Figure 23. FE fixed base model mode shape 2 comparisons

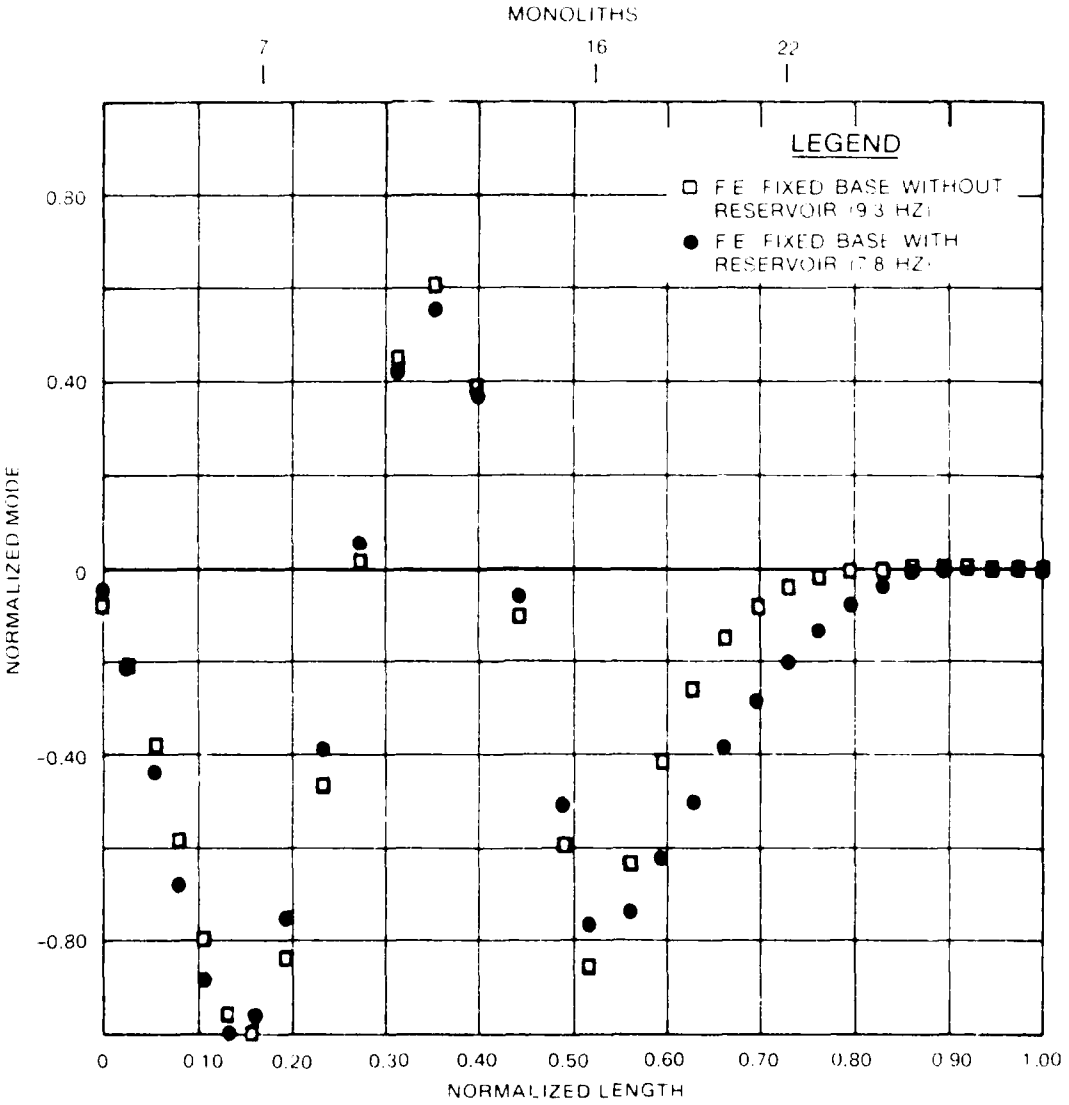

Figure 24. FE fixed base model mode shape 3 comparisons

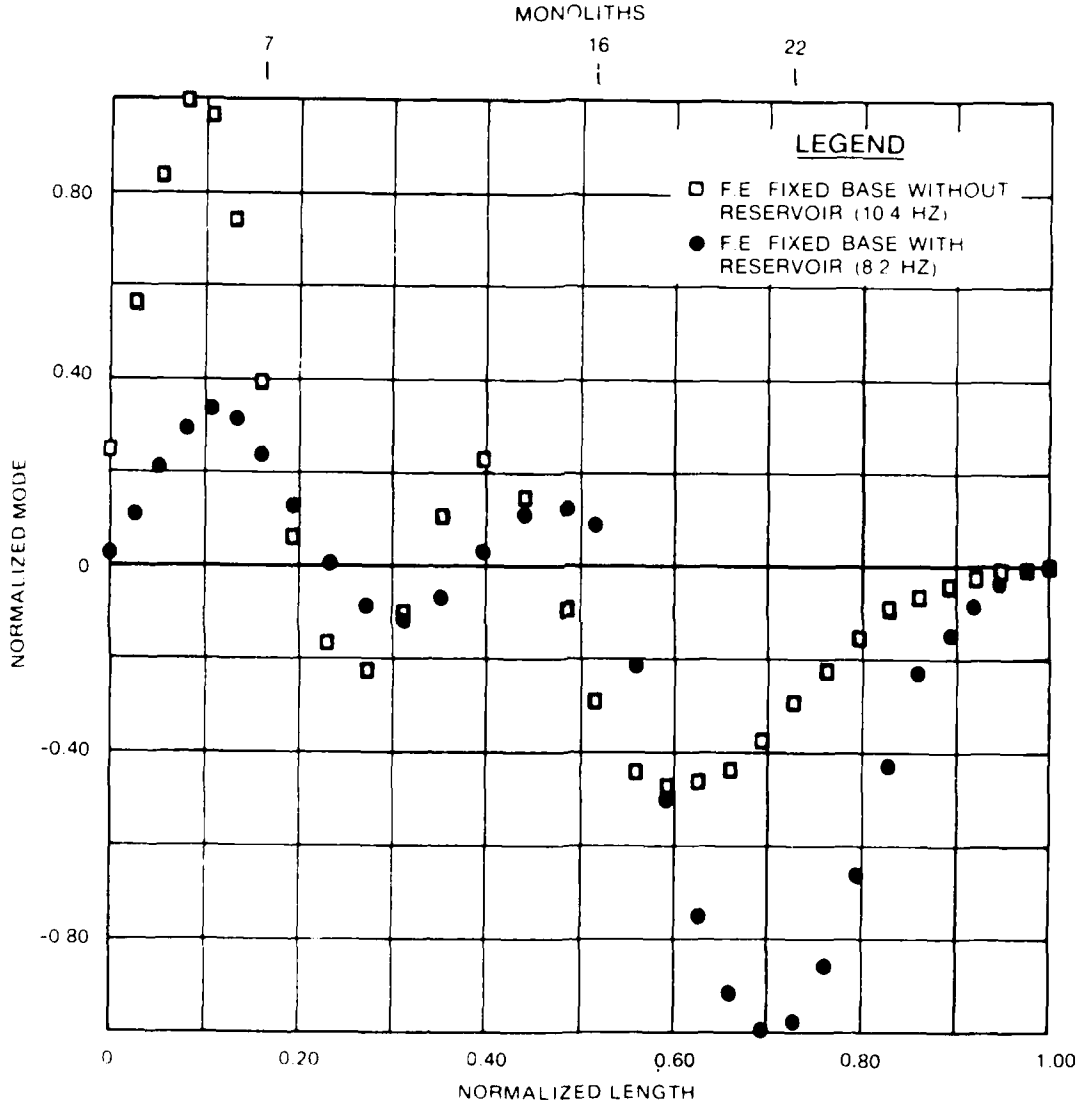

Figure 25. FE fixed base model mode shape 4 comparisons

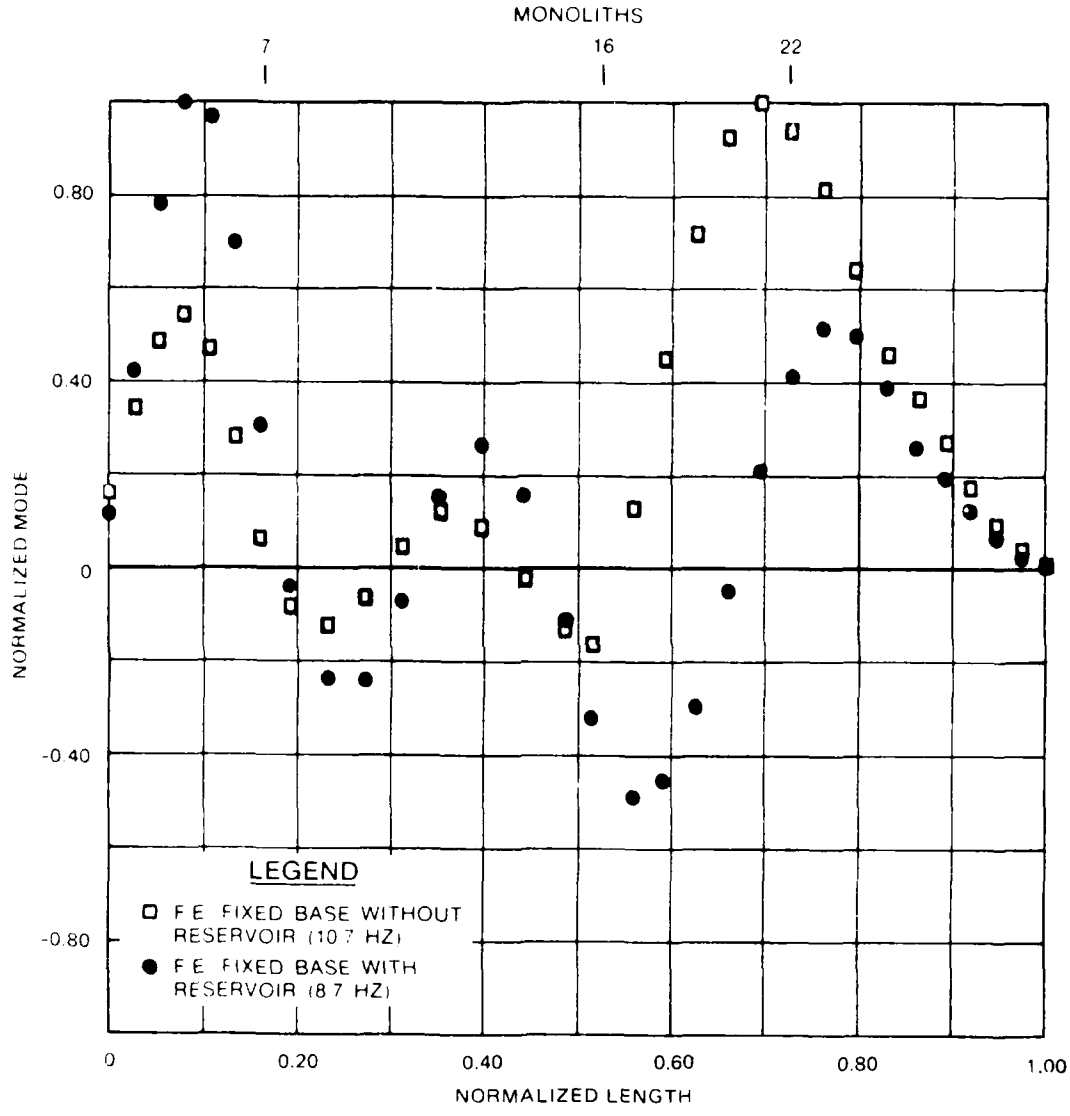

Figure 26. FE fixed base model mode shape 5 comparisons

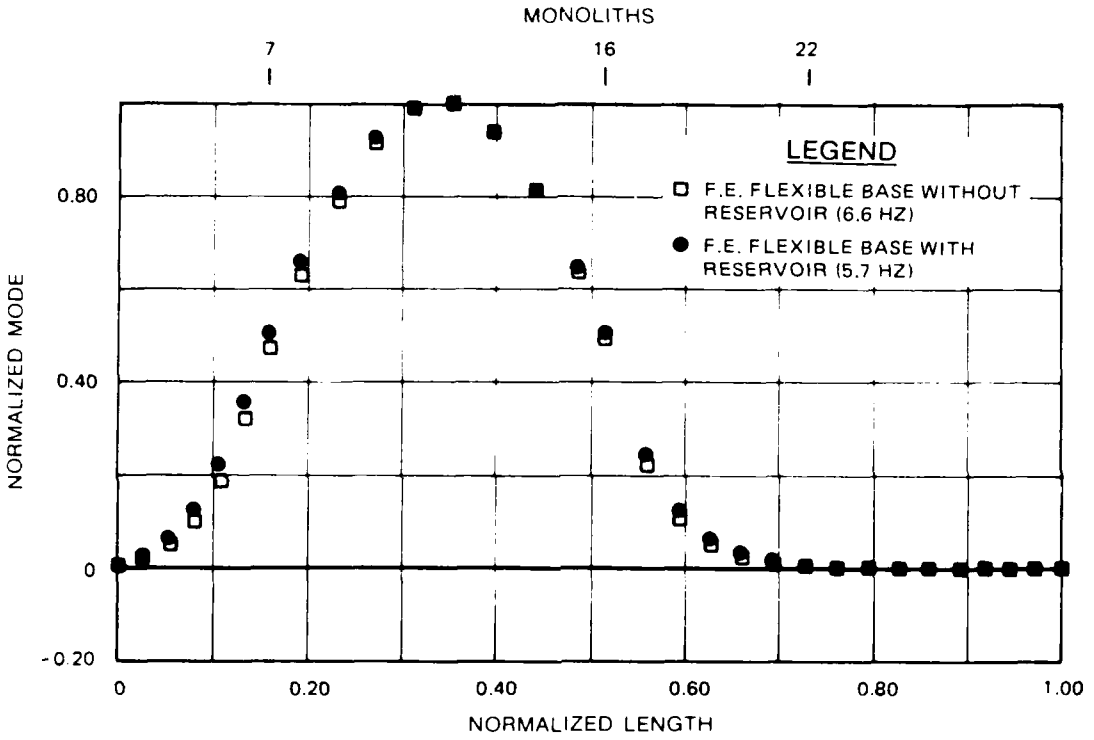

Figure 27. FE flexible base model mode shape 1 comparisons

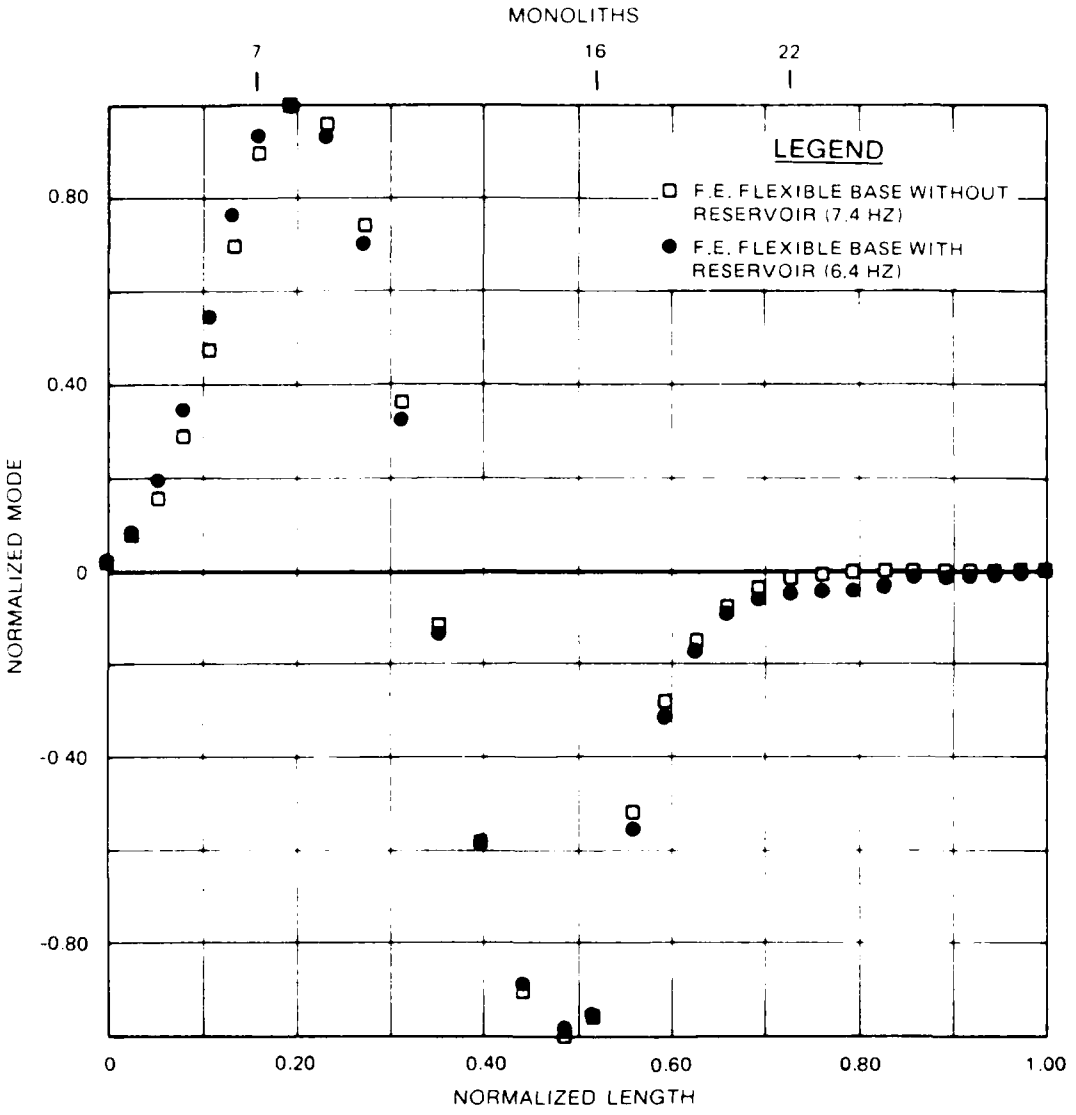

Figure 28. FE flexible base model mode shape 2 comparisons

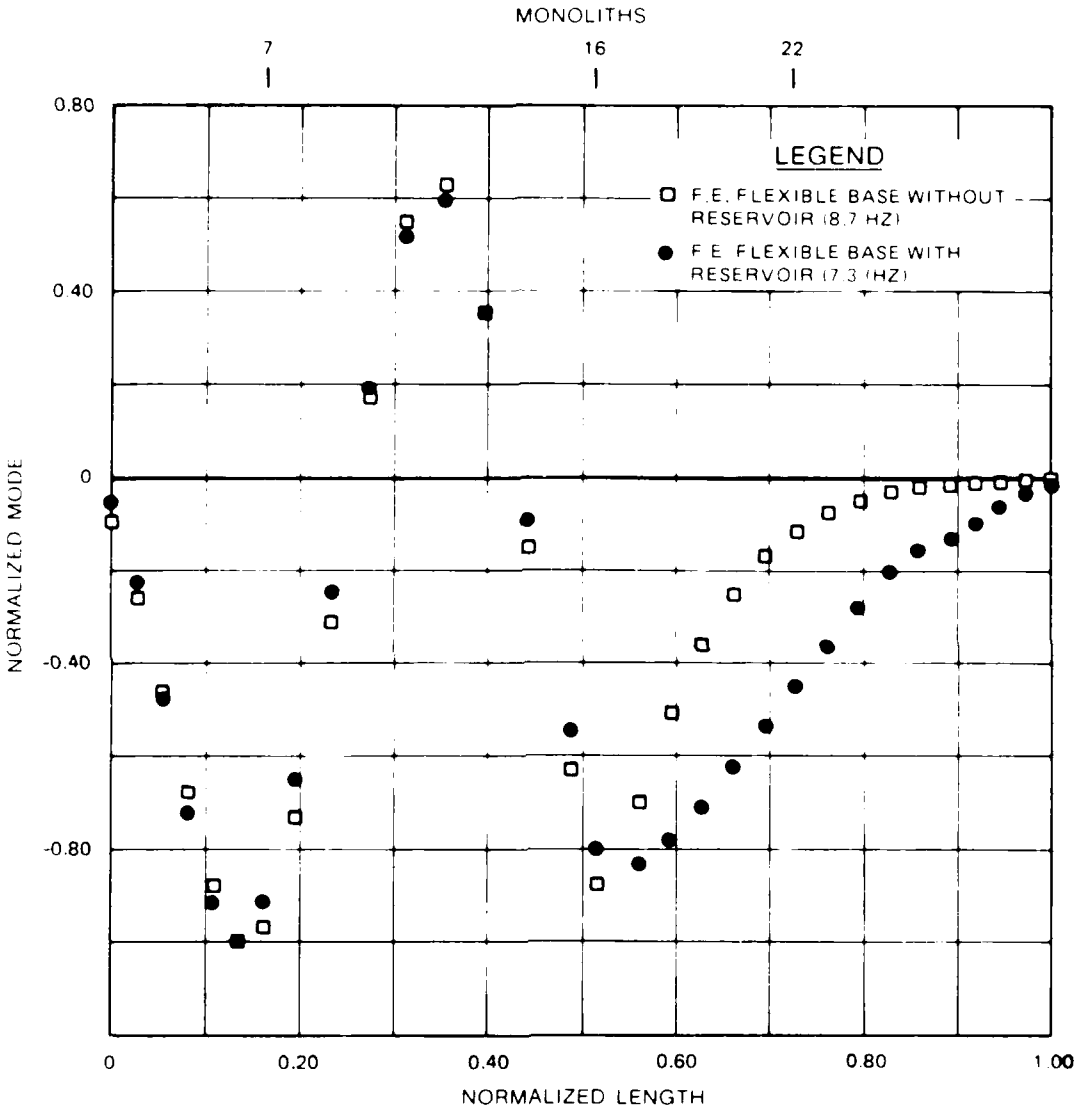

Figure 29. FE flexible base model mode shape 3 comparisons

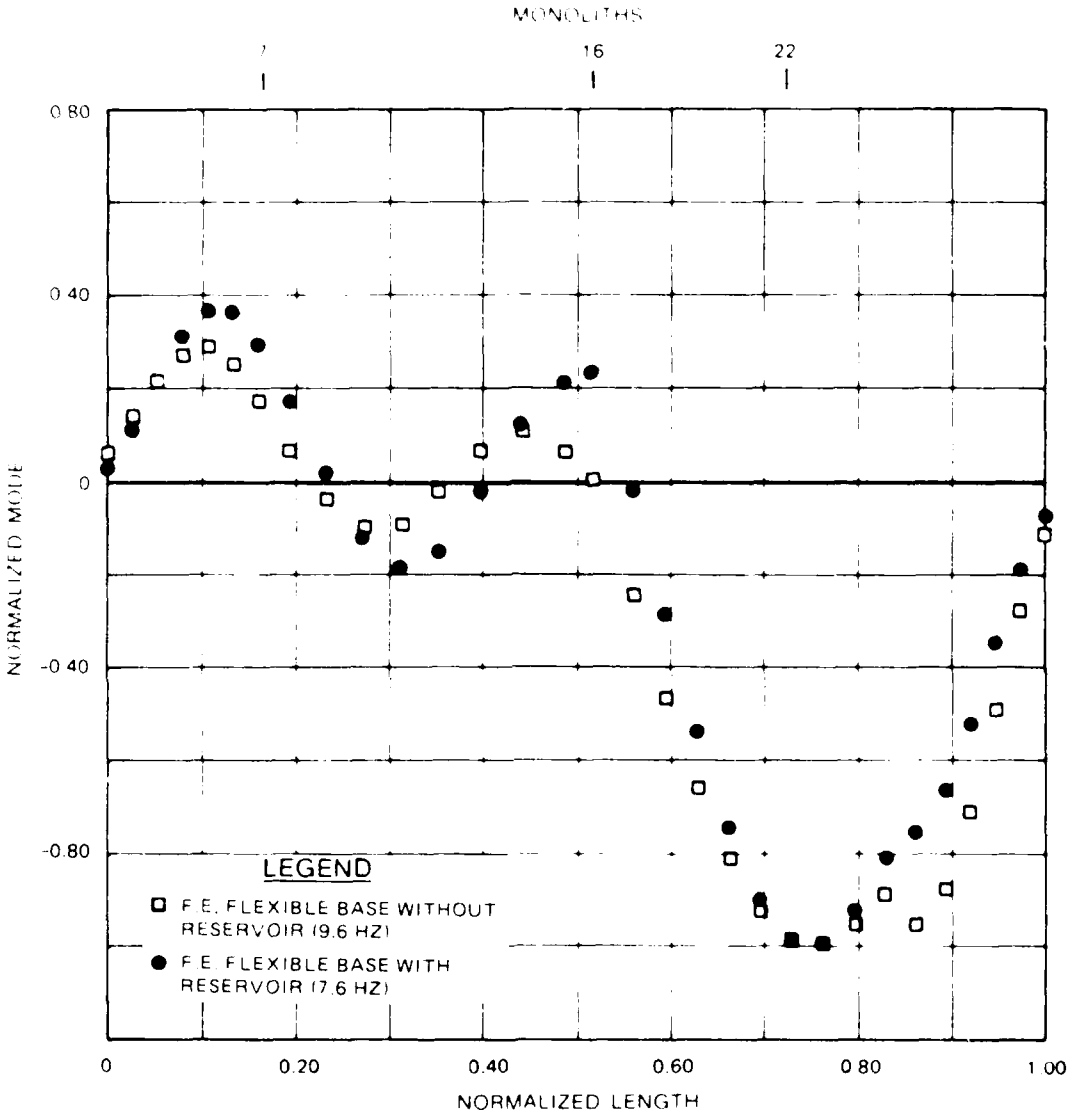

Figure 30. FE flexible base model mode shape 4 comparisons

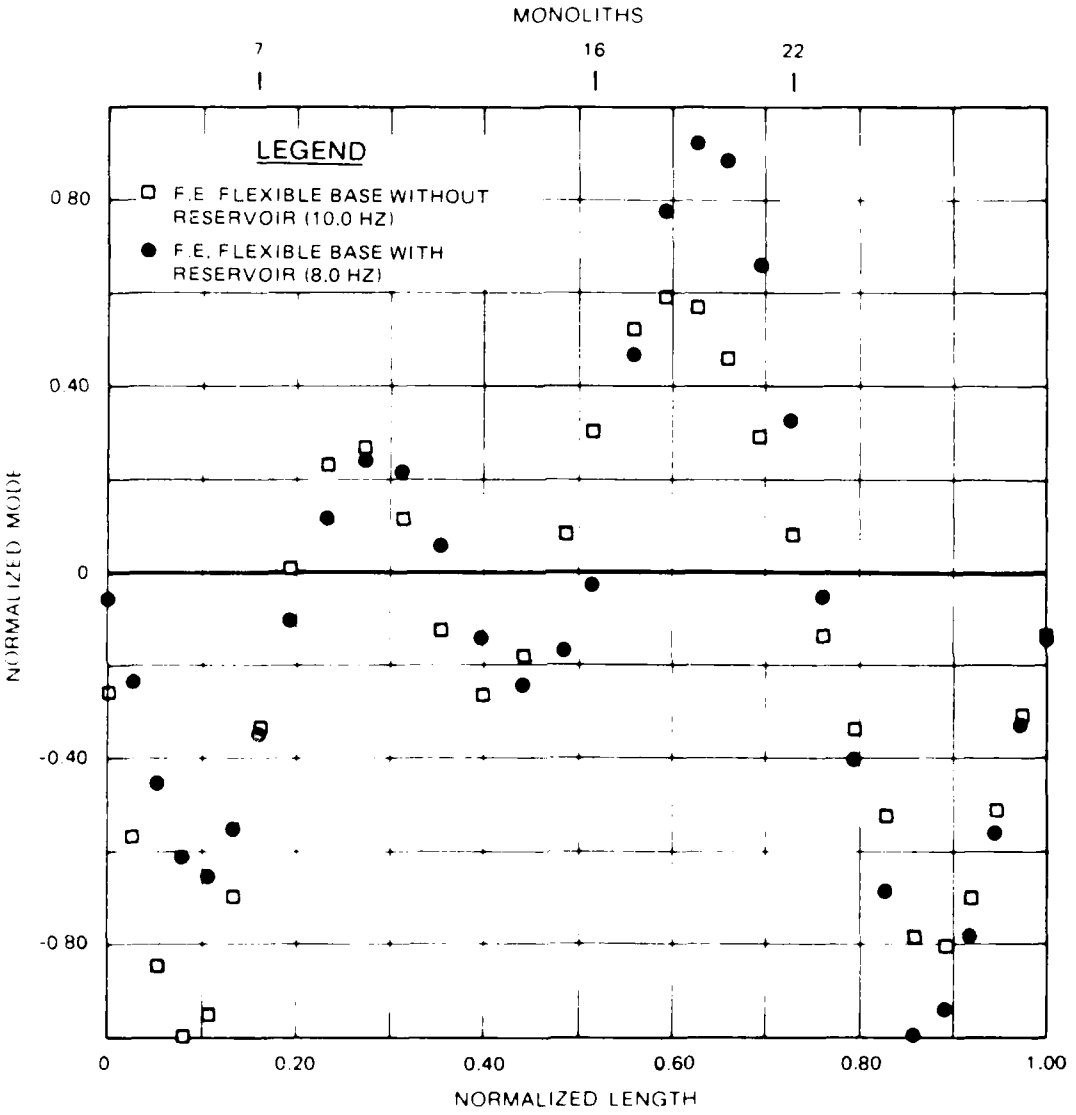

Figure 31. FE flexible base model mode shape 5 comparisons

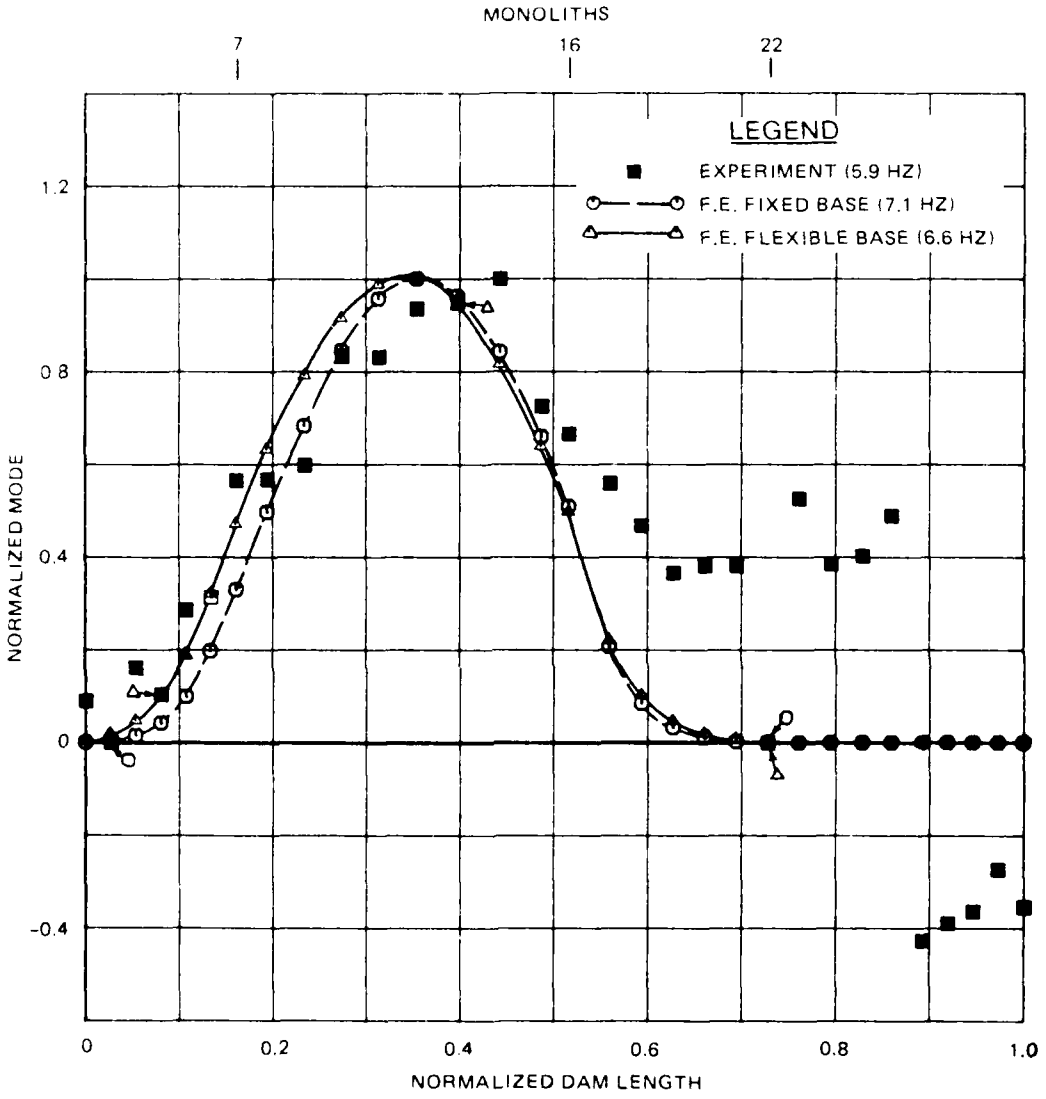

Figure 32. Analytical and experimental crest mode shape 1 comparisons for dam without reservoir

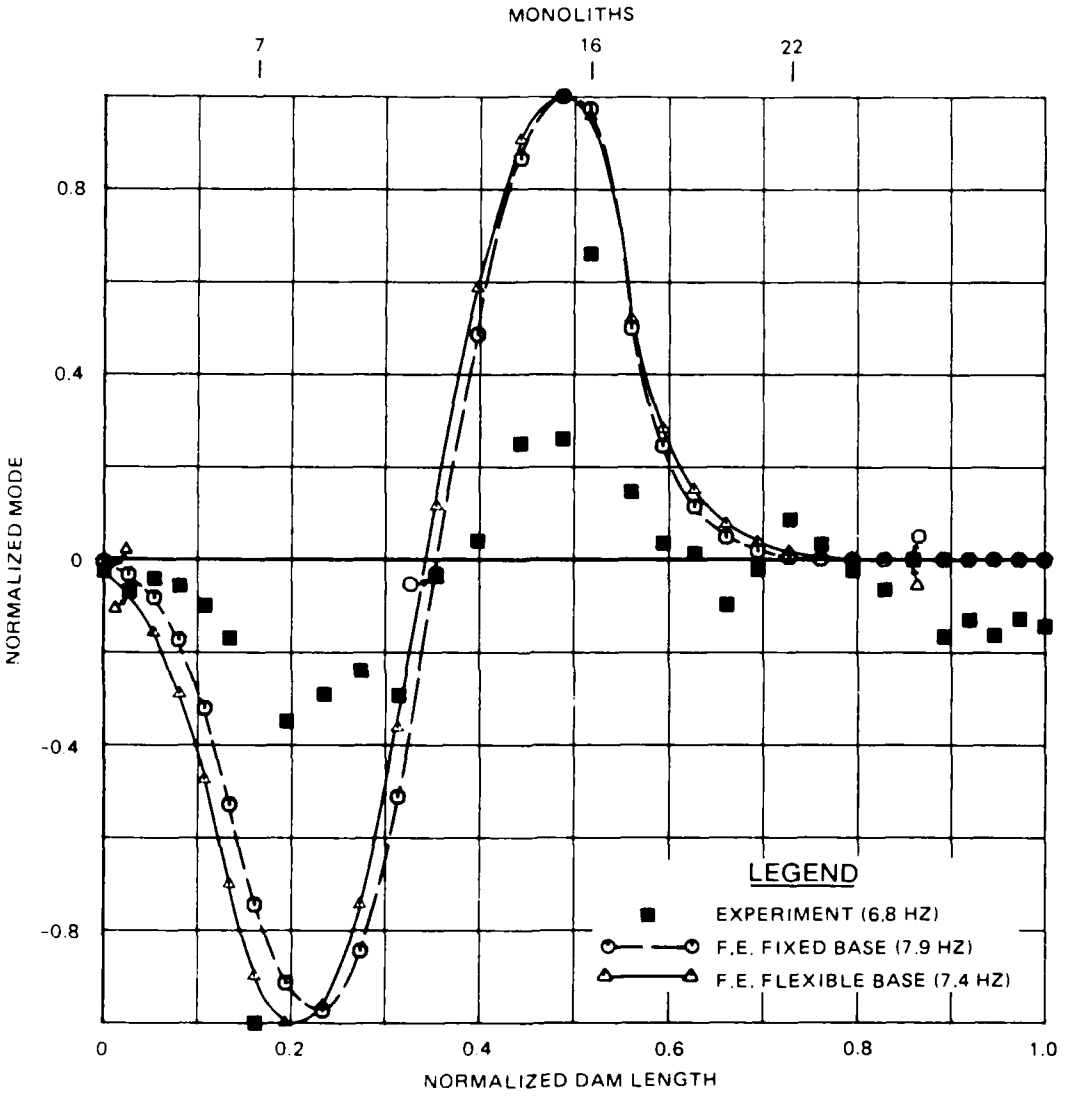

Figure 33. Analytical and experimental crest mode shape 2 comparisons for dam without reservoir

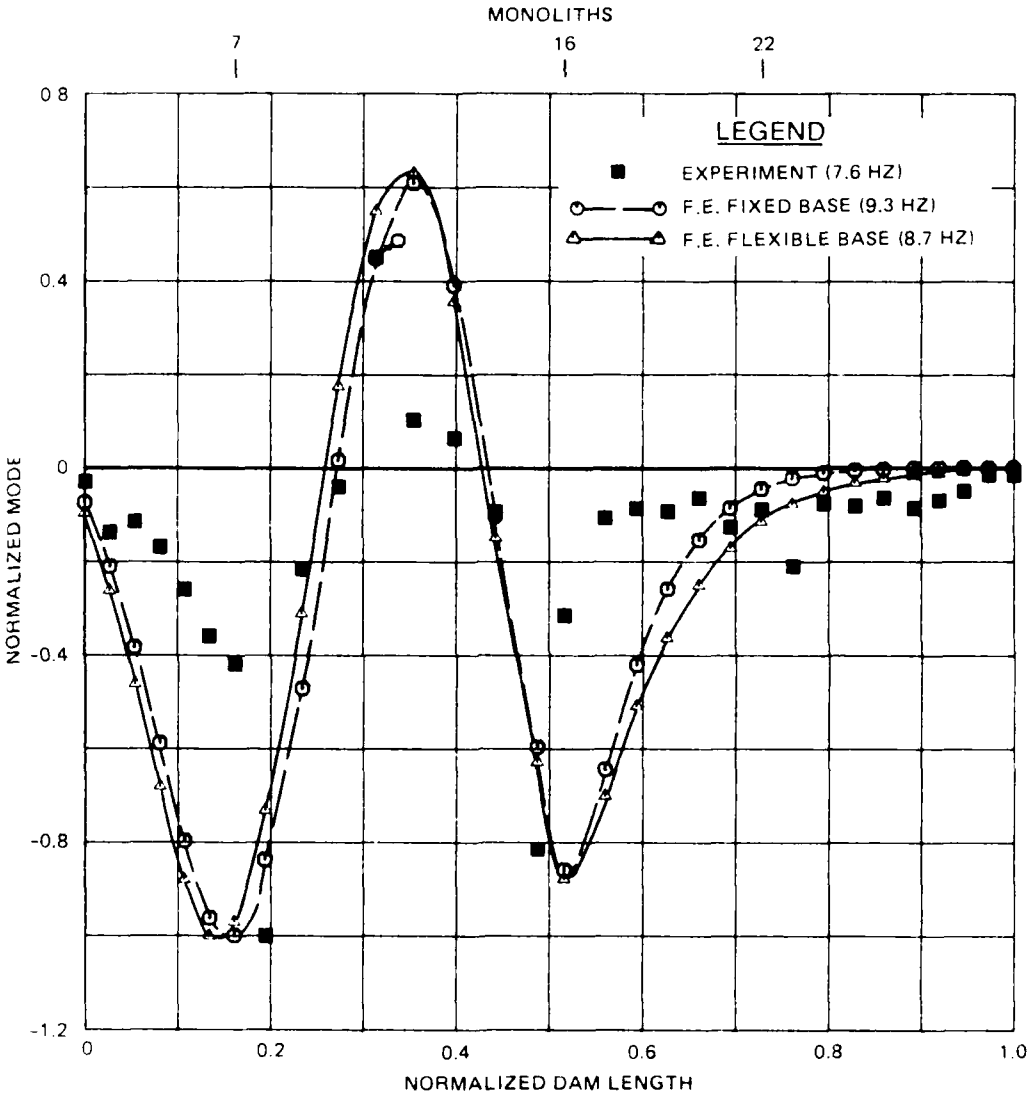

Figure 34. Analytical and experimental crest mode shape 3 comparisons for dam without reservoir

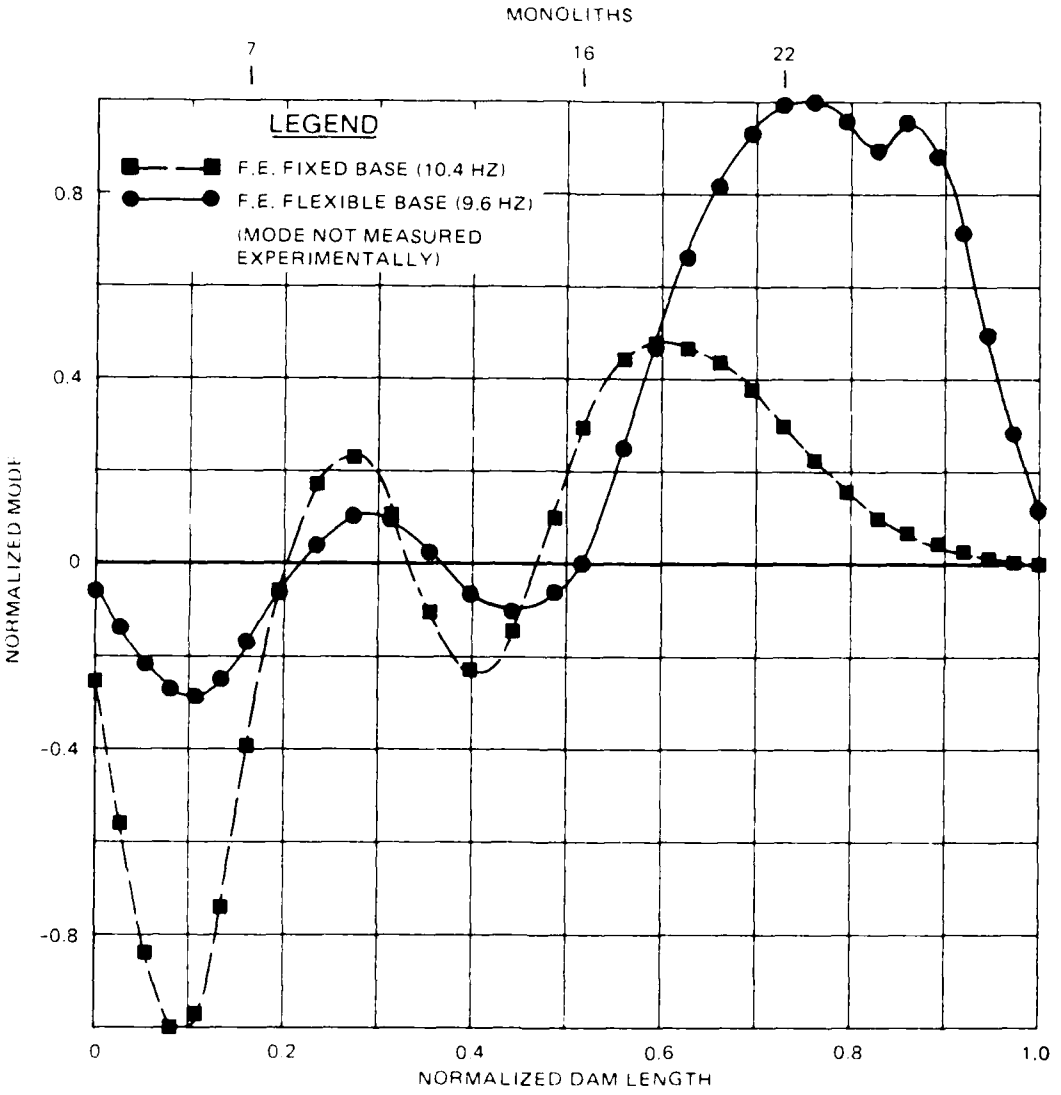

Figure 35. Analytical crest mode shape 4 comparisons for dam without reservoir

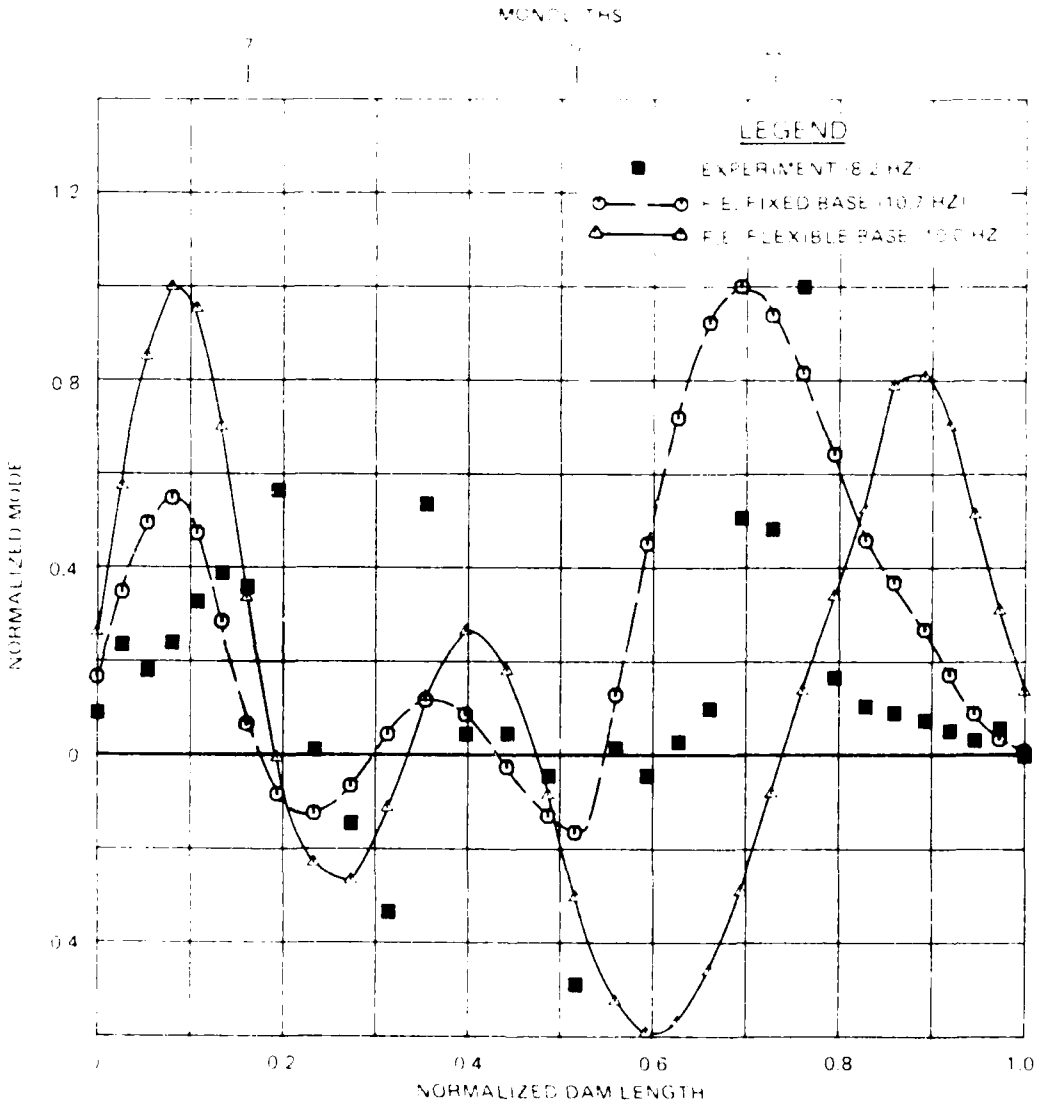

Figure 36. Analytical and experimental crest mode shape 5 comparisons for dam without reservoir

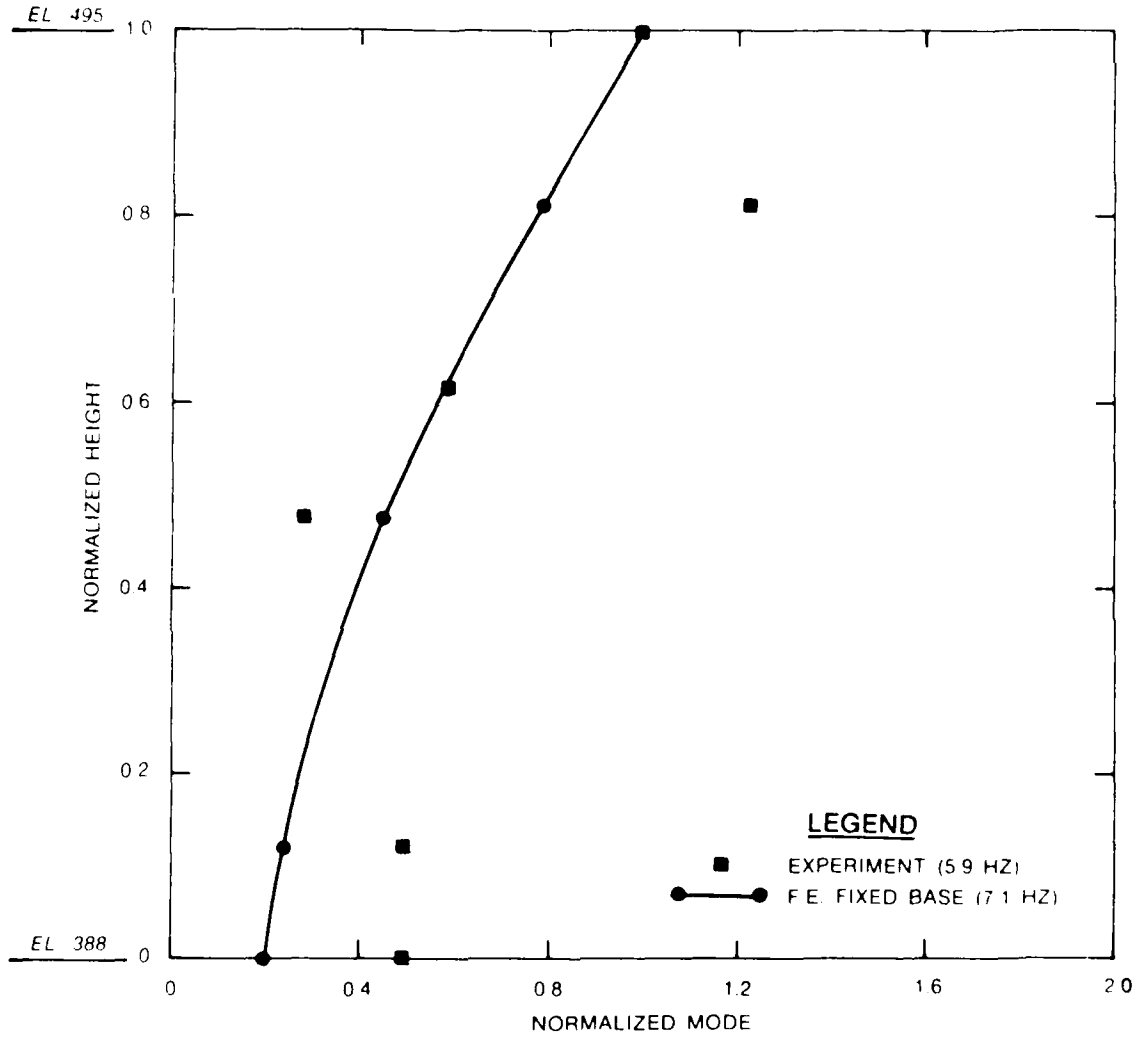

Figure 37. Cross-sectional mode shape 1 comparisons for monolith 7, upstream face, dam without reservoir

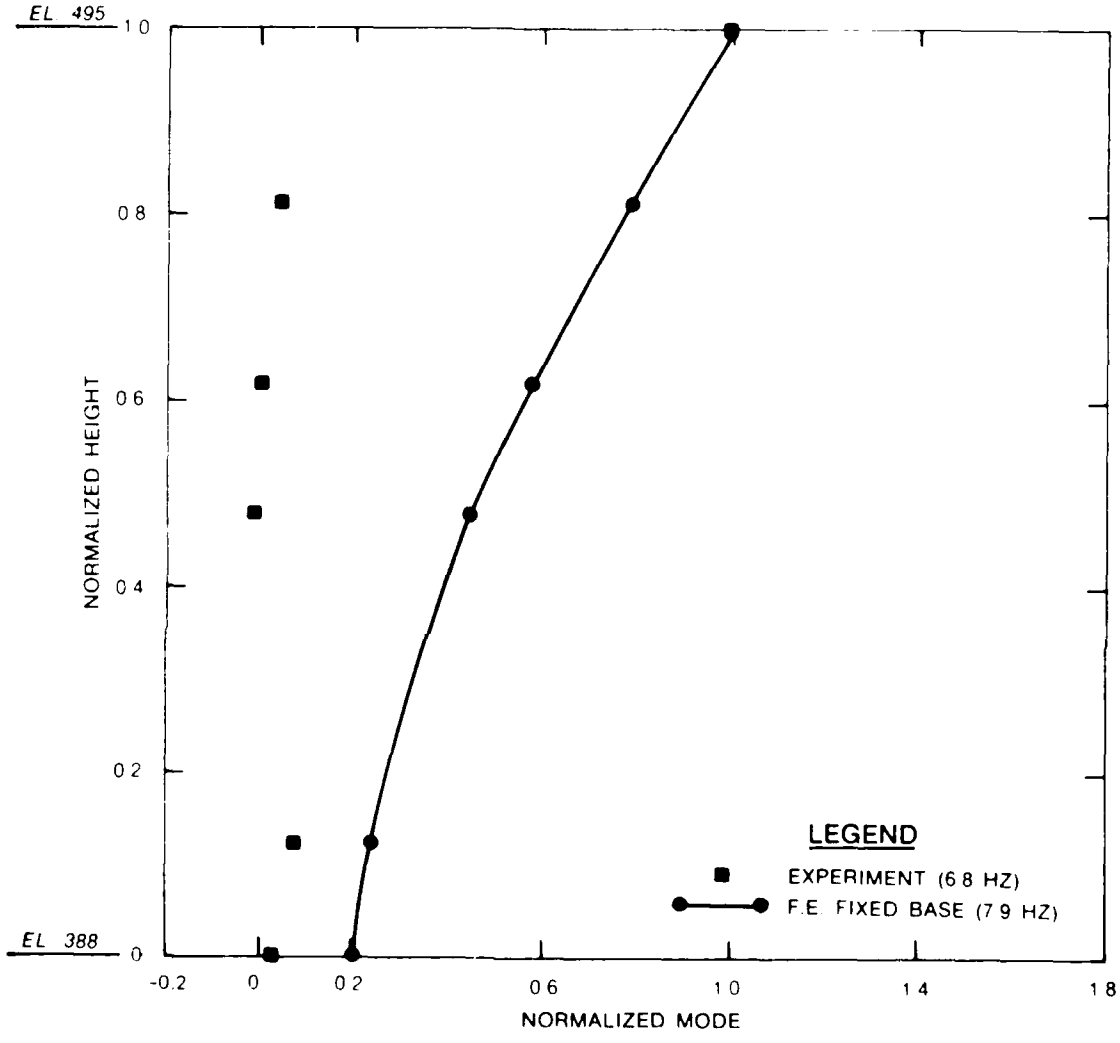

Figure 38. Cross-sectional mode shape 2 comparisons for monolith 7, upstream face, dam without reservoir

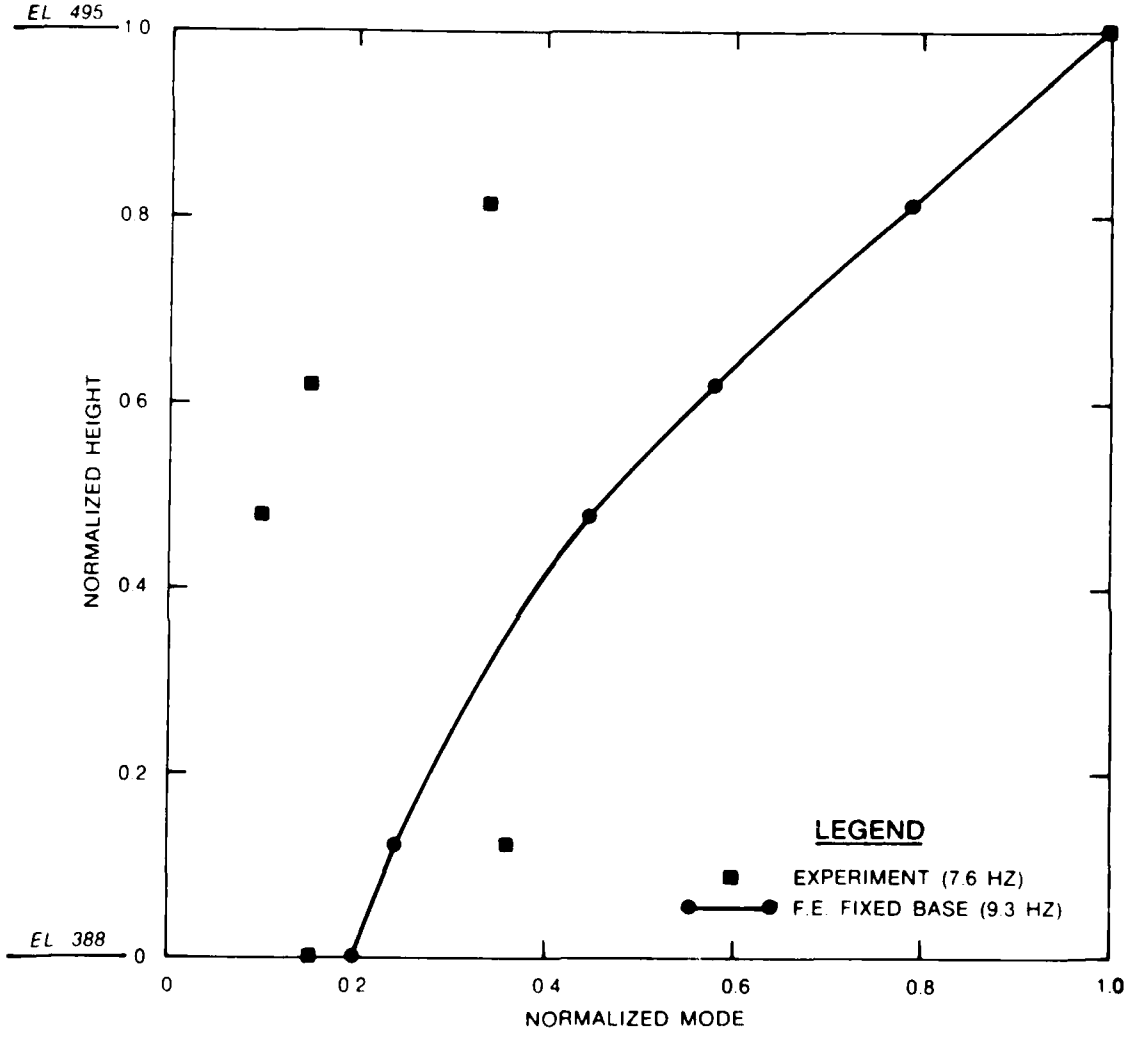

Figure 39. Cross-sectional mode shape 3 comparisons for monolith 7, upstream face, dam without reservoir

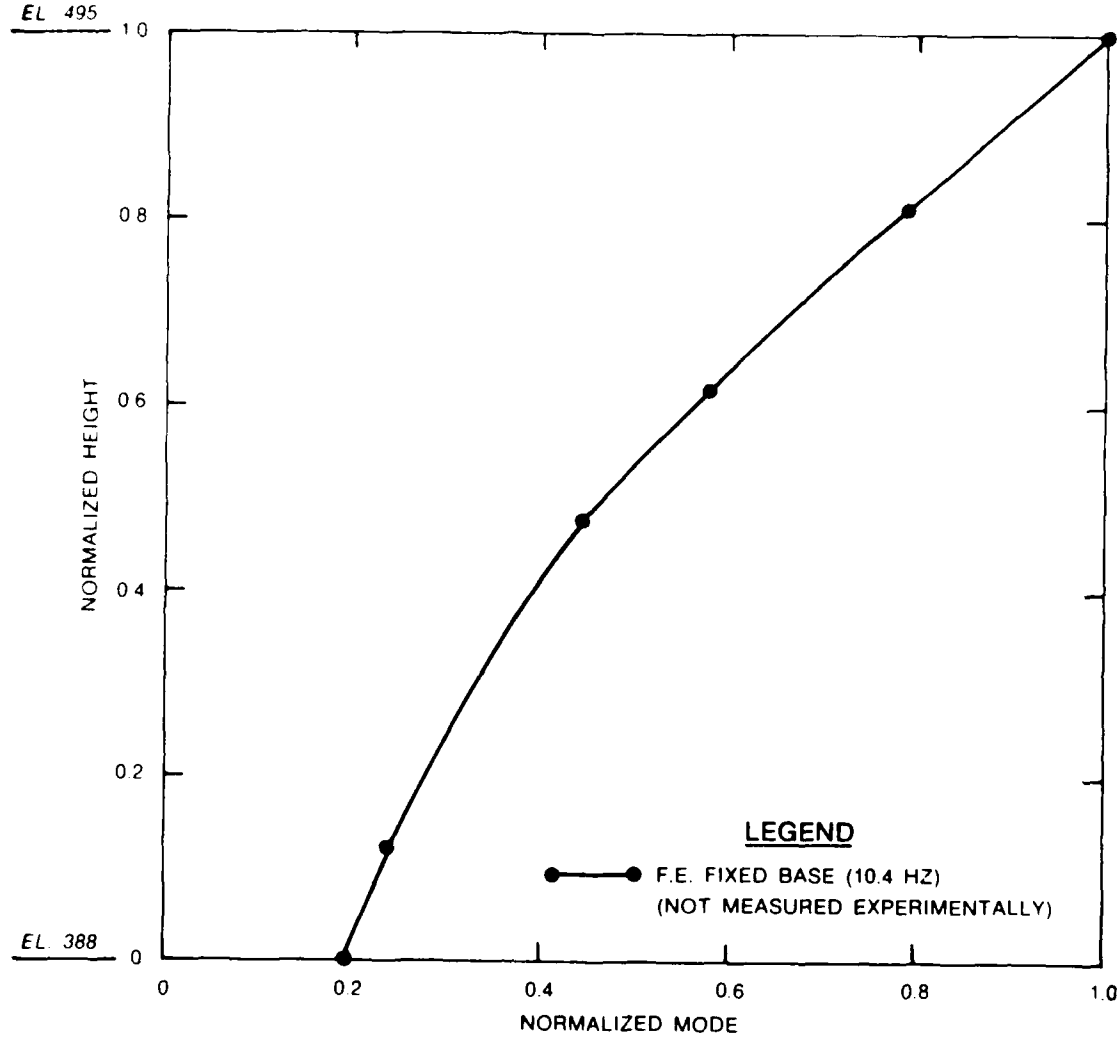

Figure 40. Cross-sectional mode shape 4 for monolith 7, upstream face, dam without reservoir

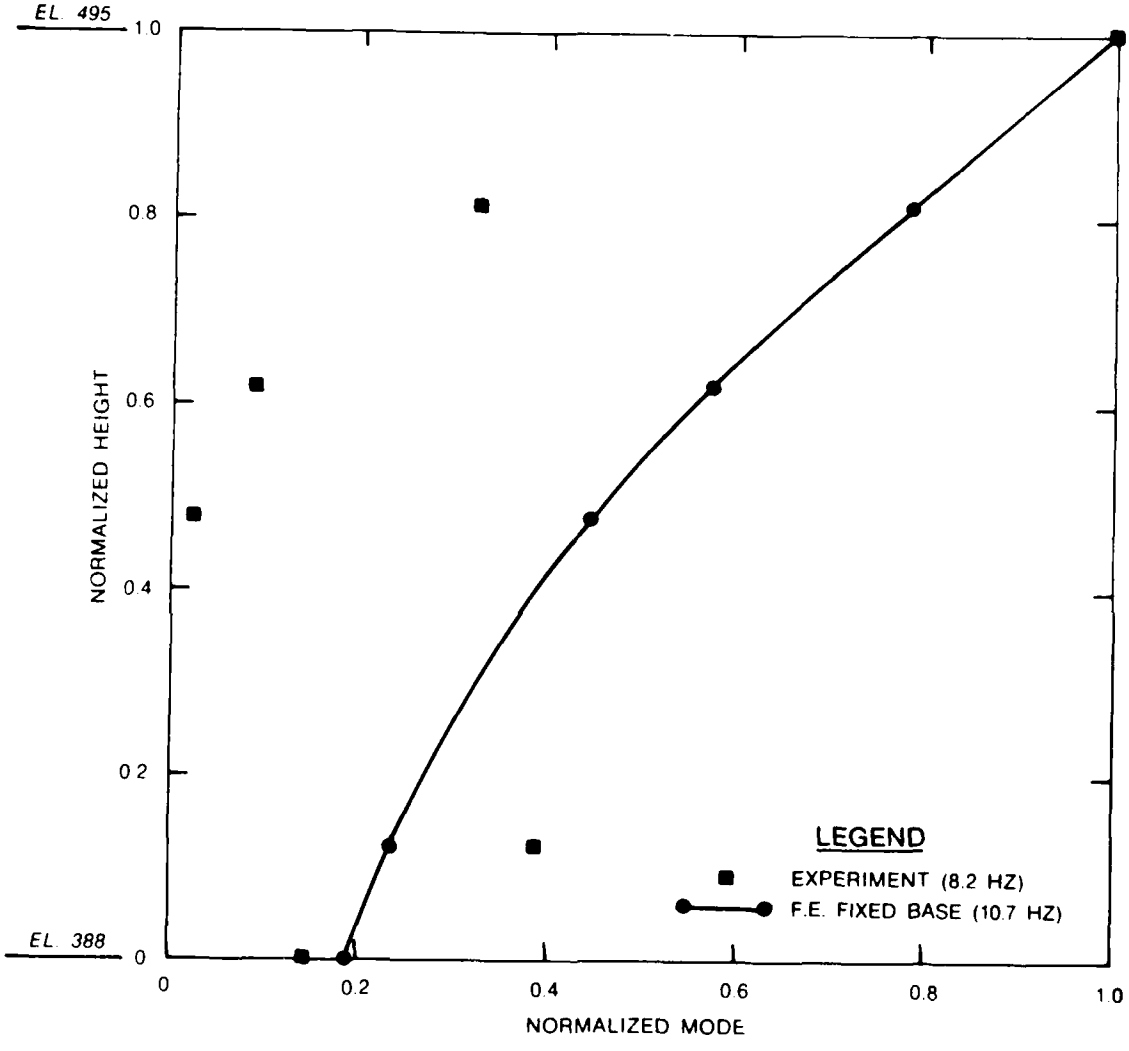

Figure 41. Cross-sectional mode shape 5 comparisons for monolith 7, upstream face, dam without reservoir

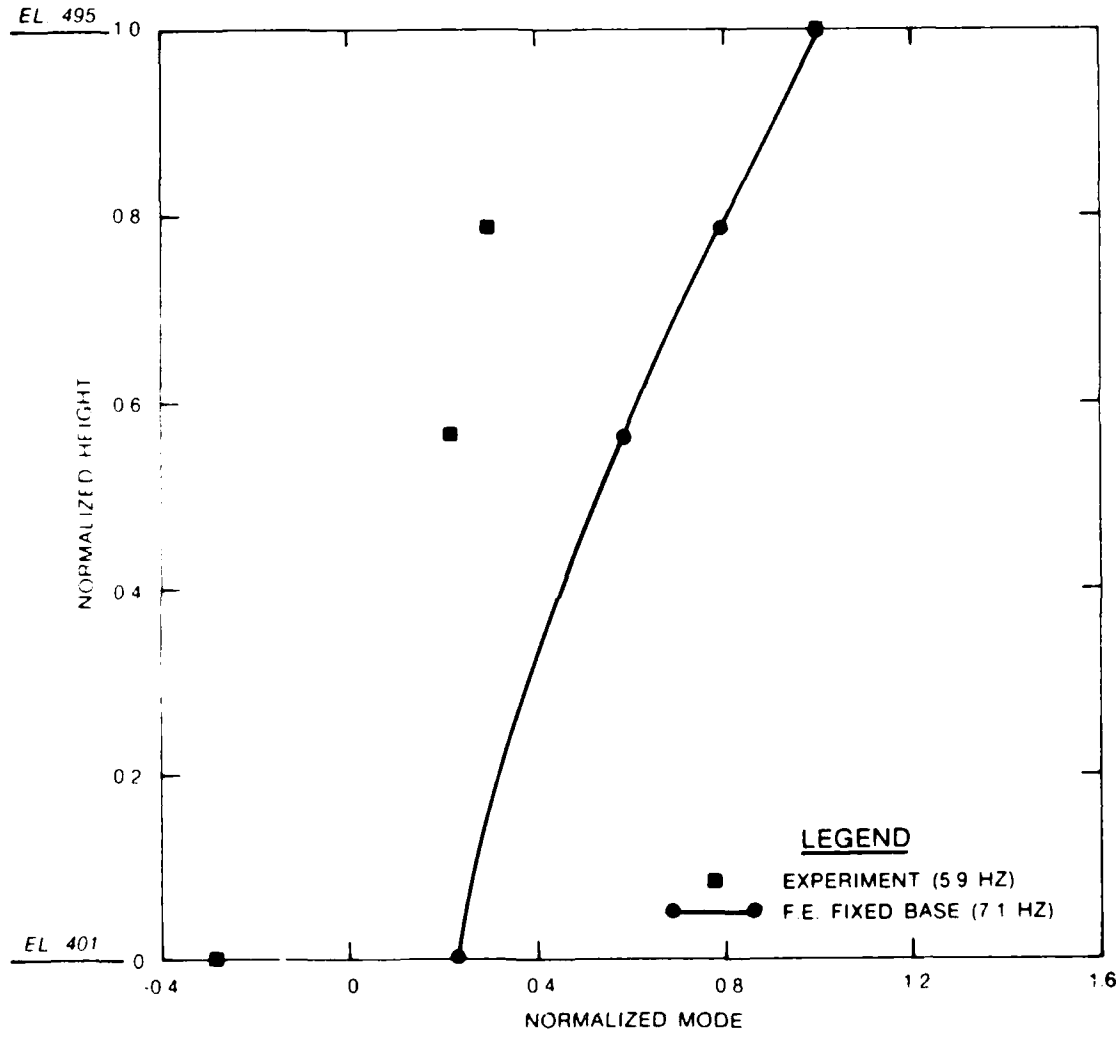

Figure 42. Cross-sectional mode shape 1 comparisons for monolith 7, downstream face, dam without reservoir

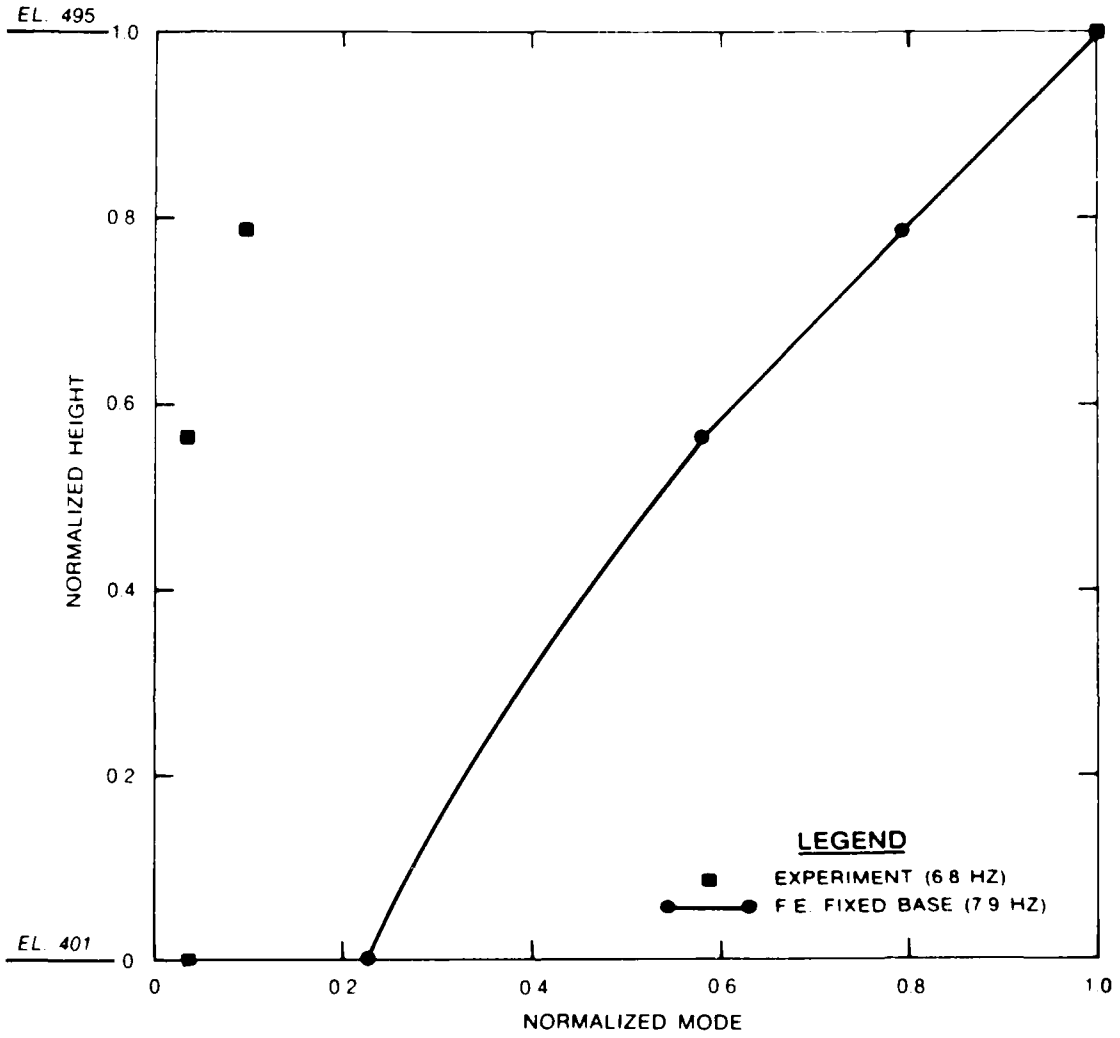

Figure 43. Cross-sectional mode shape 2 comparisons for monolith 7, downstream face, dam without reservoir

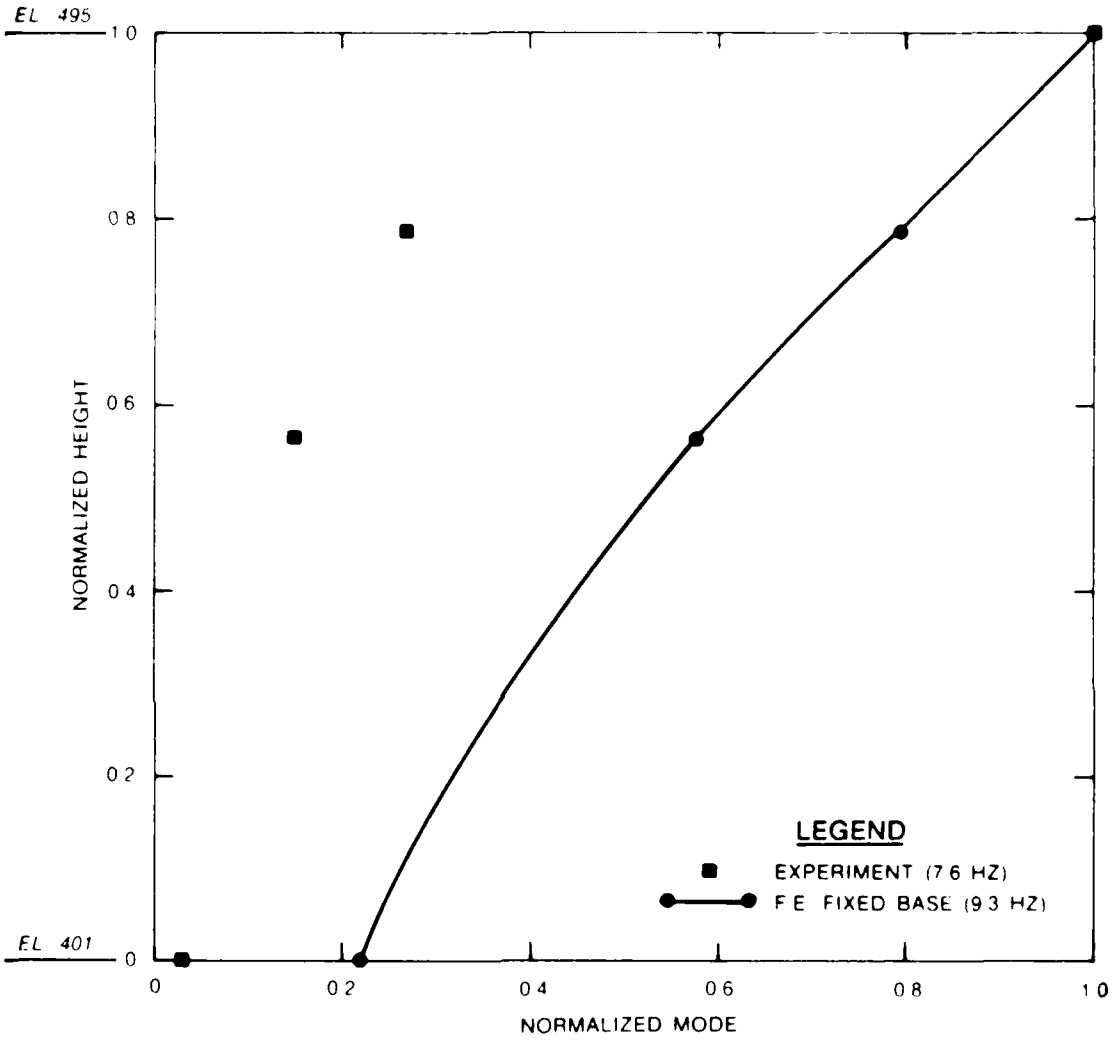

Figure 44. Cross-sectional mode shape 3 comparisons for monolith 7, downstream face, dam without reservoir

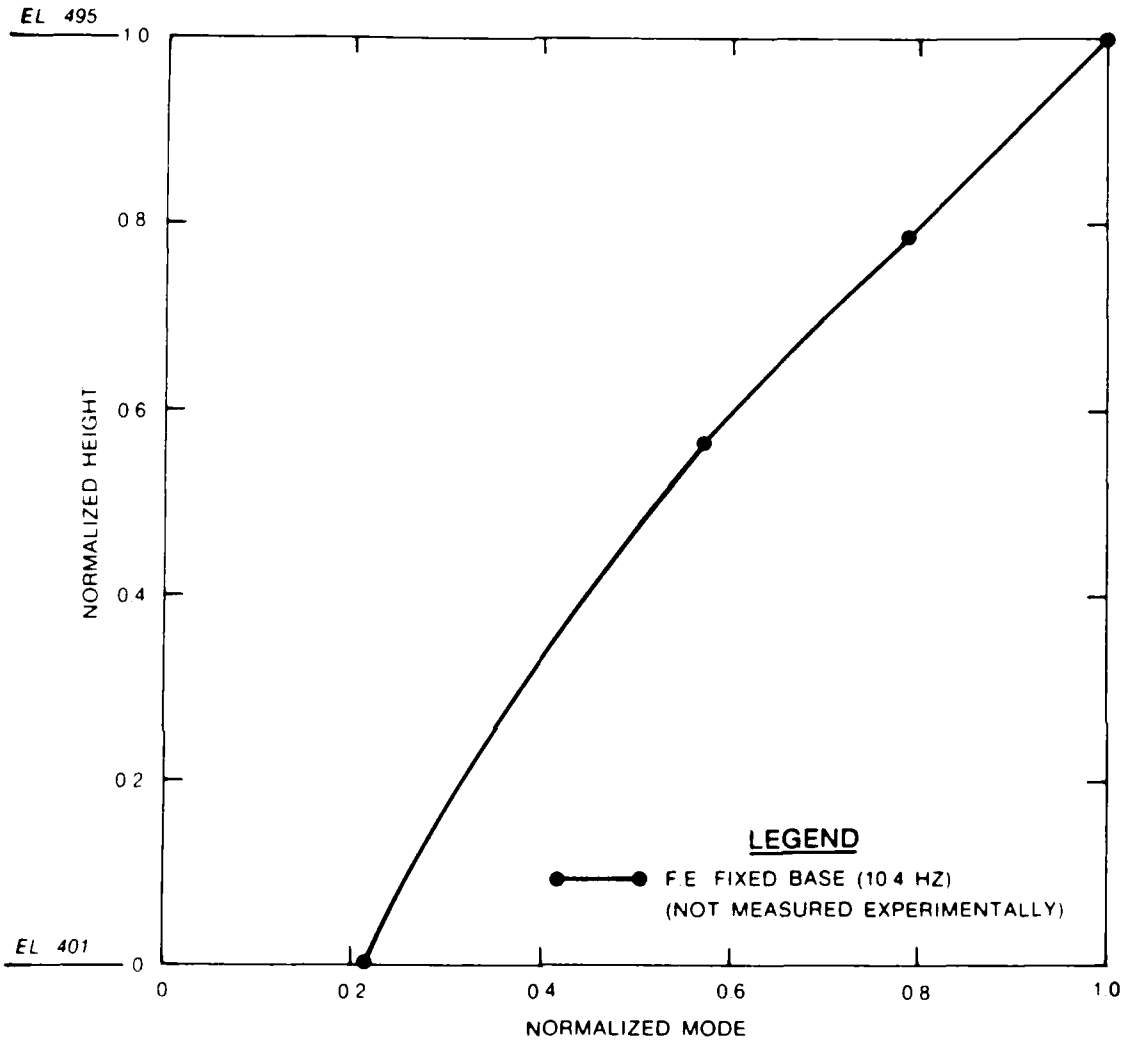

Figure 45. Cross-sectional mode shape 4 comparisons for monolith 7, downstream face, dam without reservoir

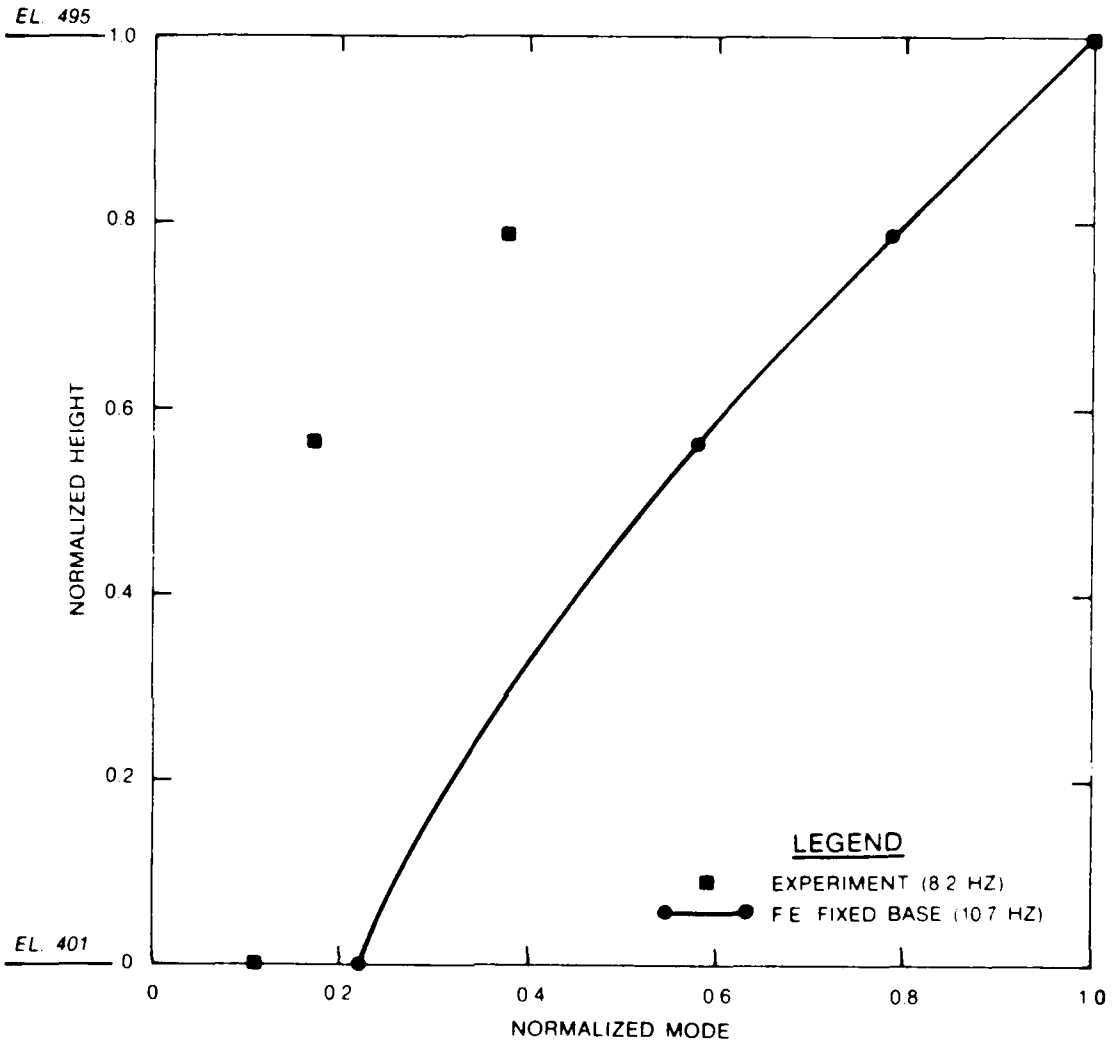

Figure 46. Cross-sectional mode shape 5 comparisons for monolith 7, downstream face, dam without reservoir

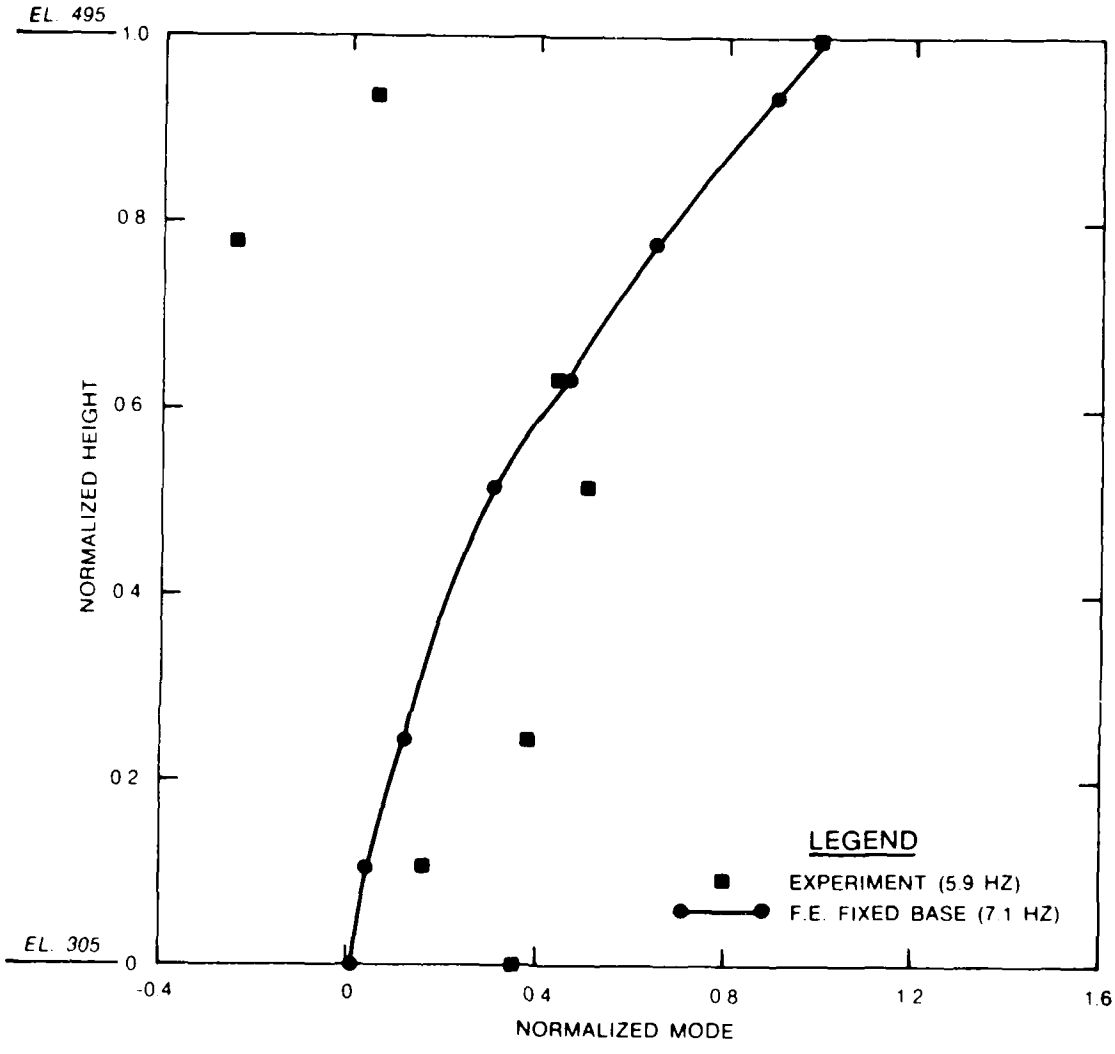

Figure 47. Cross-sectional mode shape 1 comparisons for monolith 16, dam without reservoir

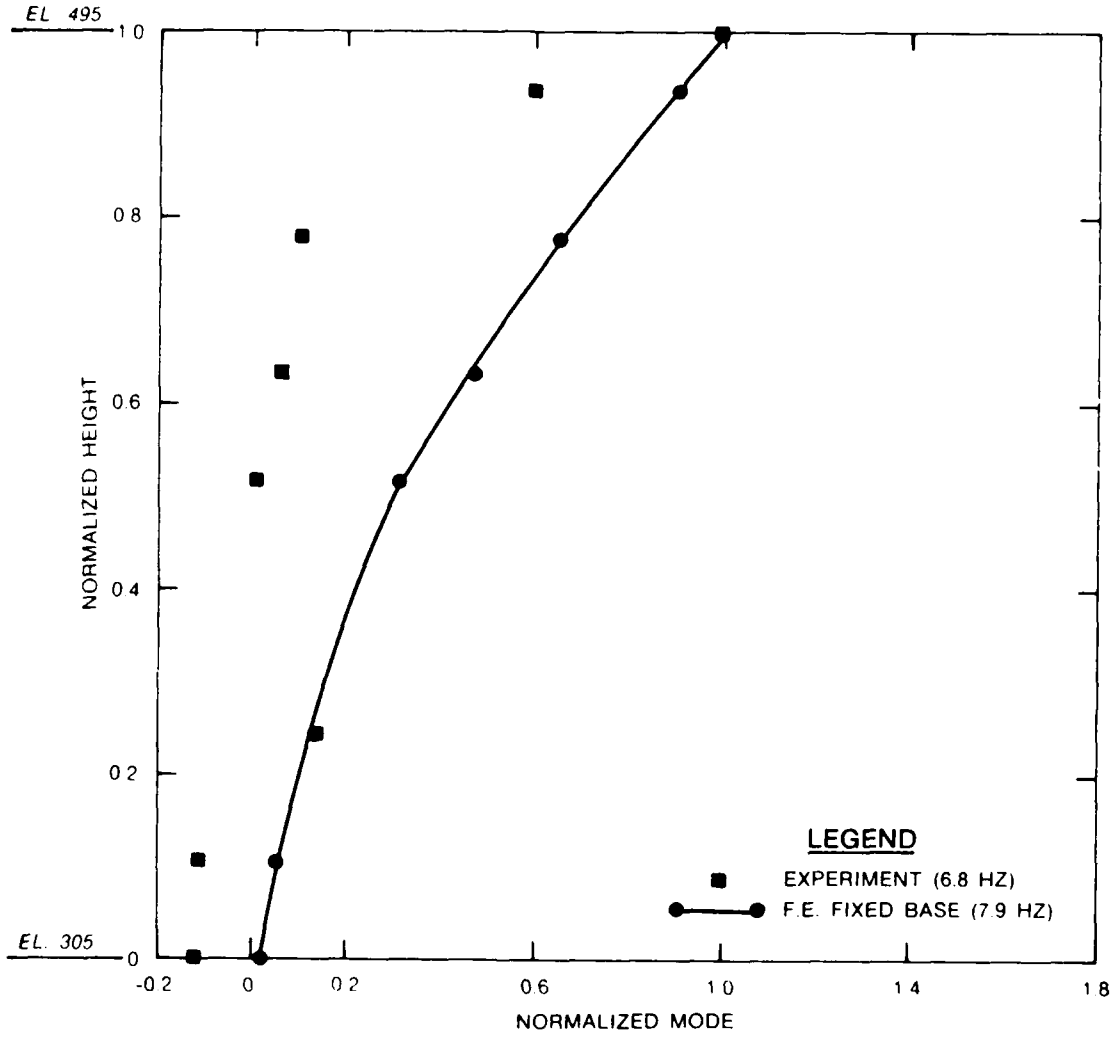

Figure 48. Cross-sectional mode shape 2 comparisons for monolith 16, dam without reservoir

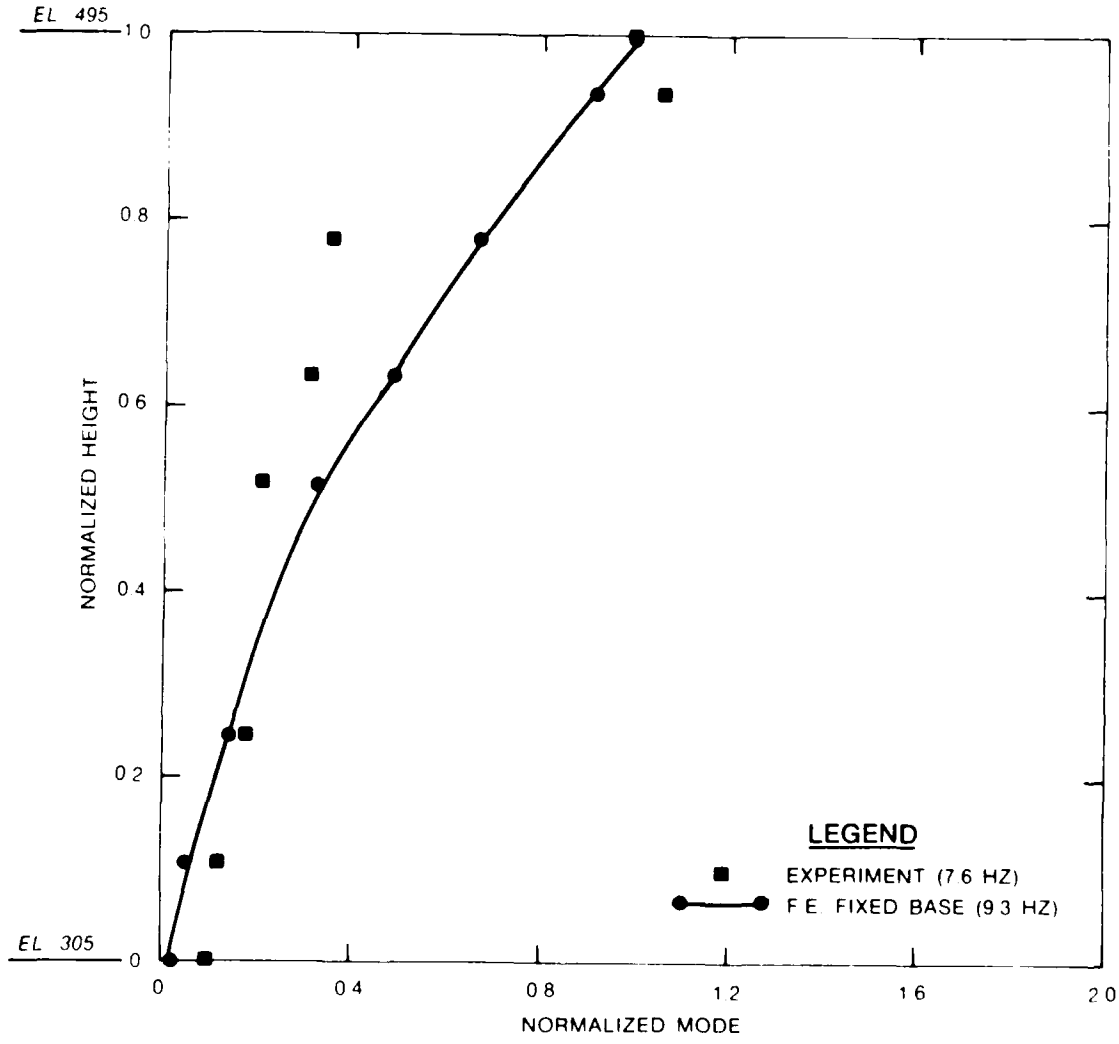

Figure 49. Cross-sectional mode shape 3 comparisons for monolith 16, dam without reservoir

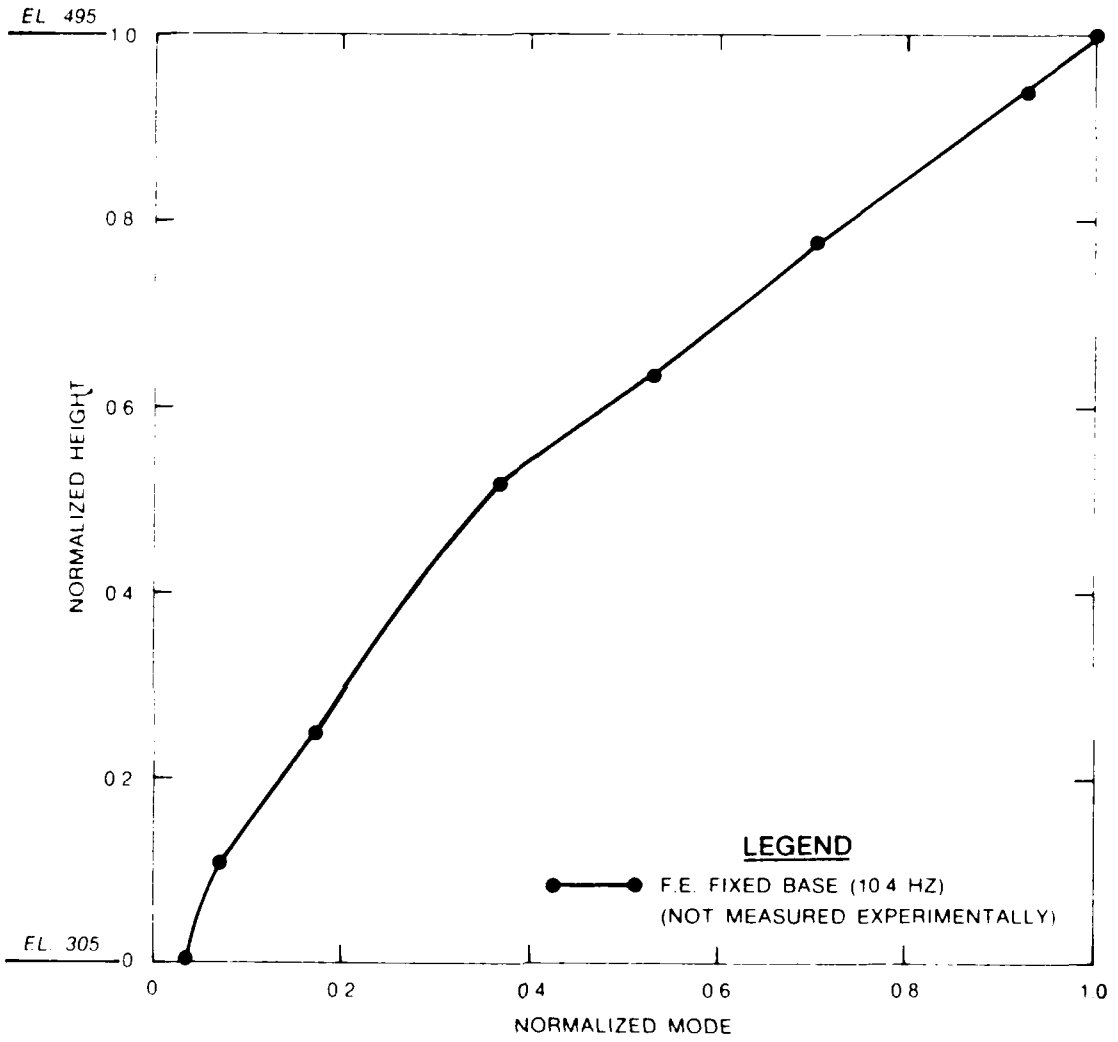

Figure 50. Cross-sectional mode shape 4 comparisons for monolith 16, dam without reservoir

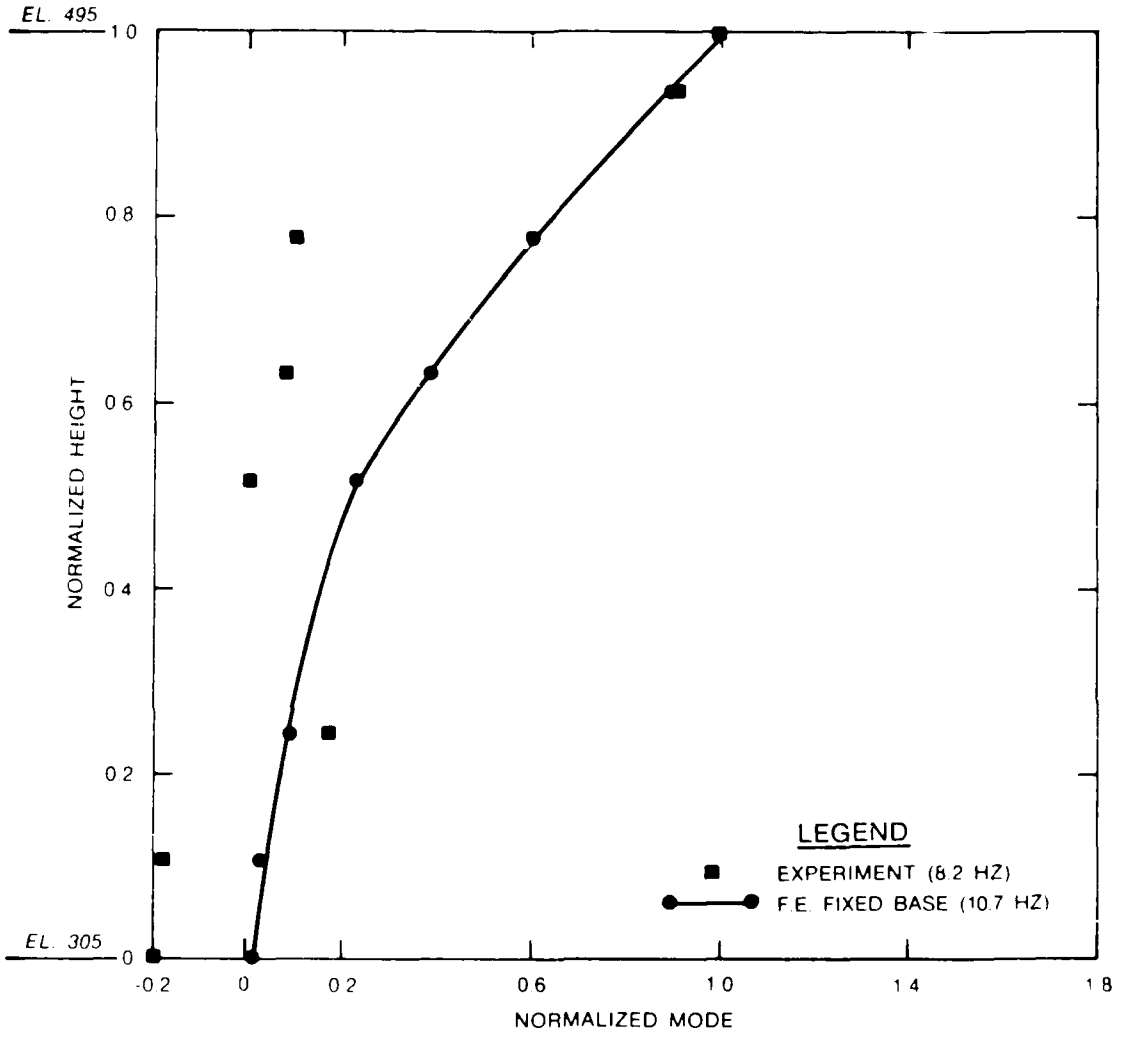

Figure 51. Cross-sectional mode shape 5 comparisons for monolith 16, dam without reservoir

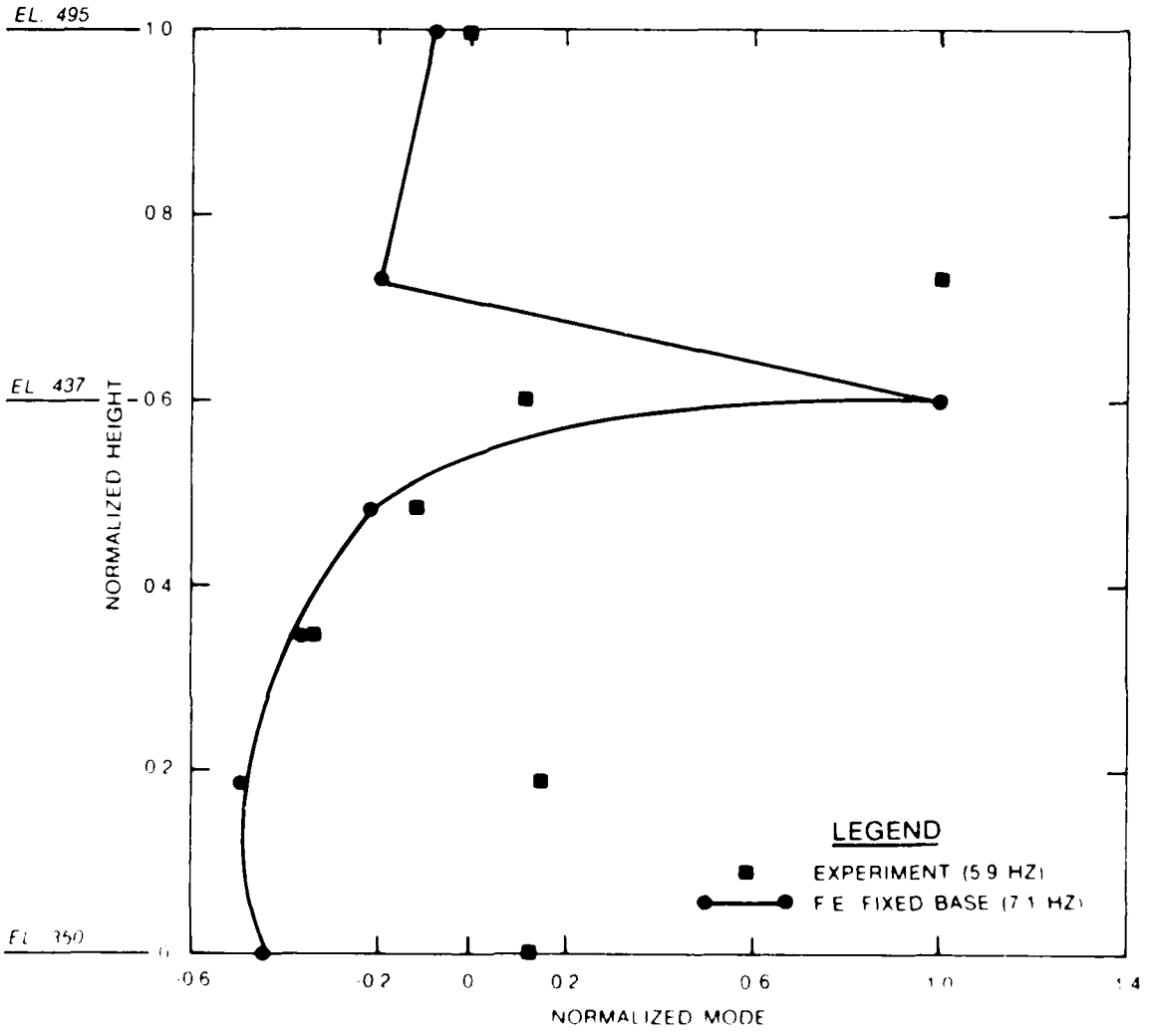

Figure 52. Cross-sectional mode shape 1 comparisons for monolith 22, dam without reservoir

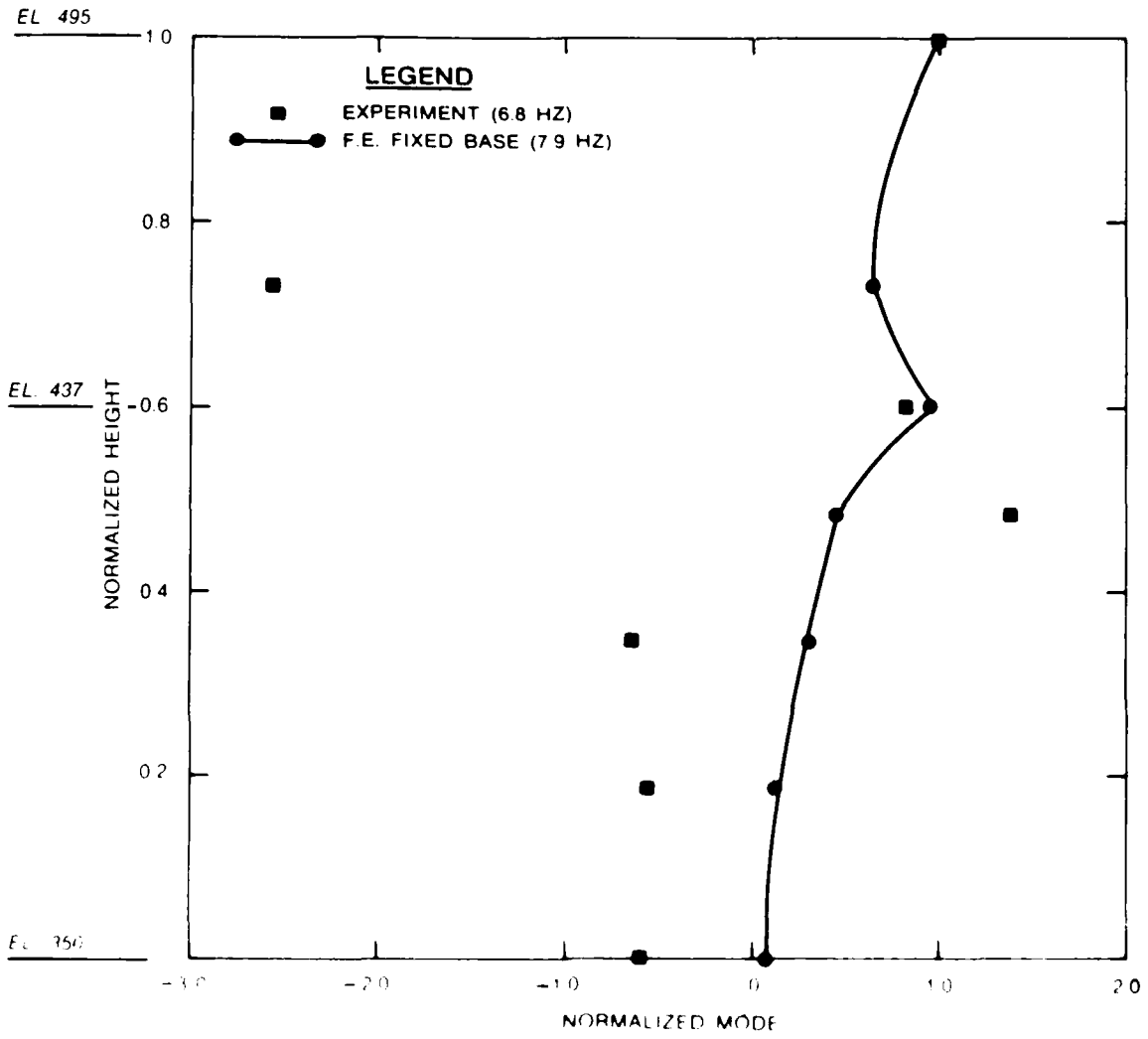

Figure 53. Cross-sectional mode shape 2 comparisons for monolith 22, dam without reservoir

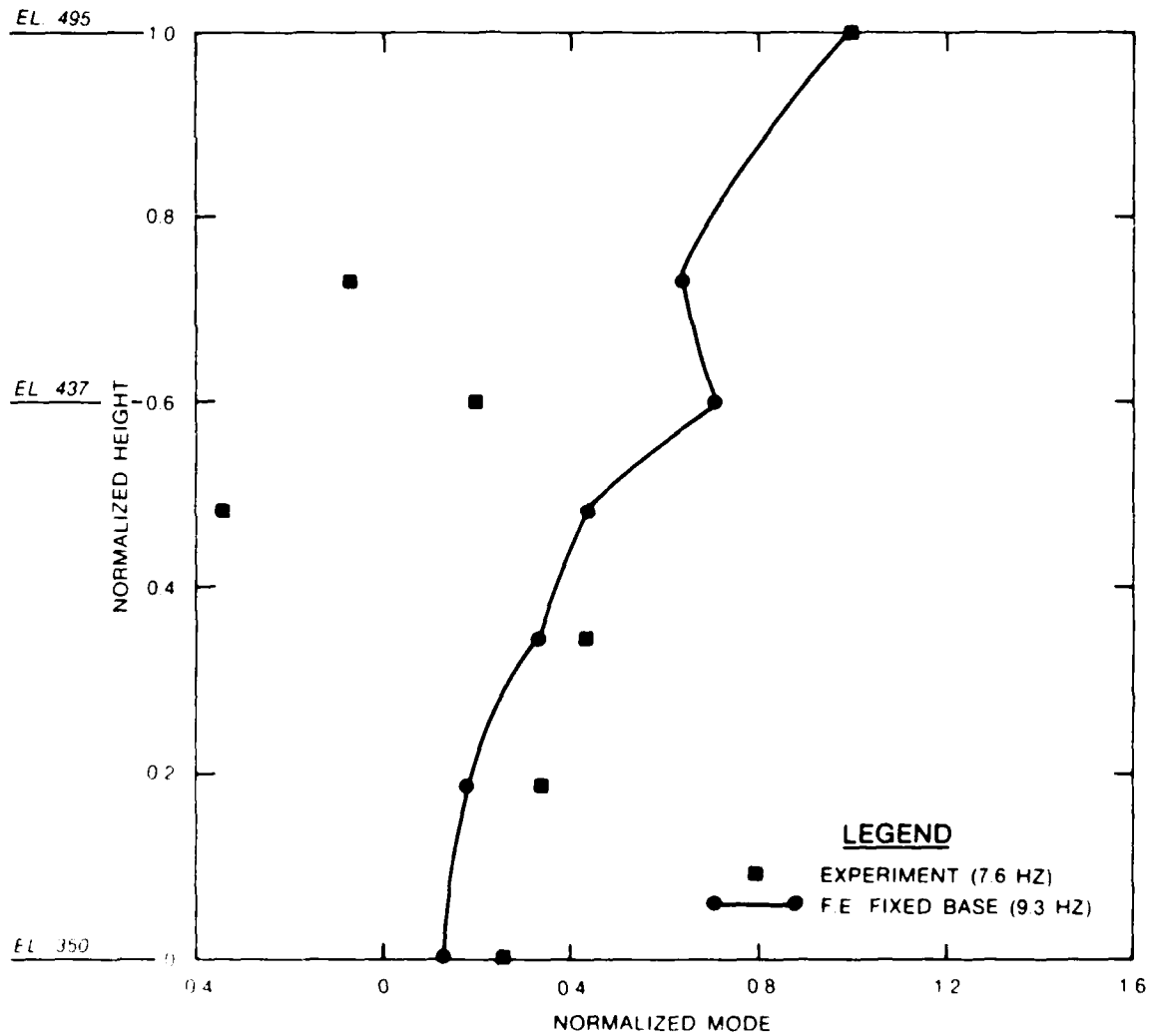

Figure 54. Cross-sectional mode shape 3 comparisons for monolith 22, dam without reservoir

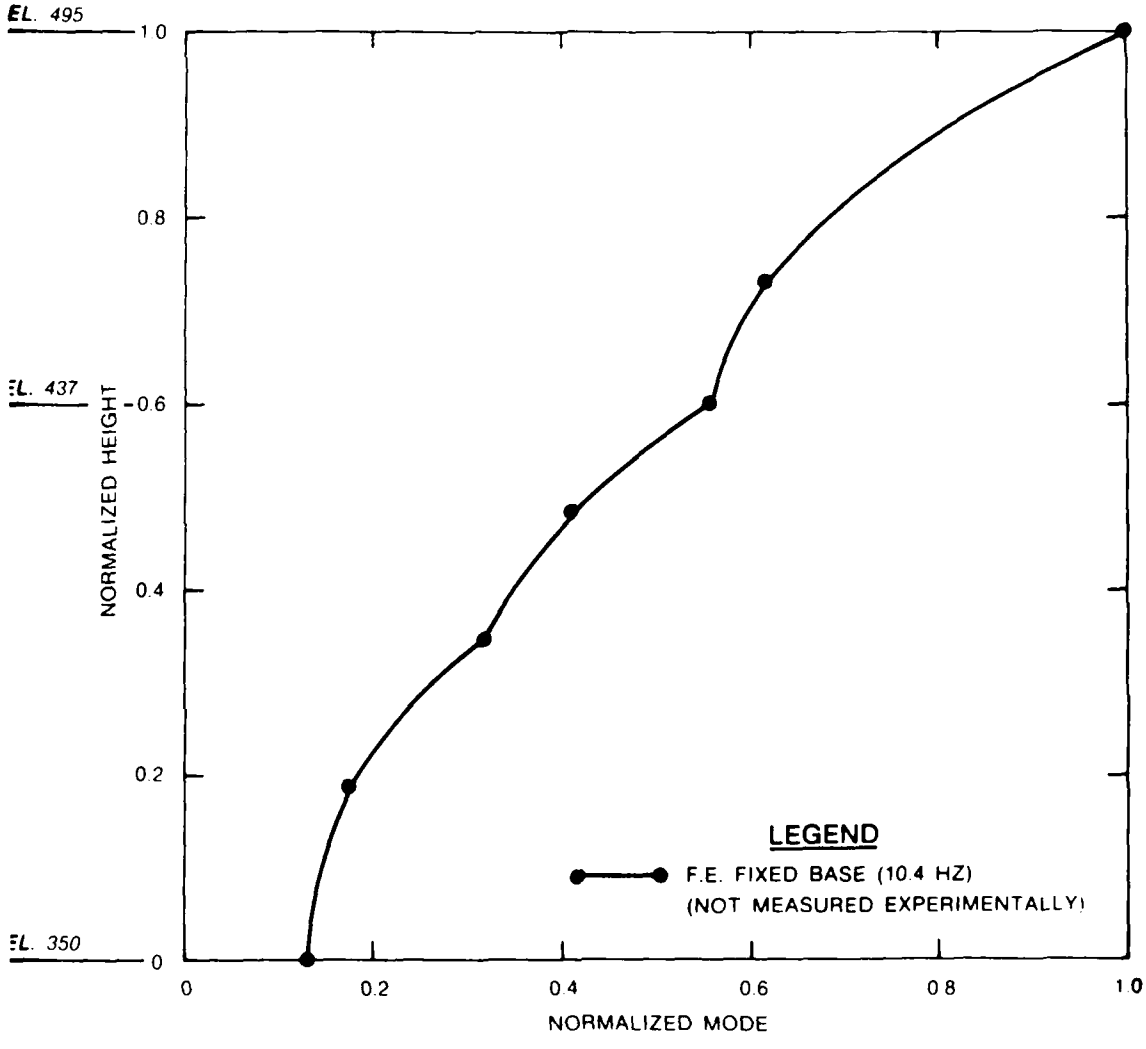

Figure 55. Cross-sectional mode shape 4 comparisons for monolith 22, dam without reservoir

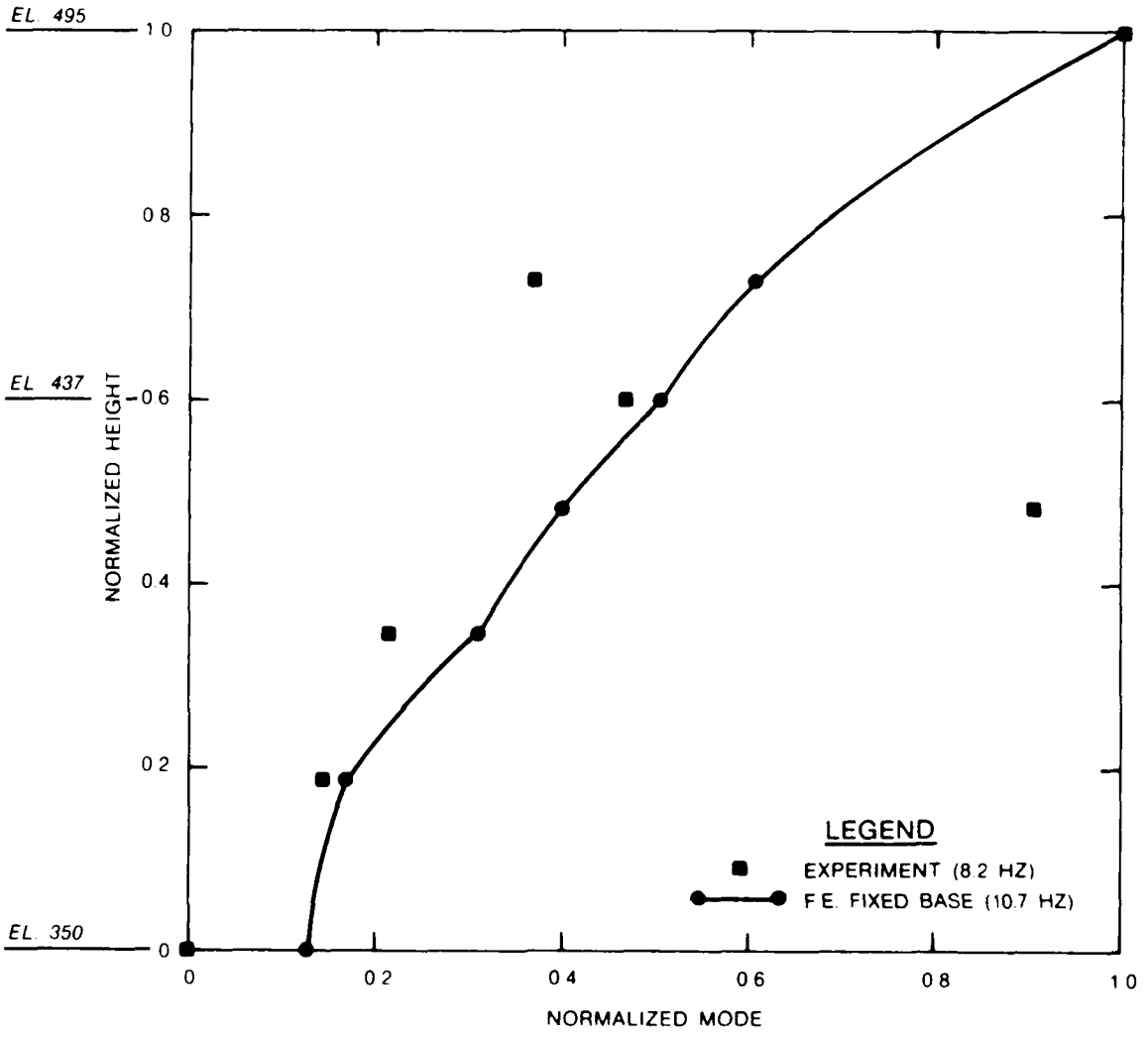

Figure 56. Cross-sectional mode shape 5 comparisons for monolith 22, dam without reservoir

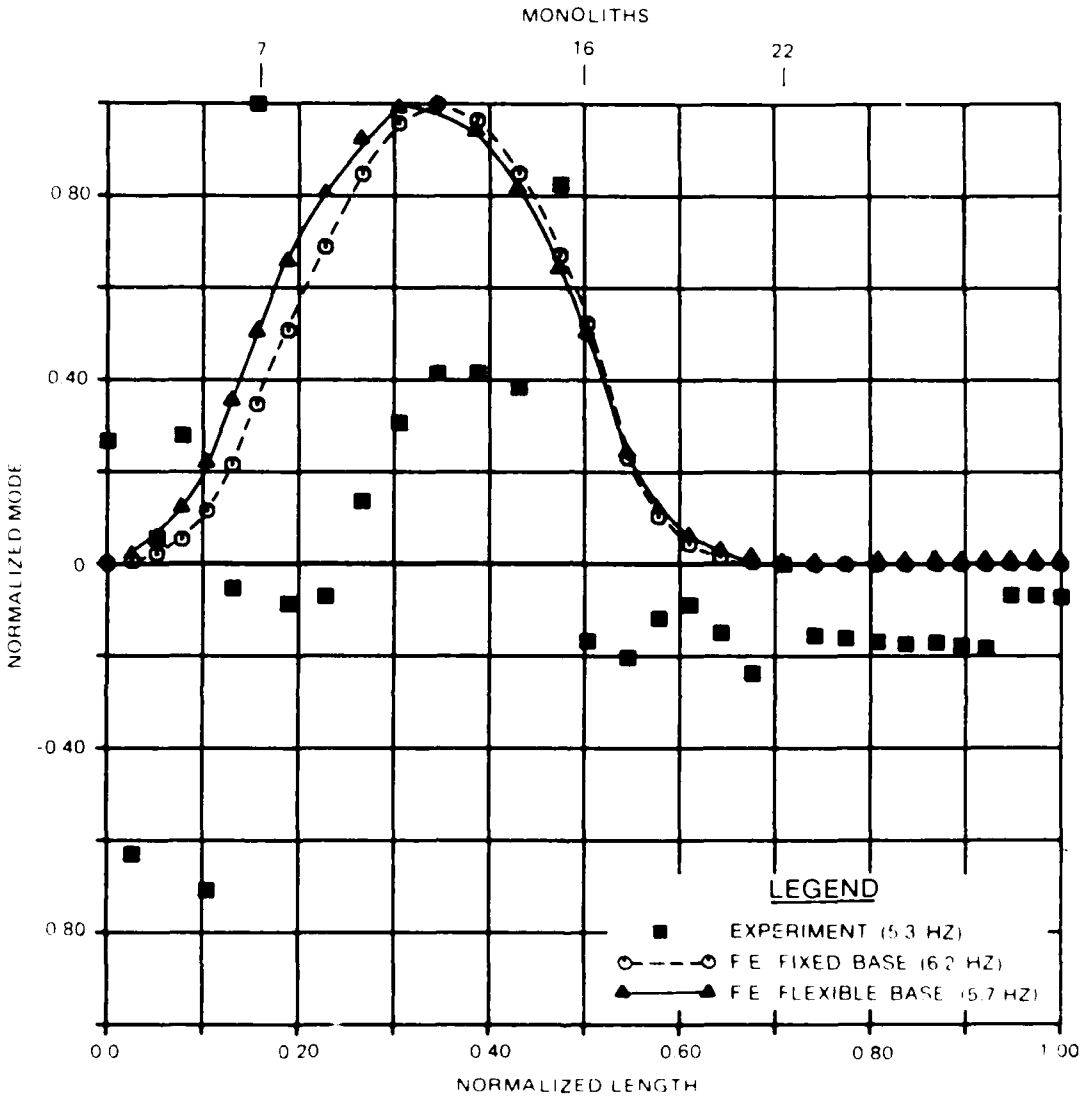

Figure 57. Analytical and experimental crest mode shape 1 comparisons for dam with reservoir

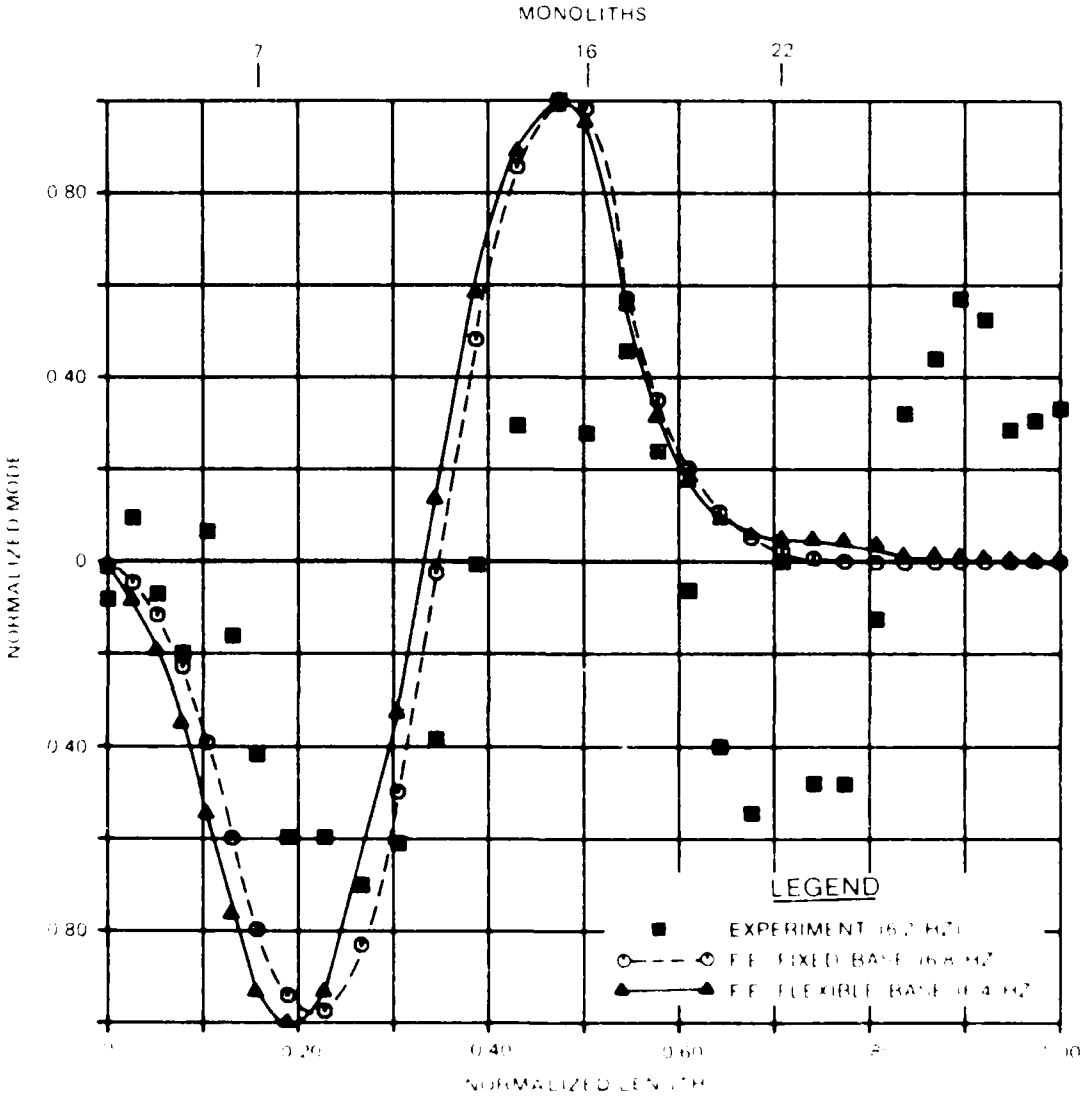

Figure 58. Analytical and experimental crest mode shape 2 comparisons for dam with reservoir

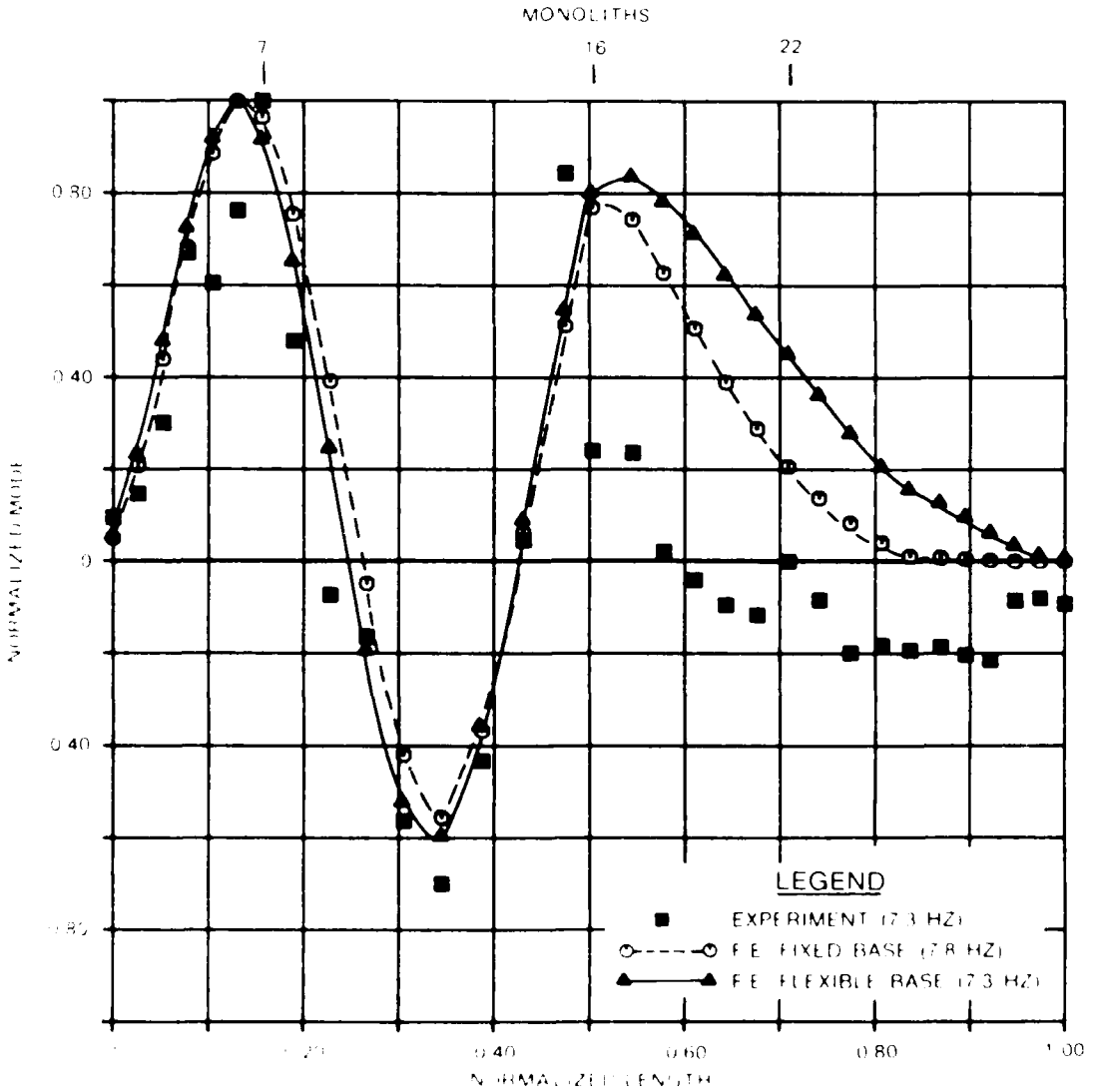

Figure 59. Analytical and experimental crest mode shape 3 comparisons for dam with reservoir

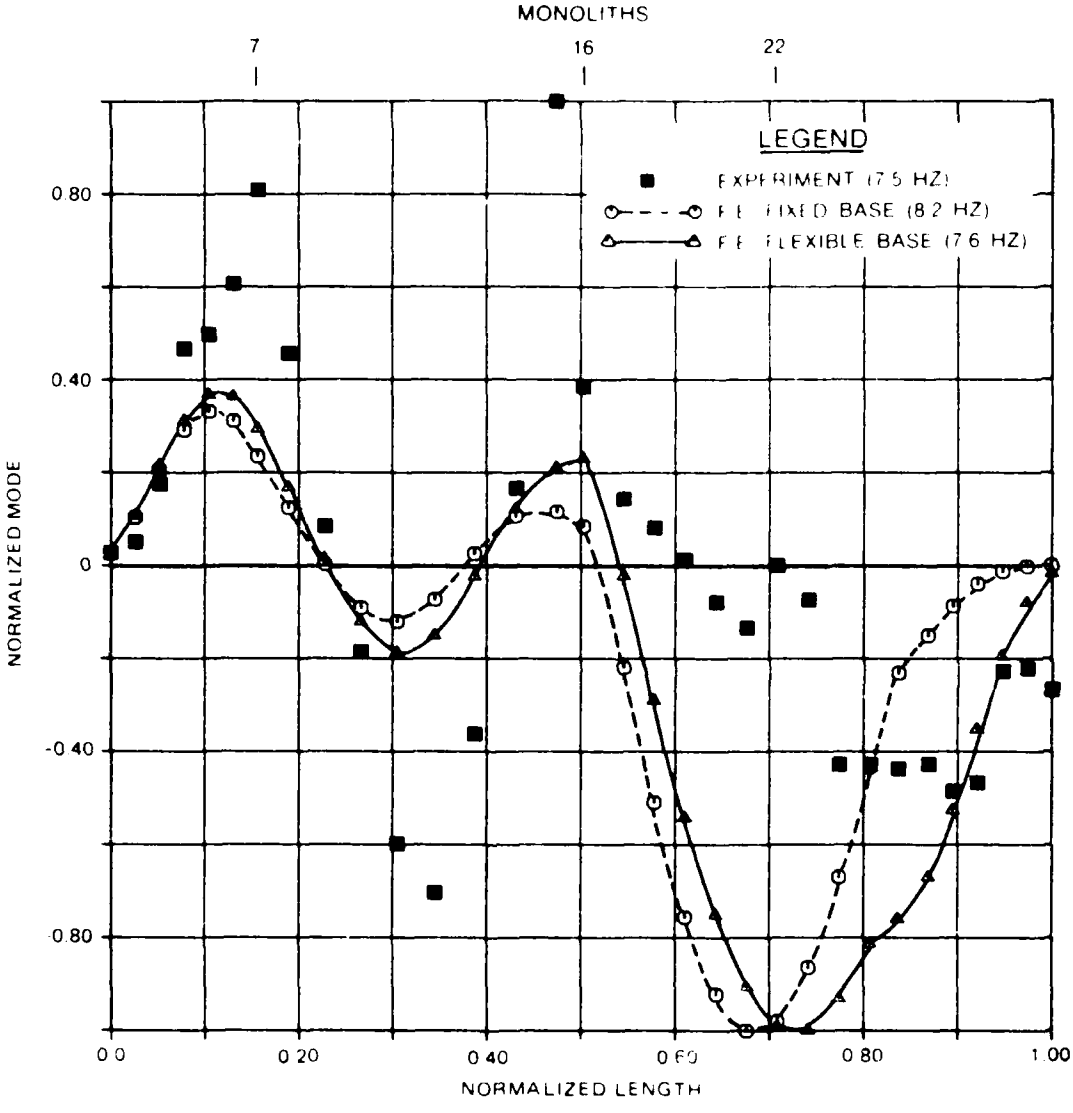

Figure 60. Analytical and experimental crest mode shape 4 comparisons for Tam with reservoir

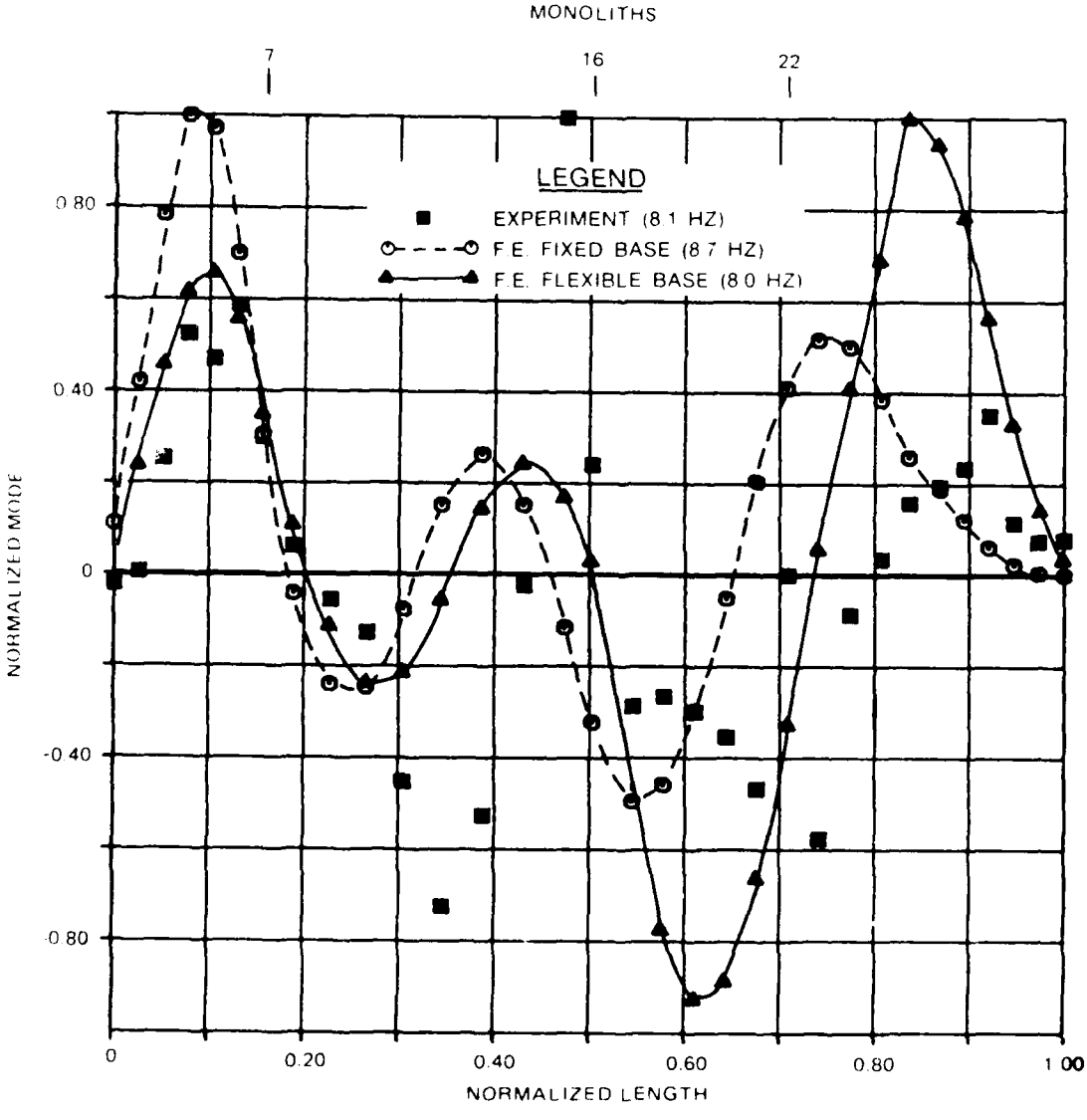

Figure 61. Analytical and experimental crest mode shape 5 comparisons for dam with reservoir

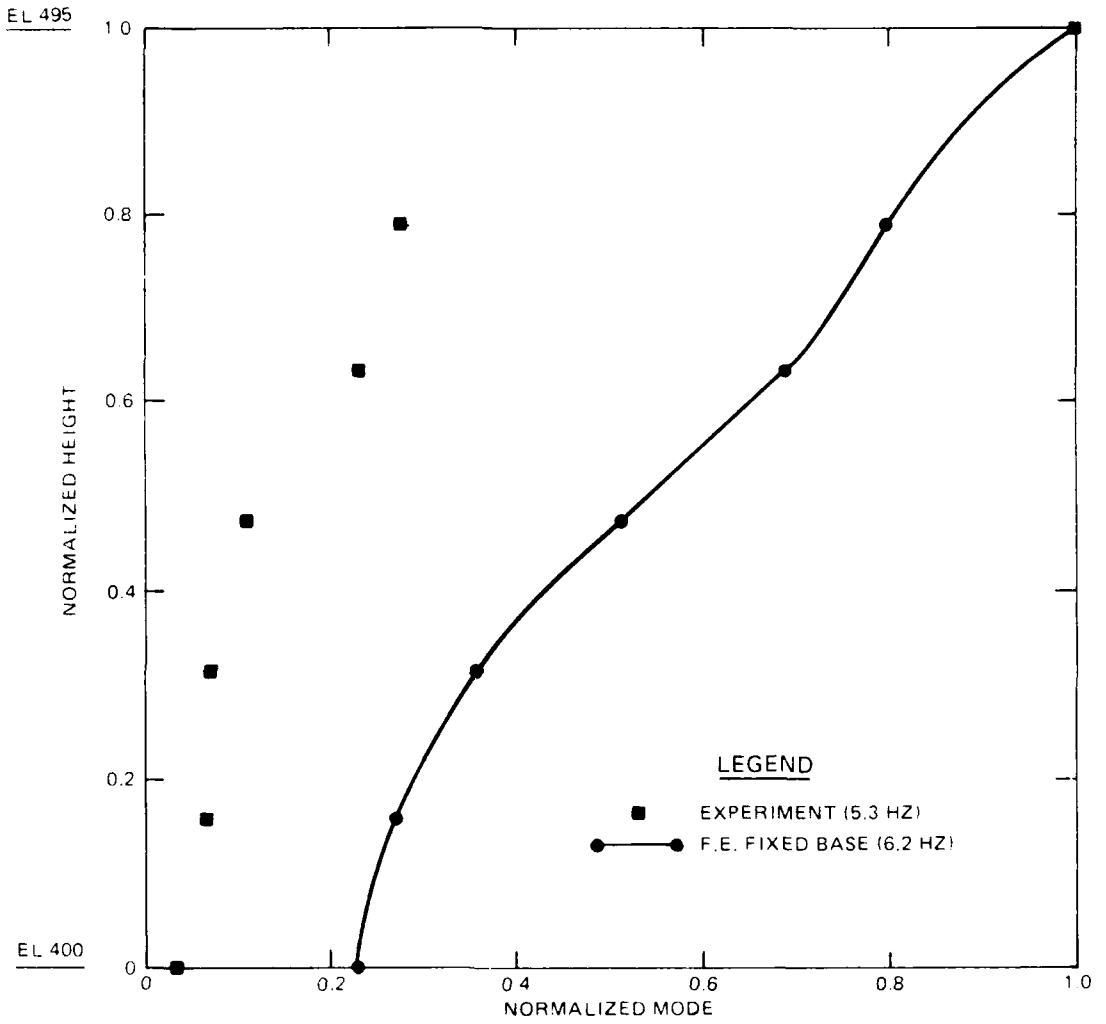

Figure 62. Cross-sectional mode shape 1 comparisons for monolith 7, downstream face, dam with reservoir

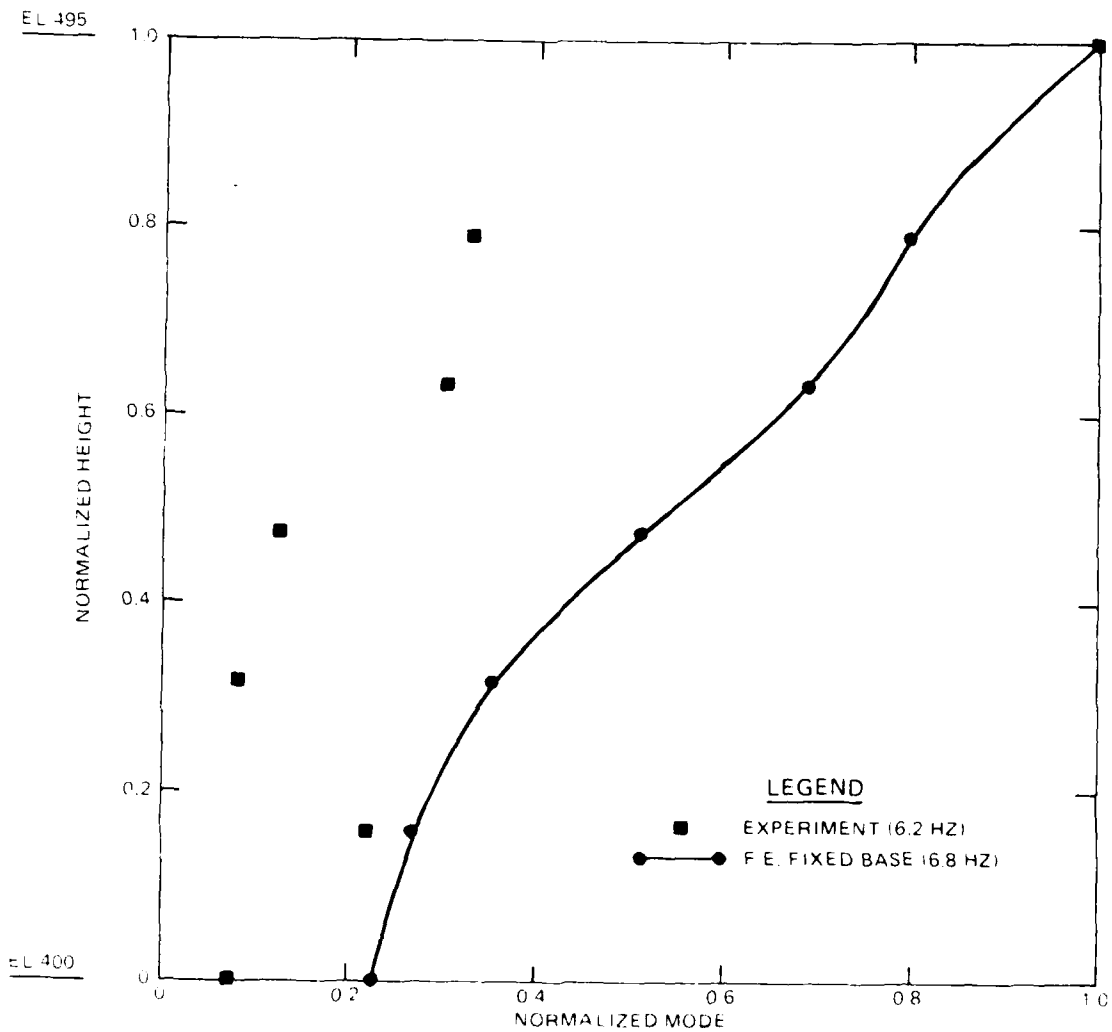

Figure 63. Cross-sectional mode shape 2 comparisons for monolith 7, downstream face, dam with reservoir

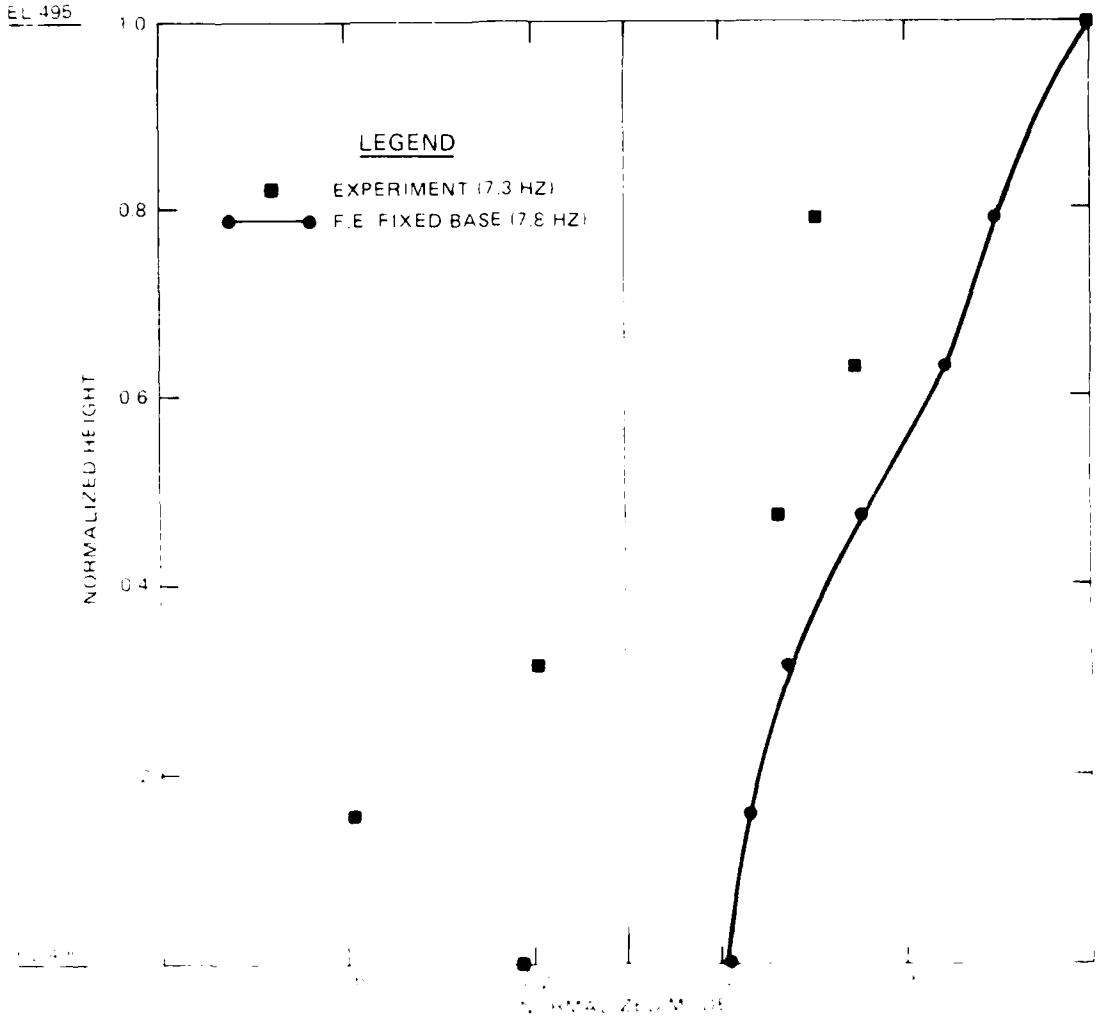

Figure 64. Cross-sectional mode shape 3 comparisons for monolith 7, downstream face, dam with reservoir

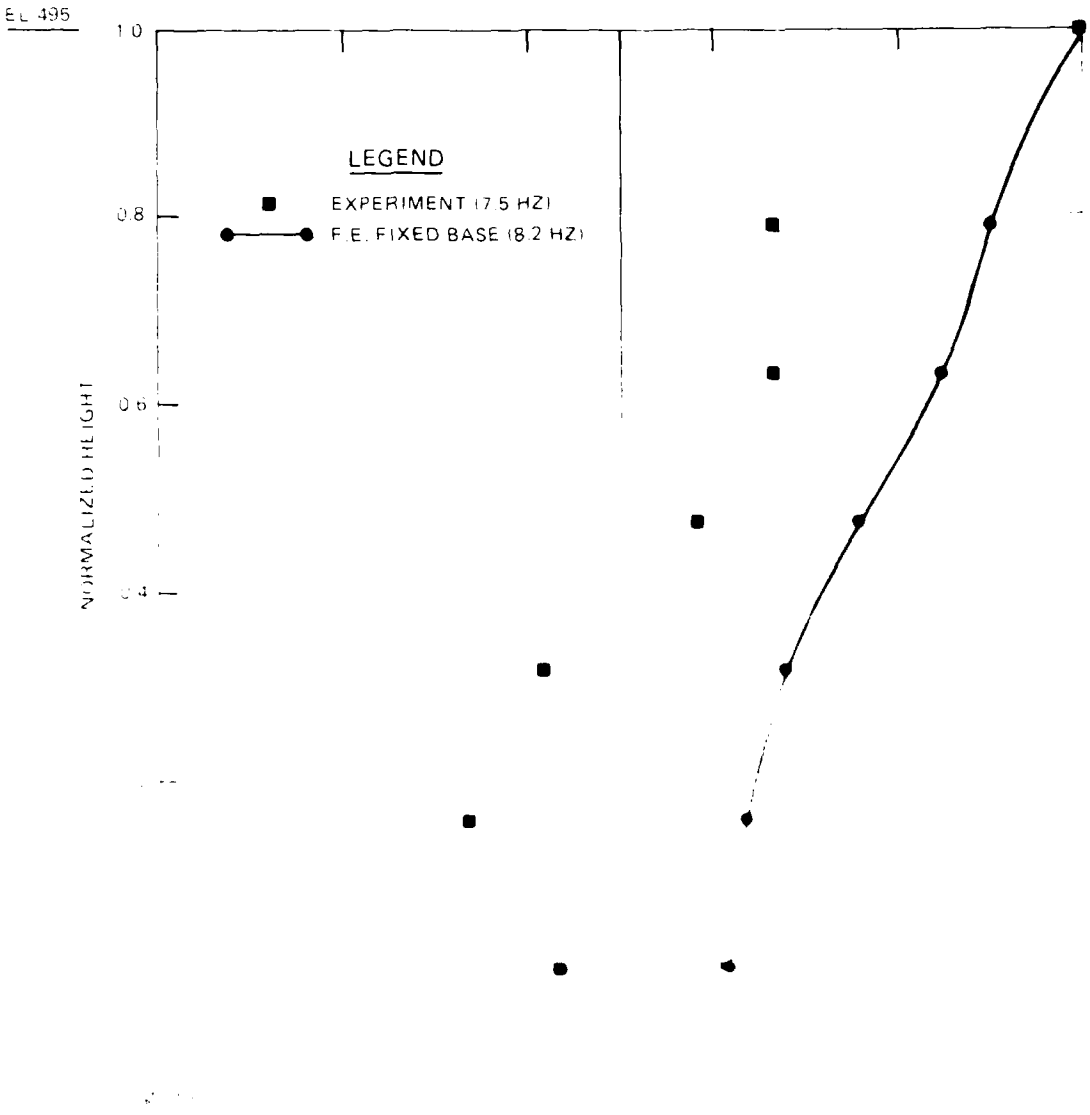
EL 495
1.0
0.8
0.6
0.4
NORMALIZED HEIGHT
LEGEND
EXPERIMENT (7.5 HZ)
F.E. FIXED BASE (8.2 HZ)

AD-A191 063 SUMMARY OF THE RICHARD B RUSSELL CONCRETE DAM VIBRATION STUDY(U) ARMY ENGINEER WATERWAYS EXPERIMENT STATION VICKSBURG MS STRUCTURES LAB R S WRIGHT ET AL FEB 88 2/2

UNCLASSIFIED WES/TR/SL-88-10 F/G 13/2 NL

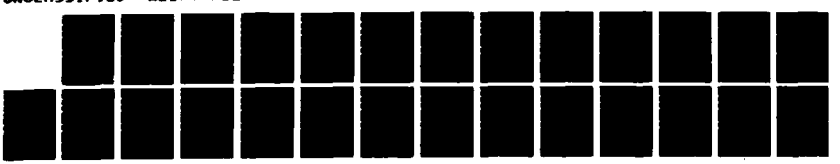

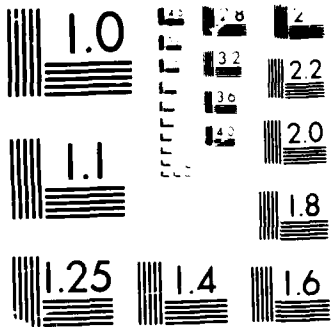

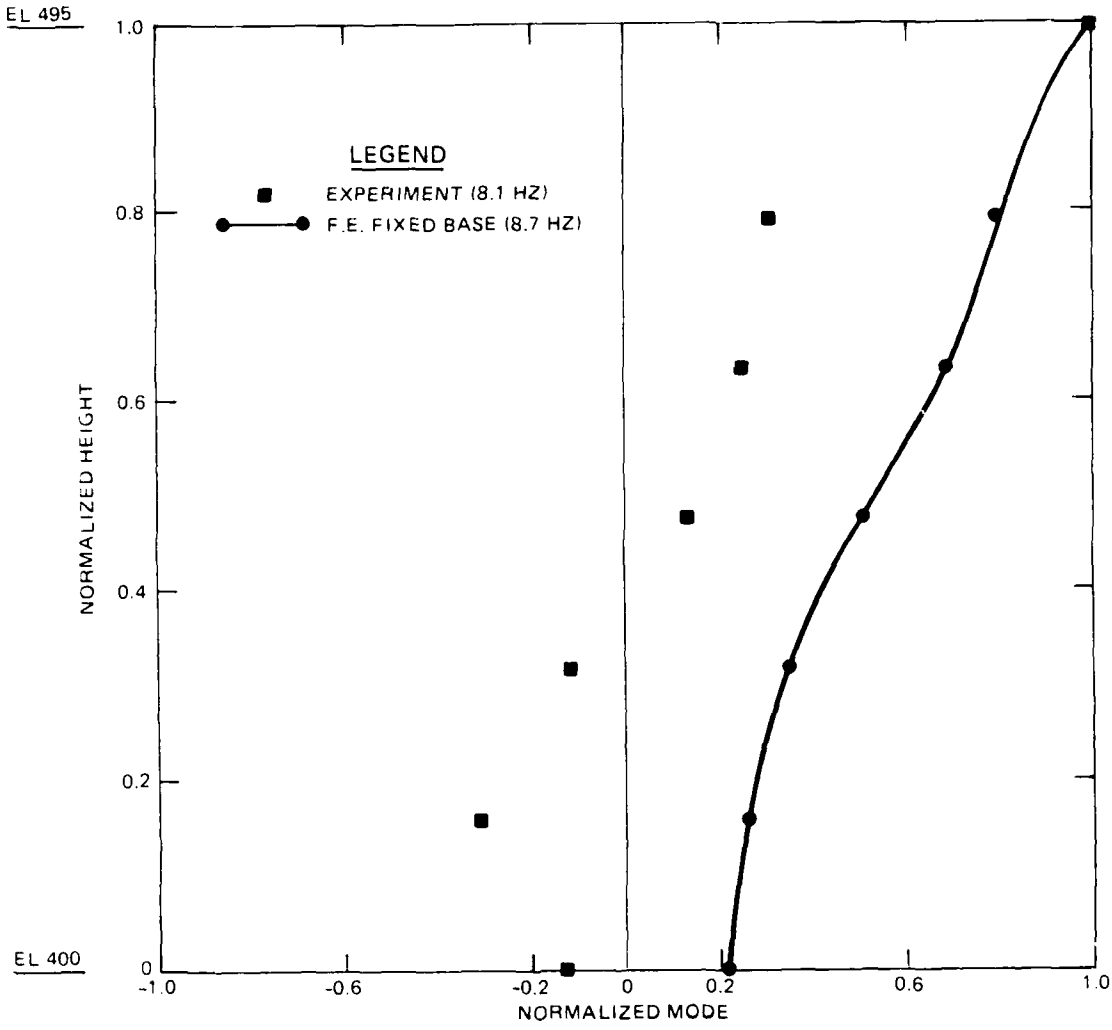

Figure 66. Cross-sectional mode shape 5 comparisons for monolith 7, downstream face, dam with reservoir

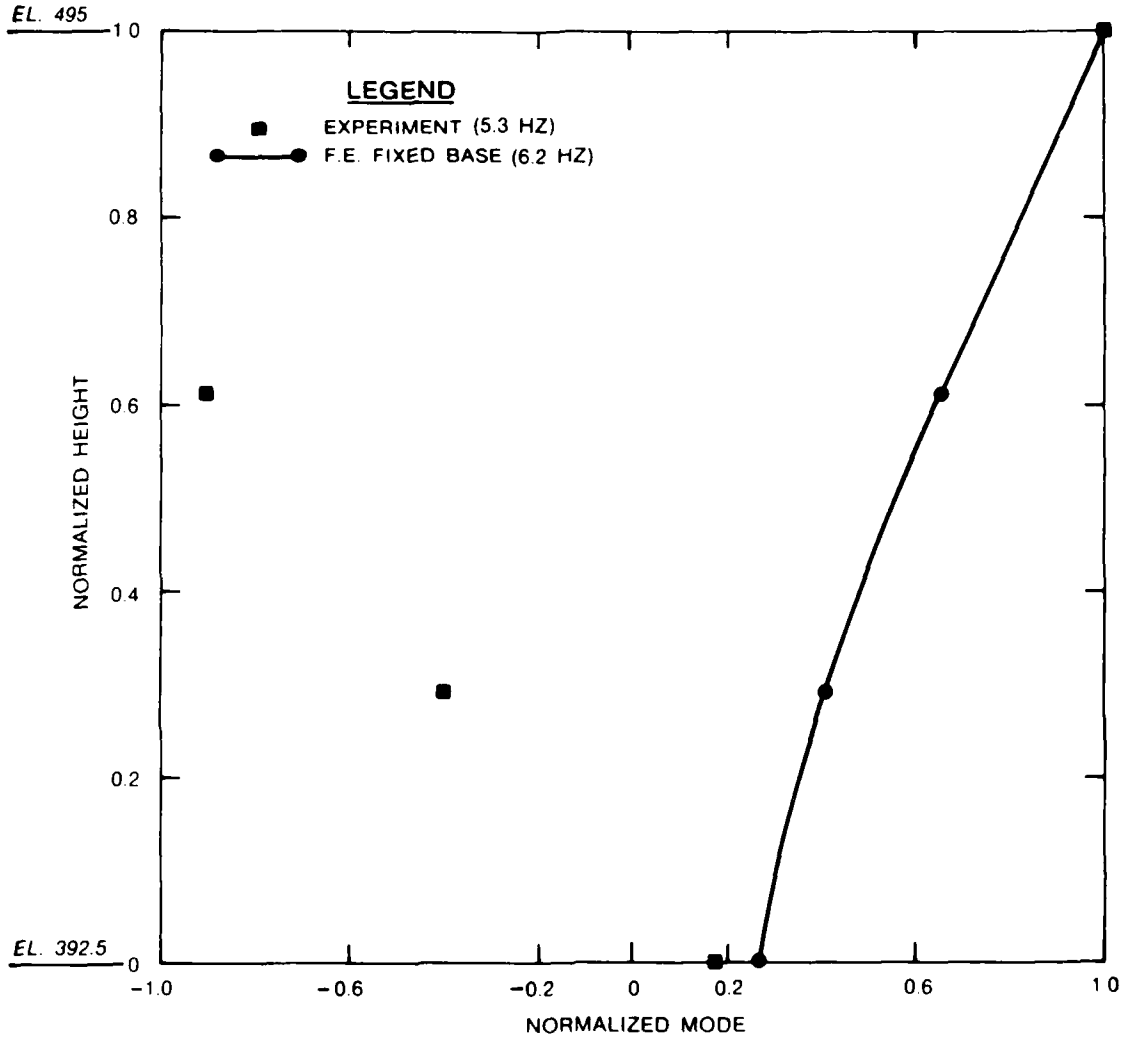

Figure 67. Cross-sectional mode shape 1 comparisons for monolith 16, dam with reservoir

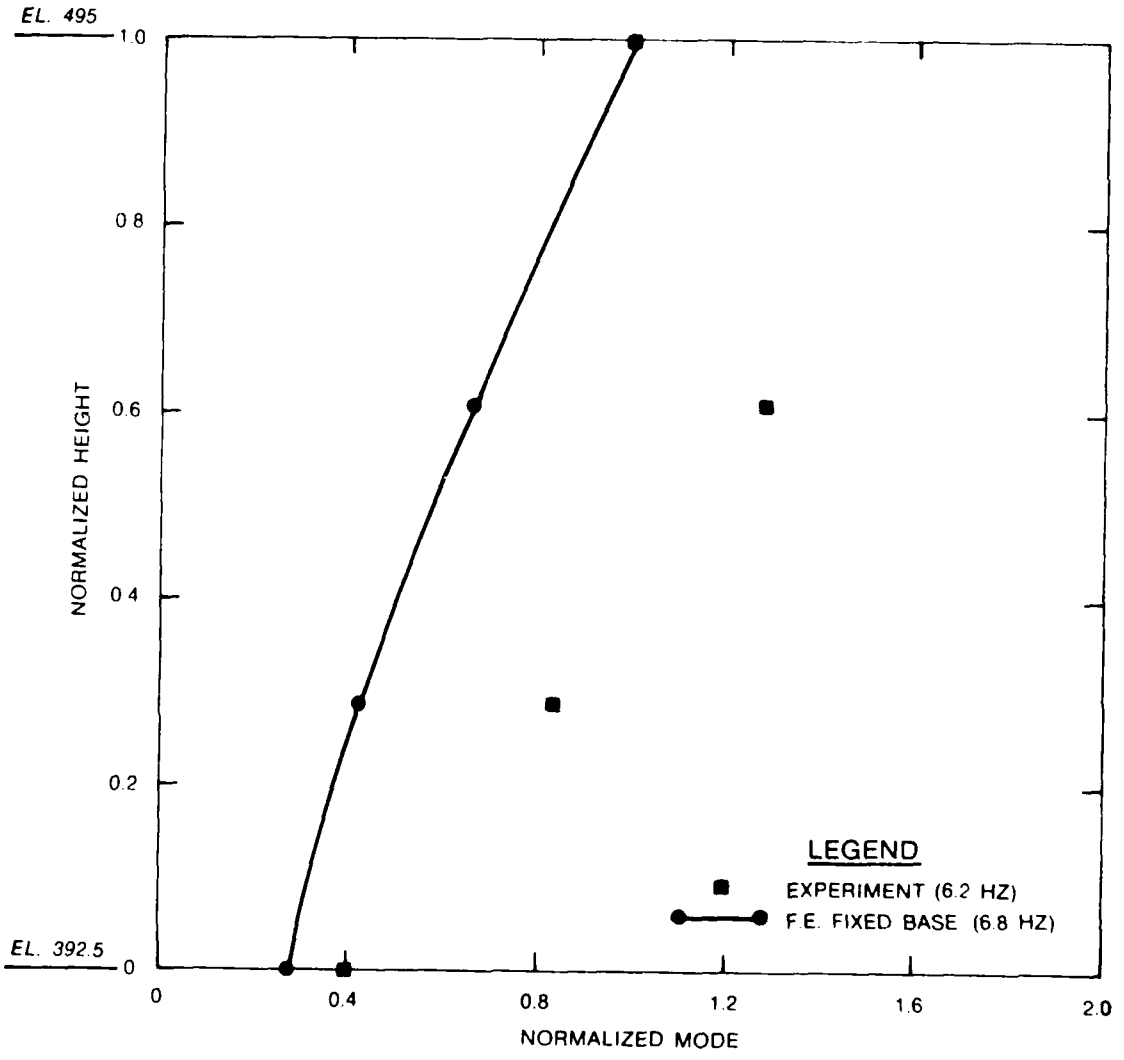

Figure 68. Cross-sectional mode shape 2 comparisons for monolith 16, dam with reservoir

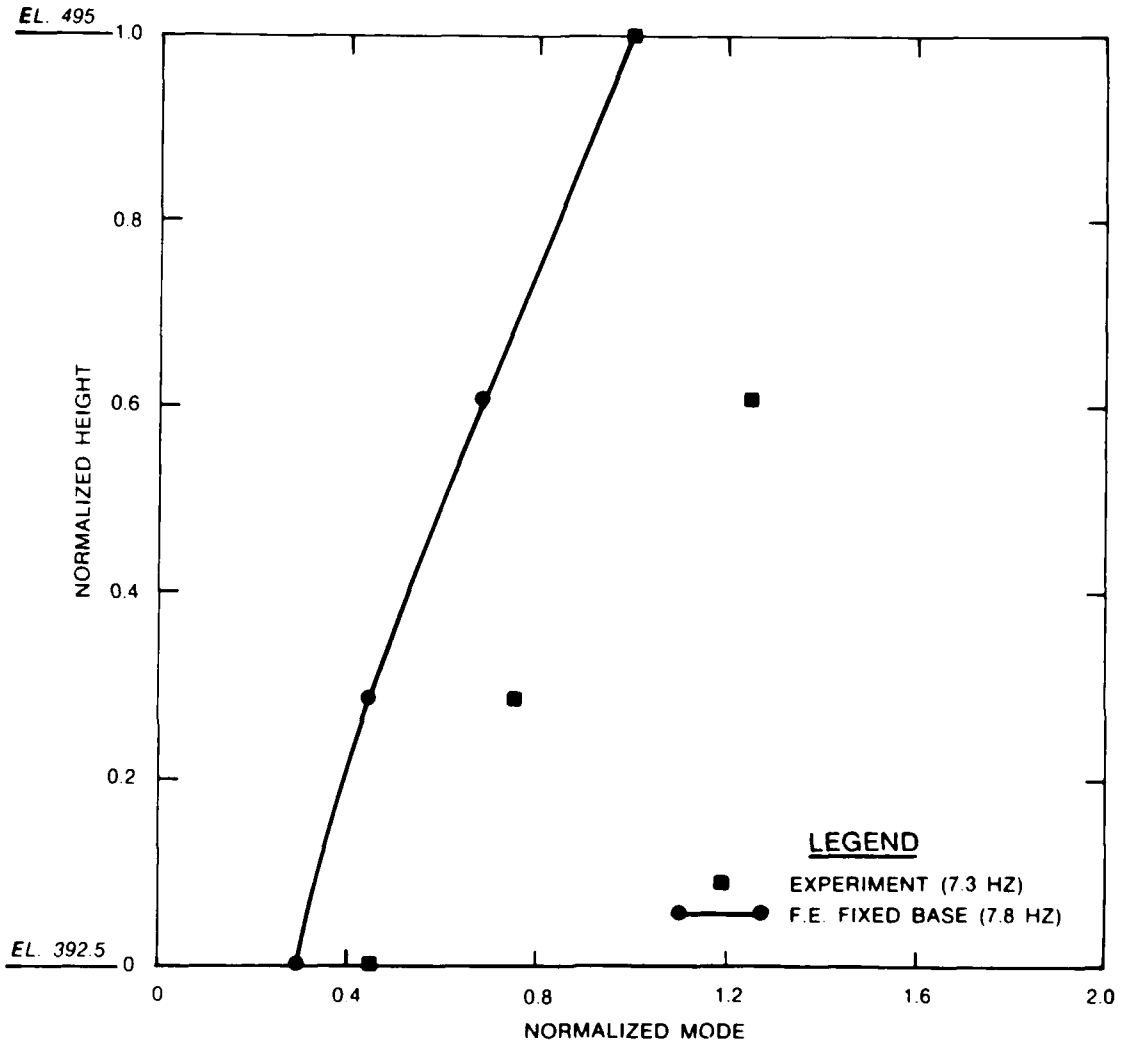

Figure 69. Cross-sectional mode shape 3 comparisons for monolith 16, dam with reservoir

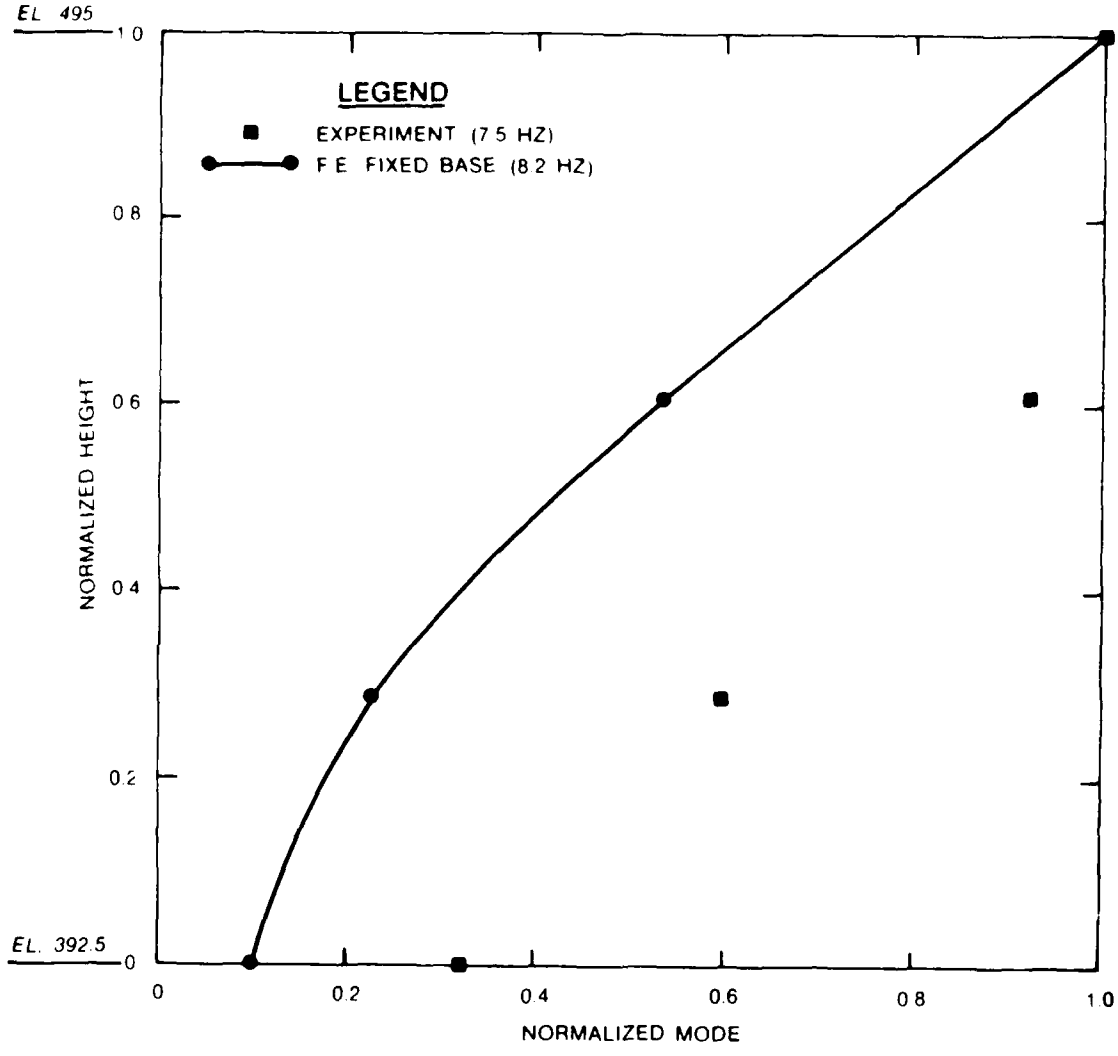

Figure 70. Cross-sectional mode shape 4 comparisons for monolith 16, dam with reservoir

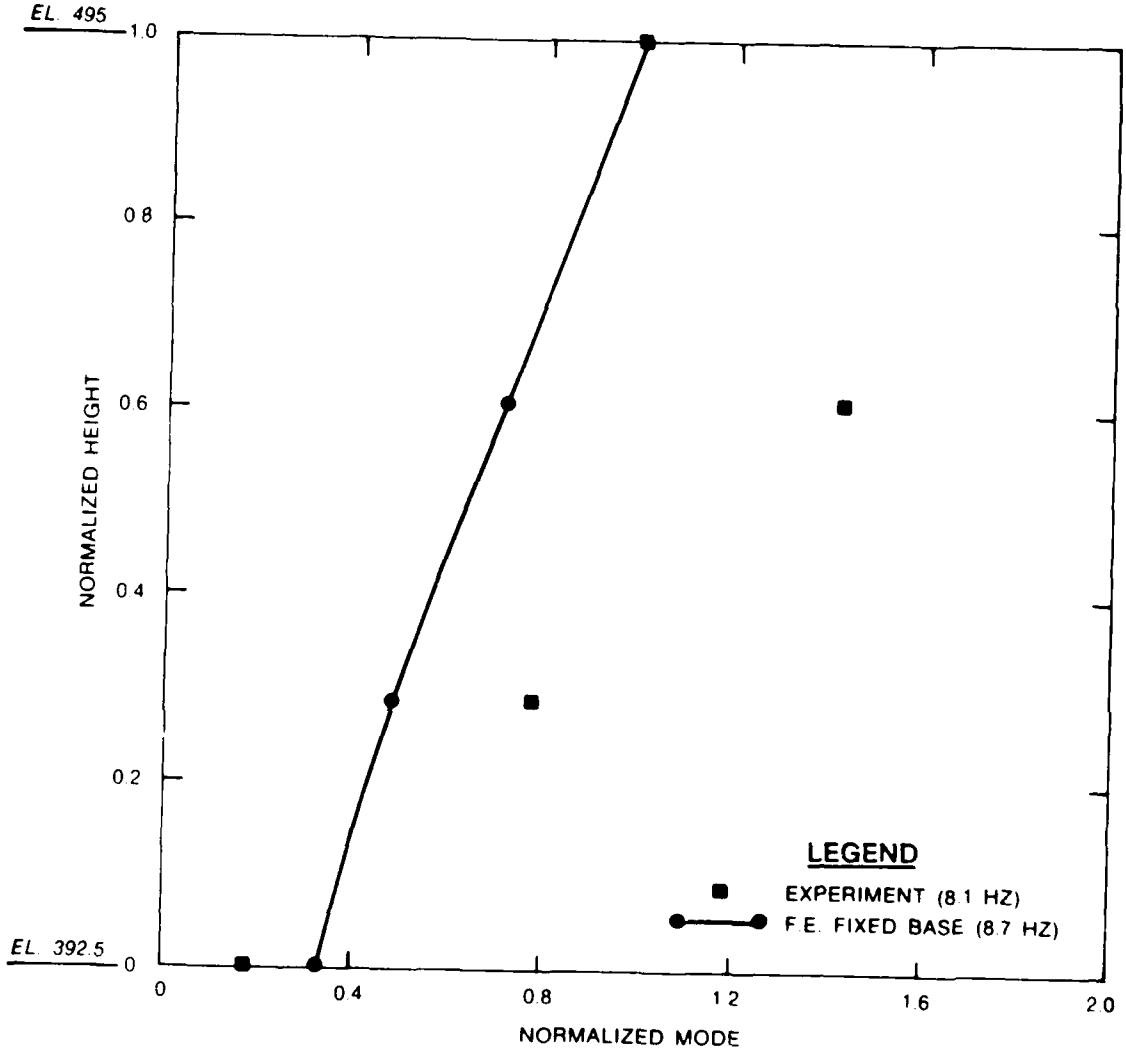

Figure 71. Cross-sectional mode shape 5 comparisons for monolith 16, downstream face, dam with reservoir

APPENDIX A: FOUNDATION INTERACTION STUDIES

1. Foundation properties are taken from Richard B. Russell Dam Design Memorandum 8, 1983. The in situ elastic modulus of the foundation, E_f, was estimated from the average dynamic modulus of elasticity, cross-hole seismic velocity and pulse velocity of rock core samples. The dynamic modulus of elasticity, E_{RC}, measured from seven rock core samples is shown in Table 4 of the main text.

$$E_{RC} = 9.6 \times 10^6 \text{ psi}$$

2. The average cross-hole seismic velocity, v_f, taken from 44 measurements was 12,810 ft/sec, with a coefficient of variation, $C_v = 0.22$. The average pulse velocity, V_{RC}, taken from 10 rock core samples was 16,130 ft/sec with $C_v = 0.20$. The velocity of waves, v, propagating through an elastic material is (Timoshenko and Goodier 1970)*

$$v = \sqrt{\frac{E}{\rho}} \tag{A1}$$

where

E = modulus of elasticity

ρ = mass density

Assuming constant mass density, E_f can be estimated from E_{RC} using Equation A1:

$$\frac{E_f}{E_{RC}} = \frac{V_f^2}{V_{RC}^2} = \frac{12{,}810^2}{16{,}130^2} = 0.63 \tag{A2}$$

Then

$$E_f = 0.63 \times 9.6 \times 10^6 \text{ psi}$$
$$= 6.05 \times 10^6 \text{ psi}$$

3. Elastic theory was used to obtain spring constants for the flexible base analysis of the entire dam. The stiffness of a semi-infinite solid acted on by a distributed loading on the boundary is (Timoshenko and Goodier 1970)

---

* See References at the end of the main text.

$$k = \frac{E\sqrt{A}}{m(1 - \nu^2)} \tag{A3}$$

where

k = stiffness

E = modulus of elasticity

A = magnitude of distributed load area

m = 0.95 for a square loading
= 0.92 for a 2:1 rectangular loading

ν = Poisson's ratio

Using m = 0.92 , Poisson's ratio = 0.2 , and an elastic modulus of foundation of 6.05×10^6 psi, spring constants were calculated for each node along the base of the dam. Because the loaded area varied, the constants varied from 283×10^8 lb/ft to 461×10^8 lb/ft. These constants gave an upper bound to results obtained from vibration tests.

4. Studies were performed on the effect of foundation interaction on the natural frequencies of individual two-dimensional (2-D) and three-dimensional (3-D) nonoverflow sections. Sections used for the 2-D and 3-D FE analyses were 1 and 48 ft wide, respectively. Tables A1 and A2 summarize comparisons of natural frequencies of the nonoverflow section using:

a. Winkler springs along base.

b. FE foundation (Figure A1).

c. Fixed foundation.

5. The grid used for the nonoverflow section in the analysis of the entire dam was also used for the individual nonoverflow section analyses with Winkler springs and fixed foundation. The grid shown in Figure A1 was used for the analysis with FE foundation. Dynamic concrete modulus of elasticity values were used, along with an elastic modulus of foundation equal to 9.60×10^6 psi. Figures A2 and A3 show the effect of spring stiffness on the fundamental frequency of the nonoverflow monolith.

6. The results indicated that a relatively low spring constant approximated the FE analysis with foundation (Figure A2). For the 2-D model, the effect of the horizontal spring constant on natural frequency is insignificant when it exceeds about 2×10^8 lb/ft, as shown in Table A1 and Figure A3.

7. As shown in Figure A2, the fundamental frequency of the 2-D model approaches the fundamental frequency with a fixed foundation for values of spring constant above 20×10^8 lb/ft. However, the fundamental frequency of

the 3-D model approaches the fundamental frequency with a fixed foundation for values of spring constant over 100×10^8 lb/ft. This indicates that the 3-D model is more flexible than the 2-D model.

8. Elastic theory predicts a much stiffer spring constant than obtained from comparison with the results using an FE foundation grid. Using a modulus of elasticity of 9.60×10^6 psi, Equation A3 gave a spring constant of 92.7×10^8 lb/ft for the 2-D model and a spring constant of 383×10^8 lb/ft for the 3-D model. The equivalent spring constants of the FE foundation grid results were 4.5×10^8 lb/ft for the 2-D model and 12.3×10^8 lb/ft for the 3-D model (Figure A2). Thus, elastic theory predicted foundation stiffness 20 to 30 times larger than an FE model with foundation grid.

Table A1

Natural Frequencies of Two-Dimensional Model of Nonoverflow Monolith

(All Frequencies in Hz)

	Boundary Spring Foundation* 5 Vertical - 5 Horizontal Springs Vertical and Horizontal Spring Constants (K_V and K_H) $\times 10^8$ lb/ft														
Mode No.	K_V / K_H	92.7 / 92.7	92.7 / ∞	46.4 / ∞	20.0 / ∞	10.0 / ∞	6.0 / ∞	4.0 / ∞	4.5 / ∞	4.5 / 4.5	4.5 / 2.25	4.5 / 0.045	1.43 / ∞	1.43 / 1.43	Finite Element Foundations* (60 elements)	Fixed Foundation
1		8.42	8.43	8.37	8.25	8.05	7.81	7.54	7.63	7.52	7.41	3.01	6.47	6.23	7.61	8.48
2		18.45	18.50	18.44	18.29	18.06	17.79	17.49	17.79	16.98	16.29	9.73	14.39	14.13	16.04	18.56
3		23.54	23.57	23.32	22.69	21.65	20.40	19.08	19.48	19.20	19.03	18.52	16.80	15.24	17.38	23.80
4		31.54	31.66	31.60	31.48	31.29	31.10	30.92	30.97	28.75	27.80	22.00	30.41	24.62	23.71	31.71
5		46.93	47.15	47.72	47.05	46.73	44.74	42.70	43.29	42.06	40.22	36.57	38.17	35.90	29.34	47.14
6		51.41	51.47	50.90	49.49	47.43	46.95	46.80	46.84	43.21	43.28	41.81	46.28	39.56	30.62	51.99
7		61.57	61.71	61.38	60.58	59.01	56.60	54.11	54.86	53.67	53.06	47.71	47.99	46.96	35.20	62.01
8		63.71	63.80	63.30	62.07	60.43	59.32	58.47	58.73	57.32	55.74	52.37	55.65	52.38	38.31	64.26
9		66.67	66.84	66.71	66.42	66.03	65.60	65.09	65.26	62.16	61.03	56.79	62.57	55.25	42.39	66.97
10		70.32	70.49	70.30	69.83	69.07	68.16	67.22	67.50	64.42	62.31	59.81	65.19	60.01	43.45	70.67

* Elastic modulus of foundation (E_f) = 9.60×10^6 psi, Poisson's ratio $\nu = 0.20$.

Table A2

Natural Frequencies of Three-Dimensional Isolated Model of Nonoverflow Monolith

(All Frequencies in Hz)

	Boundary Spring Foundation* 10 Vertical-10 Horizontal Springs $K_V = K_H$ (10^8 lb/ft)					Finite Element Foundation 60 elements	Fixed Foundation
Mode No.	4.5	10.0	20.0	46.35	92.69		
1	3.62	5.0	6.4	7.8	8.6	5.43	9.8
2	6.65	9.5	12.5	16.7	19.1	14.66	21.5
3	10.57	13.9	16.1	18.2	20.3	15.48	26.3
4	20.28	22.5	25.9	30.6	33.2	23.21	37.5
5	36.51	37.9	40.3	44.1	46.8	26.33	50.9
6	40.38	41.0	42.1	45.2	50.0	29.67	52.4
7	49.09	50.4	50.5	50.7	50.7	31.45	54.5
8	49.81	51.1	51.6	52.0	52.2	32.25	55.2
9	50.23	51.1	53.0	53.9	54.1	35.63	55.3
10	51.32	52.4	53.5	54.4	54.5	37.32	56.7

* Elastic modulus of foundation (E_f) = 9.60×10^6 psi, Poisson's ratio $\nu = 0.20$.

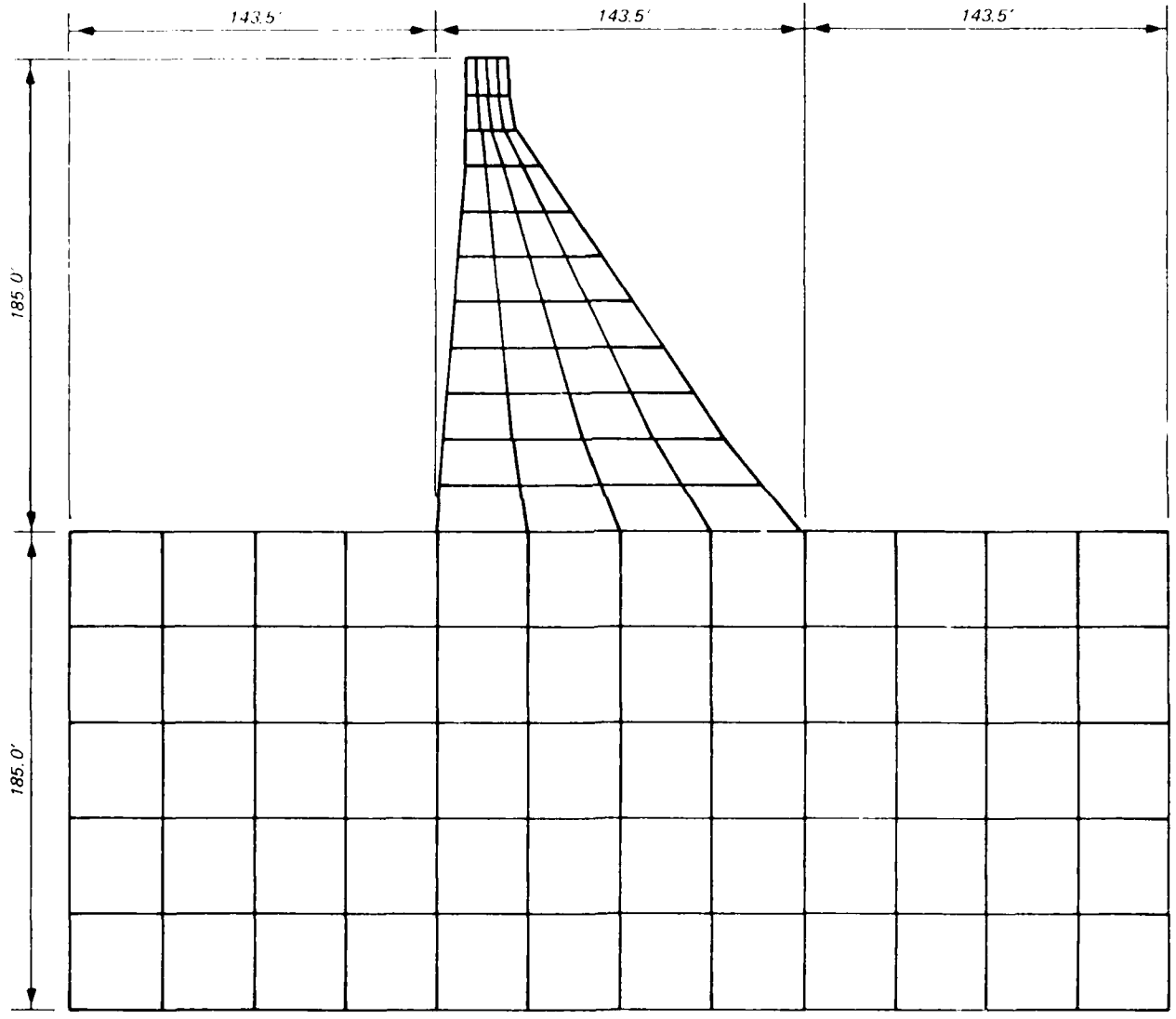

Figure A1. Finite element nonoverflow monolith and foundation grid

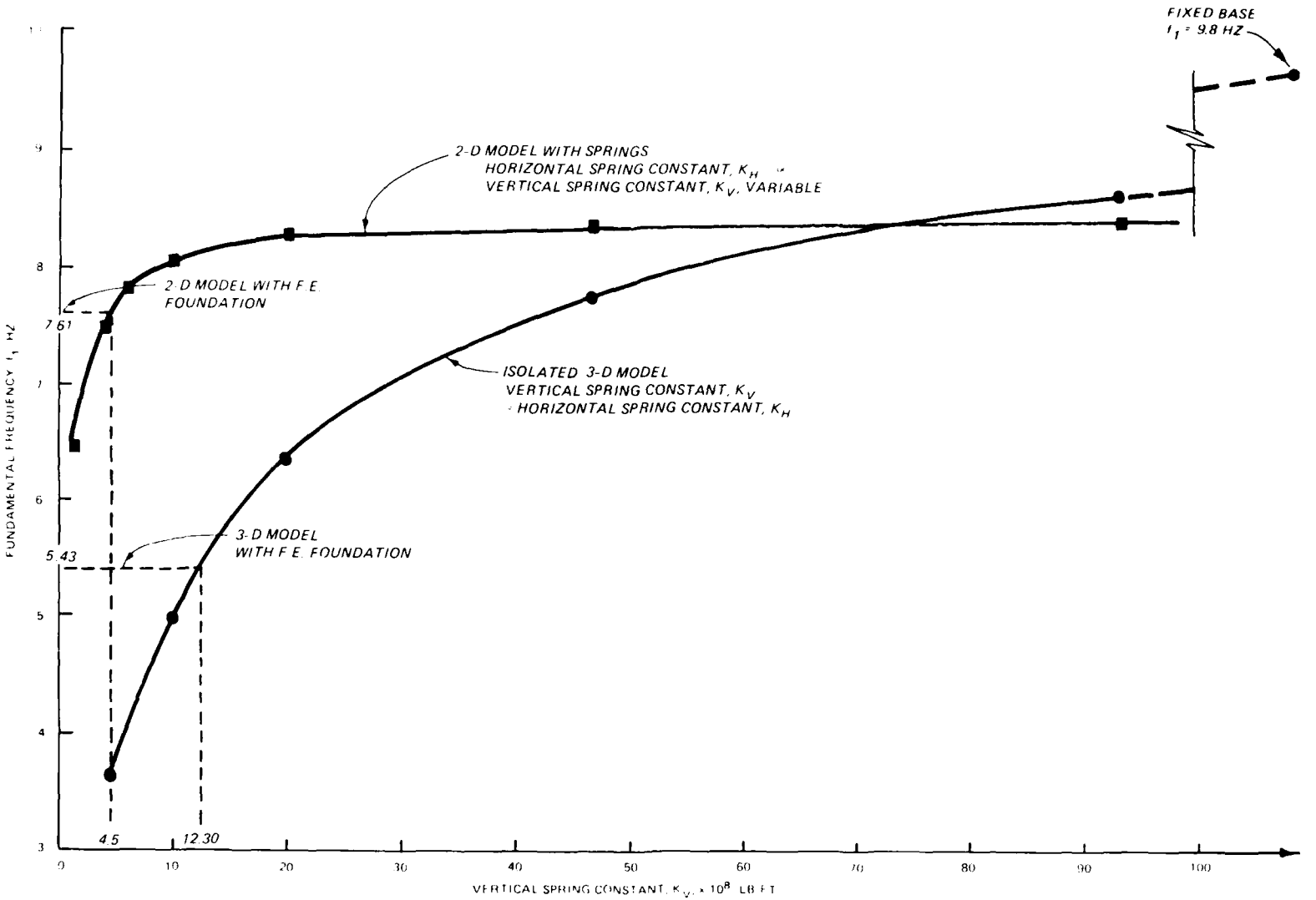

Figure A2. Effect of vertical spring stiffness on fundamental frequency of nonoverflow nomolith

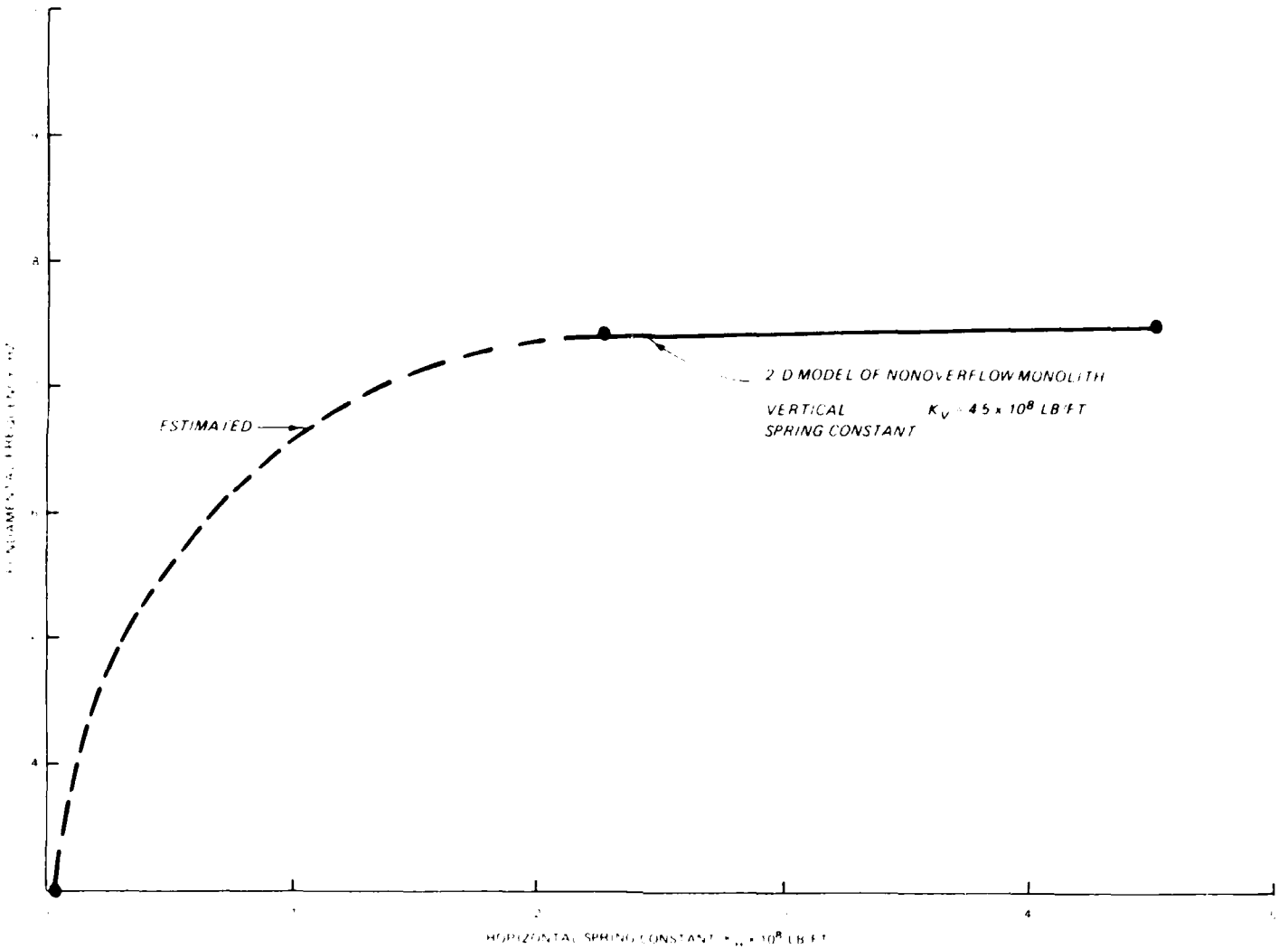

Figure A3. Effect of horizontal spring stiffness on fundamental frequency of nonoverflow monolith (1 lb/ft = 14.6 N/m)

APPENDIX B: MODAL ASSURANCE CRITERION*

1. The modal assurance criterion (MAC) is a measure of the consistency between estimates of modal vector. This criterion was used to indicate quantitatively how well the mode shapes compared. The modal assurance criterion is defined as

$$MAC(c,d) = \frac{|MOM(c,d)|^2}{MOM(c,c)\ MOM(d,d)} \tag{B1}$$

where

MAC(c,d) = MAC for vectors c and d

MOM(c,d) = cross moment of the modal vectors c and d

MOM(c,c) = auto moment of the mode vector c

MOM(d,d) = auto moment of the mode vector d

For real modes, Equation B1 reduces to

$$MAC \frac{\left[\sum_{i=1}^{n} \phi_i 0_i\right]^2}{\left(\sum_{i=1}^{n} \phi_i^2\right)\left(\sum_{i=1}^{n} 0_i^2\right)} \tag{B2}$$

where

ϕ_i = element of mode vector ϕ

0_i = element of mode vector 0

MAC = MAC of vectors ϕ and 0

2. The MAC criterion will have values from zero, representing no correspondence, to one, representing a consistent correspondence.

---

* Allemang and Brown (1982). See References at the end of the main text.

APPENDIX C: HYDRODYNAMIC INTERACTION

1. Westergaard (1933)* derived an approximate formula for the added mass of water on the vertical upstream face of a dam during earthquakes. As shown in Figure C1, Westergaard assumed a parabolic added mass distribution. Using consistent units:

$$b = \frac{7}{8}\sqrt{hy} \tag{C1}$$

where

b = width of added water mass

h = depth of reservoir

y = vertical distance from top of dam

Westergaard neglected the effects of flexibility of the dam and compressibility of water.

2. Chopra (1978) developed an approximate analysis method accounting for the flexibility of the dam and compressibility of water. The approximate natural period of vibration of the dam with reservoir effects is

$$\bar{T}_s = R_1 \; 1.4 \; \frac{H_s}{\sqrt{E}} \tag{C2}$$

where

$\bar{T}_s$ = vibration period with water, sec

R_1 = ratio of fundamental vibration periods of dam with and without water, plotted (Chopra 1978) against depth of water for various values of concrete modulus of elasticity

H_s = height of dam, ft

E = concrete modulus of elasticity, psi

3. For the Richard B. Russell Dam, assume that height of dam = 185 ft, depth of water = 170 ft, and concrete modulus of elasticity = 5×10^6 psi. Then R_1 = 1.31 , and the vibration period computed by Equation C2 is 0.1517 sec. Therefore, the fundamental natural frequency of the dam with water is 6.59 Hz using Chopra's approximate analysis.

---

* See References at the end of the main text.

4. As discussed below, a modified Westergaard formula was used to compute a fundamental natural frequency nearly the same as that computed using Chopra's procedure. As shown in Figure C1, the mass distribution from Equation C1 was factored by 0.5, producing a total water force of 43,832 lb on a 1-in.-wide face of dam:

$$b = \frac{7}{16}\sqrt{hy} \tag{C3}$$

5. As shown in Figure C1, the constant reservoir width, W , that produced the total water force from Equation C3 was calculated.

$$W = \frac{\text{total water force}}{\gamma_w h} \tag{C4}$$

where

W = constant reservoir width

γ_W = weight density of water

h = depth of reservoir

With γ_W = 62.4 lb/ft^3 , h = 170 ft , and total water force = 43,832 lb/in., the constant reservoir width, W , from Equation C4 is 49.6 ft. A fundamental natural frequency of 6.62 Hz was obtained from a two-dimensional dynamic finite element (FE) analysis of the section shown in Figure C1 with concentrated masses applied to the nodes in contact with the constant 49.6-ft reservoir width. The same dimensions and material properties of the section used in Chopra's analysis were used in this FE analysis.

6. The fundamental natural frequency of dam with reservoir calculated from the uniform width of reservoir (6.62 Hz) compared well with the result from Chopra (1978) (6.59 Hz, or 0.5-percent difference). Therefore, the uniform reservoir width concept was used to obtain added masses on the model of the entire dam. As a first approximation, a constant 49.6-ft-wide mass of reservoir was applied at all sections of the dam. Concentrated masses due to the reservoir were applied at nodes assumed to be in contact with the reservoir.

7. Additional studies on hydrodynamic interaction would use Chopra's mass distribution in the vertical direction and a modified nonuniform mass distribution in horizontal direction along the length of the dam.

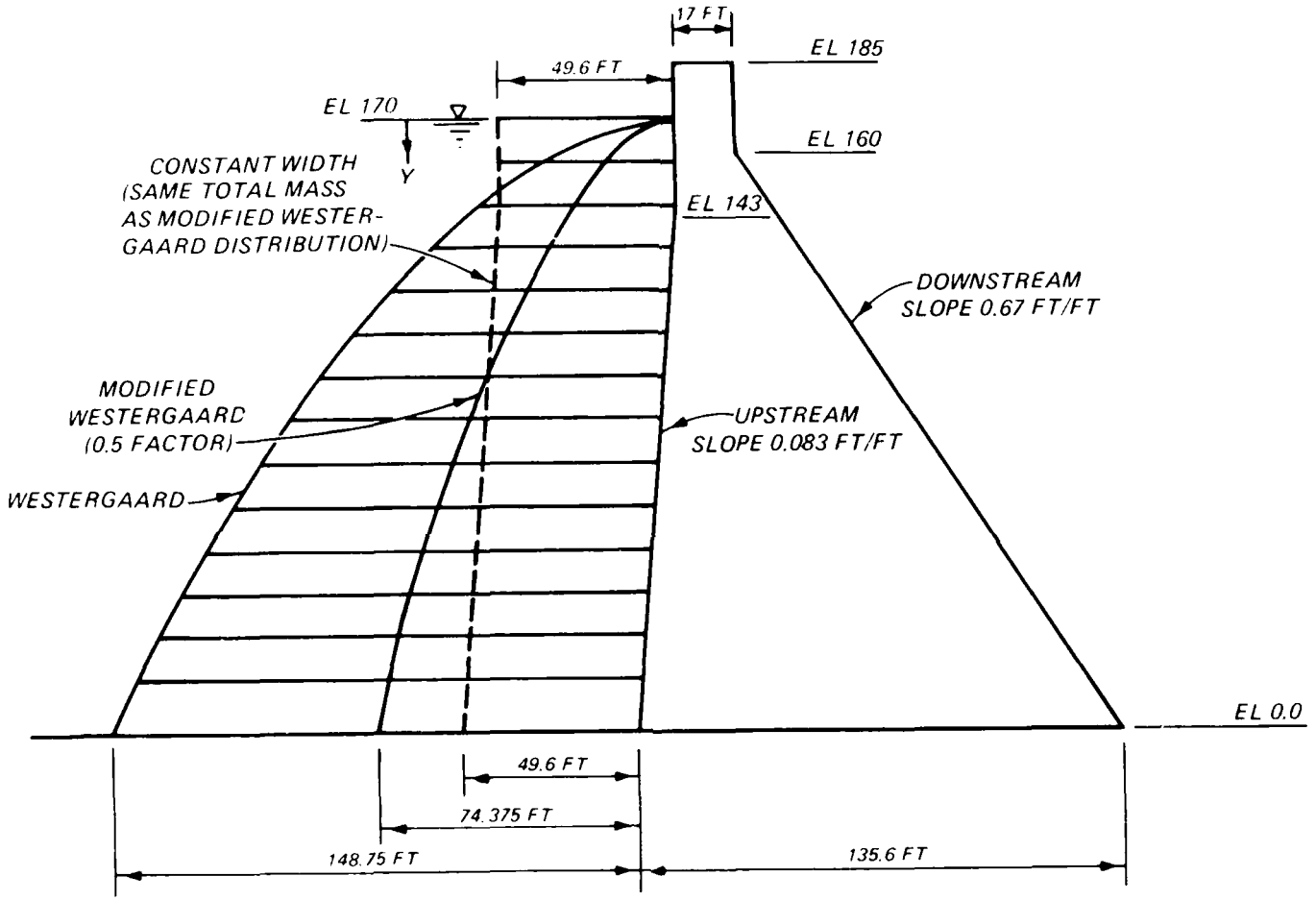

Figure C1. Added mass distributions due to reservoir

APPENDIX D: COMPARISON OF ANALYTICAL AND DESIGN CROSS-SECTIONAL MODES

1. The modal assurance criterion (MAC) (Allemang and Brown 1982)* was used to quantitatively compare mode shapes in cross section from finite element (FE) results with the design mode shape proposed by Chopra (1978).

2. In Figures D1 to D3, the design mode shape is compared with three mode shapes from three-dimensional (3-D) FE analyses to the Richard B. Russell Dam without reservoir, fixed base, for nonoverflow monolith 6, spillway monolith 7, and intake monolith 11, respectively. The three FE modes shapes are at the normal frequencies corresponding to the first three FE normal mode shapes of the dam crest. All shapes resemble the fundamental mode shape of a cantilever beam. As summarized in Table D1, the high value of the MAC indicates that the analytical and design mode shapes compare well.

3. The analytical mode shapes compared well with the experimental mode shapes in cross section as stated in the report. It can be concluded that the design mode shape would also compare well with the experimental results.

---

* See References at the end of the main text.

Table D1

Design and Analytical Mode Shape Comparisons

Section	Finite Element Fixed Base Analysis--Dam Without Reservoir	Modal Assurance Criterion
Nonoverflow	Mode 1	0.99
	Mode 2	0.99
	Mode 3	0.99
Intake	Mode 1	0.97
	Mode 2	0.98
	Mode 3	0.98
Spillway	Mode 1	0.98
	Mode 2	0.98
	Mode 3	0.99

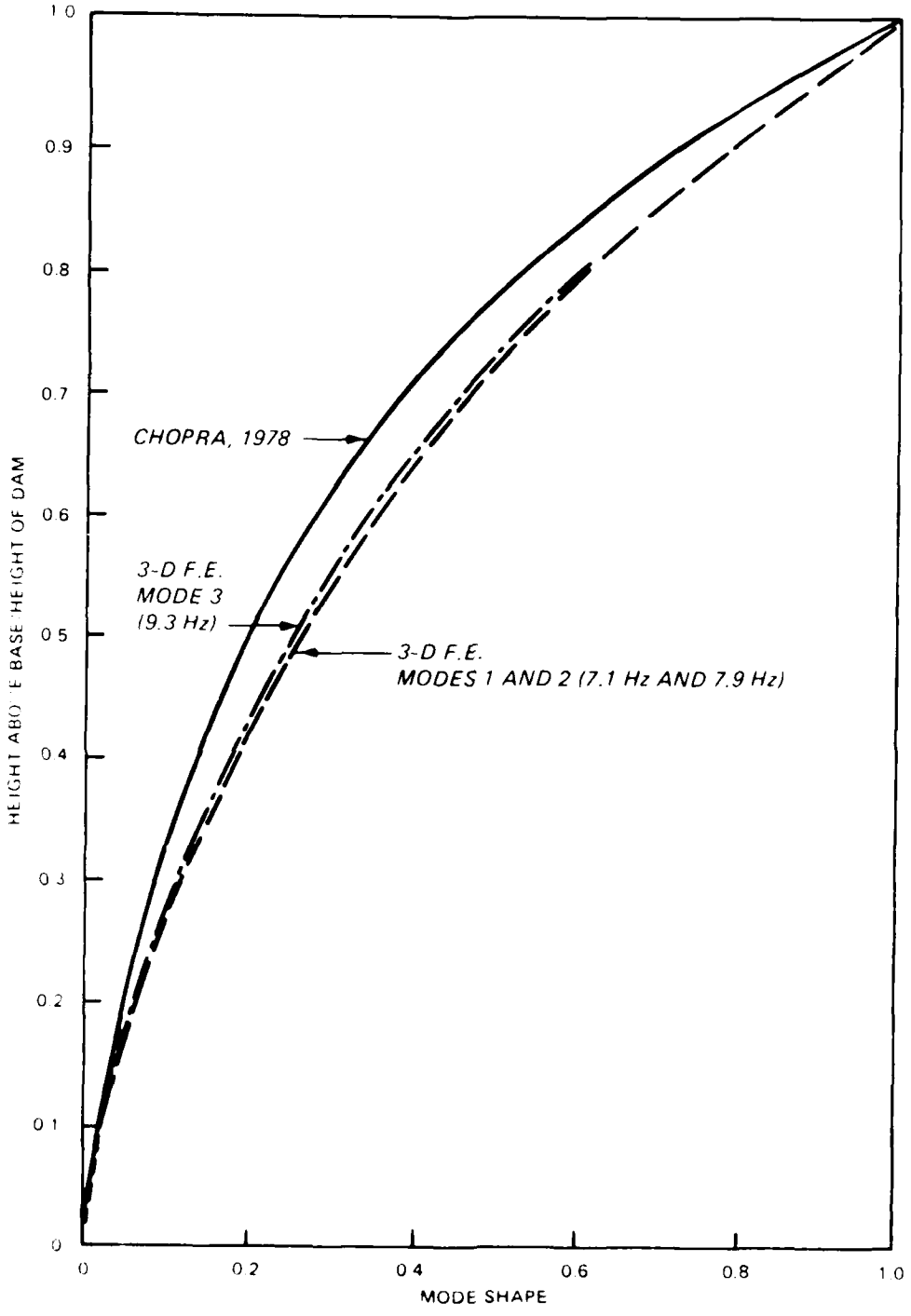

Figure D1. Analytical and design mode shape comparisons for nonoverflow monolith 6

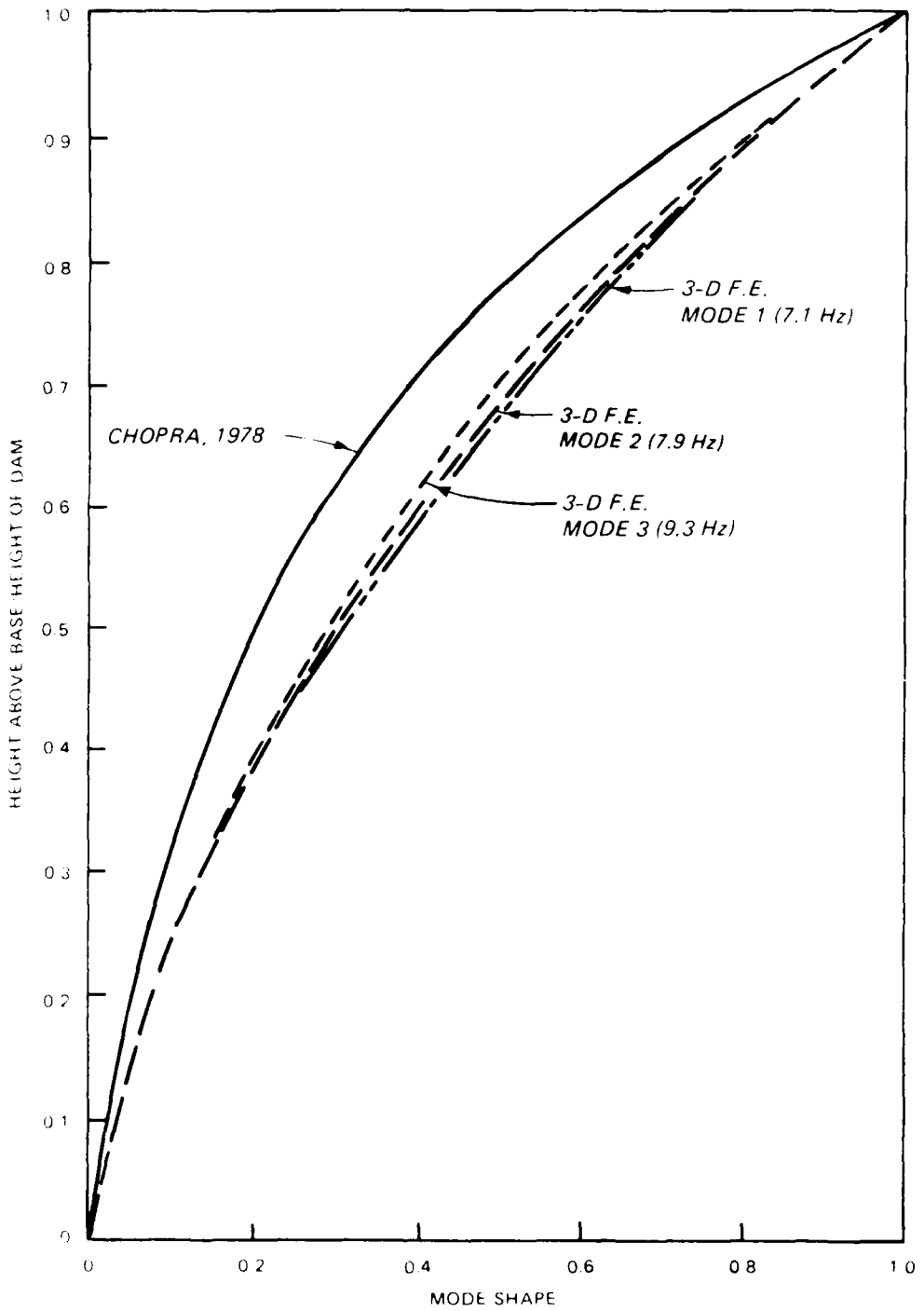

Figure D2. Analytical and design mode shape comparisons for spillway monolith 17

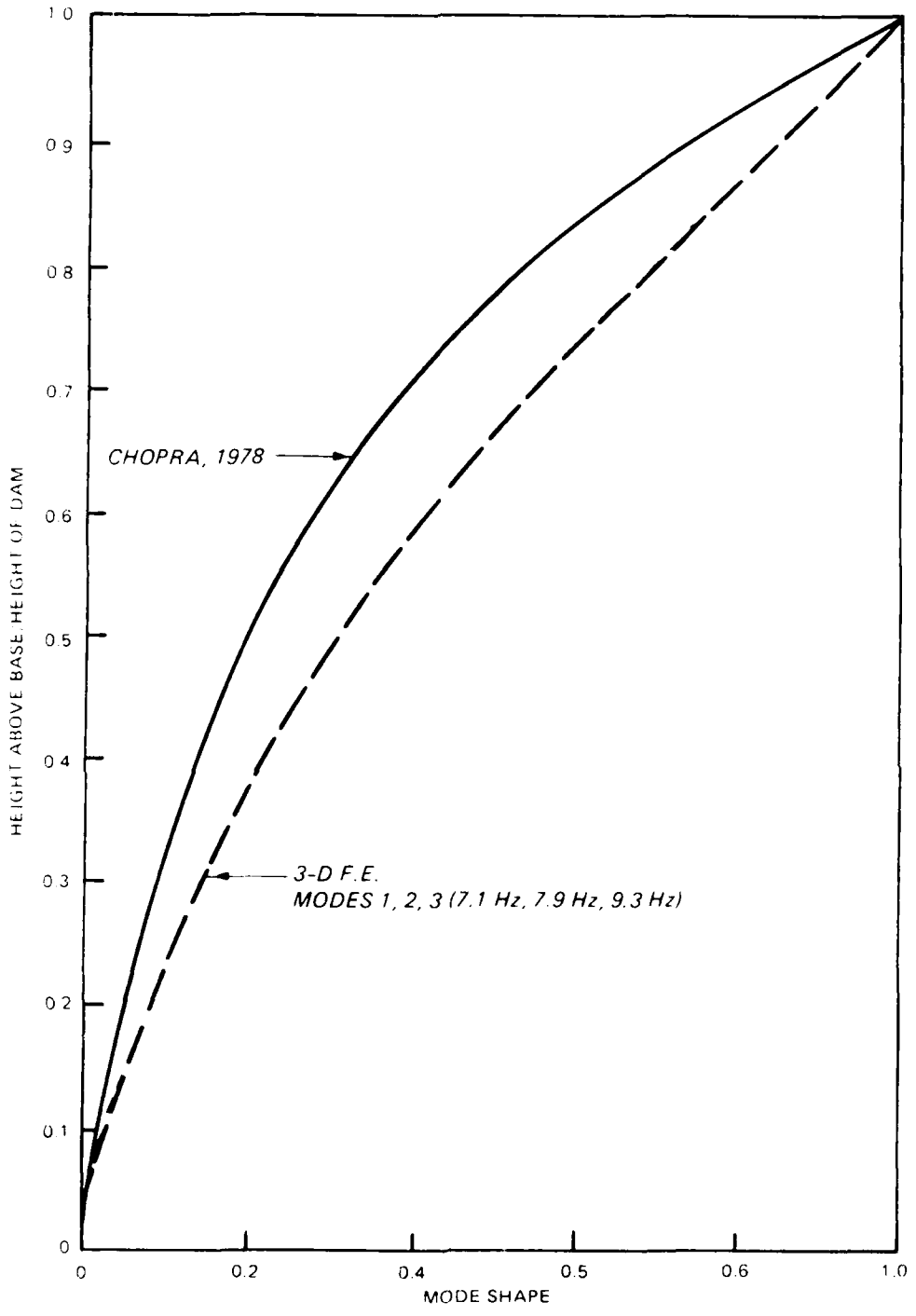

Figure D3. Analytical and design mode shape comparisons for intake monolith 11

APPENDIX E: GLOSSARY

Acceleration - A vector quantity that indicates the time rate of change of velocity.

Coherence Function - The coherence function for an input/output pair measures what ratio of the output acceleration is linearly caused by a measured input force.

Coupled Modes - Modes of vibration that are dependent upon other modes of vibration due to energy transfer. (See "Mode of vibration.")

Critical Damping - The minimum amount of damping for which no oscillation occurs when a displaced system returns to its original position.

Cycle - A set of values that occurs during one complete performance of a periodic process.

Damped Natural Frequency - Frequency of free vibration of a damped linear system.

Damping - Energy loss of a system due to friction and other resistances.

Damping Ratio - Ratio of the actual amount of damping of a system to the critical damping of the system.

Degrees-of-freedom - The number of independent coordinates required to define the motion of a system.

Dynamic Modulus of Elasticity - A measure of the material elasticity under dynamic loads, calculated from the measurement of the fundamental resonant frequency of vibration.

Eigenvalue - Frequency of a normal mode of vibration.

Eigenvector - A configuration of a vibrating system, or normal mode of vibration in which all particles are in harmonic or sinusoidal motion at the same frequency. Each eigenvector can exist independently of other eigenvectors of the system.

Excitation - An external force acting on a system that causes the system to respond in a particular way.

Forced Vibration - Vibration or oscillation of a system due to excitation (external forces).

Free Vibration - Oscillation of a system under the action of internal forces of the system, without external excitation.

Frequency - The reciprocal of the period or repetition time of oscillation, expressed in cycle per unit time. Hertz (Hz) is cycle per second.

Frequency Response Function (Transfer Function) - The complex (i.e., composed of real and imaginary parts) ratio of the measured output acceleration to the measured input force.

Fundamental Frequency - The lowest natural frequency of a system.

Fundamental Mode of Vibration - Mode that has the lowest natural frequency.

Inertial Mass - The acceleration of mass (inertial mass) creates a resisting inertial force equal to the product of mass and acceleration.

Linear System - System in which the response of every element is proportional to the excitation.

Modal Assurance Criterion - (MAC) (Appendix B). A measure of the consistency between estimates of modes of vibration.

Mode of Vibration - A configuration of a vibrating system in which all particles are in harmonic, or sinusoidal, motion at the same frequency.

Natural Frequency - Frequencies of the normal modes of vibration of a system.

Nonlinearities - Nonlinearities in a system cause the response of certain elements to be disproportional to the excitation.

Normal Mode of Vibration - A mode of vibration that can exist independently of other modes of vibration of a system.

Oscillation - Variation, usually with time, of displacement magnitude from one extreme limit to another with respect to a fixed reference.

Period - The recurring time of an oscillatory motion.

Phase Angle - The angle by which the response vector lags behind the force or input vector.

Phase Function - The phase angle of the transfer function versus frequency.

Resonance - A condition in which the frequency of excitation coincides with one of the natural frequencies of a system.

Resonant Frequency - Frequency of a system in which a resonance exists.

Signal-to-Noise Ratio (SNR) - A function of the coherence that measures how much of the response signal is contaminated by noise. A high SNR indicates most of the output vibration is linearly caused by a measured input force.

Stiffness - Ratio of change of force (or torque) to the resulting change in the static (or dynamic) deflection of an elastic element.

Subspace Iteration - The subspace iteration method uses portions or subspaces of the system matrix to solve for the natural frequencies and mode shapes in dynamic finite element analysis.

Transfer function - (See "Frequency Response Function.")

Undamped Natural Frequency - Frequency of free vibration of a system neglecting energy losses due to friction and other resistances.

END
DATE
FILMED
5-88
DTIC